CONCEPTUALIZATION AND DEVELOPMENT OF IN VITRO VASCULAR MODELS FOR STUDYING ALZHEIMER'S DISEASE

by

Tiffany Cameron

B.Sc., The University of Prince Edward Island, 2019

A THESIS SUBMITTED IN PARTIAL FULFILLMENT OF

THE REQUIREMENTS FOR THE DEGREE OF

MASTER OF APPLIED SCIENCE

in

THE FACULTY OF GRADUATE AND POSTDOCTORAL STUDIES

(Biomedical Engineering)

THE UNIVERSITY OF BRITISH COLUMBIA

(Vancouver)

April 2022

The following individuals certify that they have read, and recommend to the Faculty of Graduate and Postdoctoral Studies for acceptance, a thesis/dissertation entitled:

Conceptualization and development of in vitro vascular models for studying Alzheimer's Disease

submitted by Tiffany Cameron in partial fulfillment of the requirements for

the degree of Master of Applied Science

in Biomedical Engineering

Examining Committee:

Dr. Karen Cheung, Biomedical Engineering, UBC
Co-supervisor

Dr. Cheryl Wellington, Pathology, UBC
Co-supervisor

Dr. Sarah Hedtrich, Pharmaceutical Sciences, UBC
Supervisory Committee Member

Dr. Rizhi Wang, Materials Engineering, UBC
Supervisory Committee Member

Abstract

The human brain is an extraordinarily complex organ that is regulated by the input of nutrients and oxygen and the removal of waste via the vascular network. Understanding how the local microenvironment of cells that make up the neurovascular unit influences the health of the human brain could allow for better understanding of disease pathology, such as Alzheimer's Disease (AD). Traditional animal-based models are limited in some of their physiological similarities with humans; therefore, human-based in vitro models are desirable. Standard cell culture is often performed in a 2-dimensional, static well plate, which lacks many of the physiological properties seen in the human brain. Moving towards in vitro models that include defined cellular architectures and includes flow on the endothelial cell layer could overcome some of the challenges associated with standard well plate models.

In this thesis, in vitro models of the capillary and arteriole are conceptualized and developed. Two capillary-based microfluidic designs are developed, with a focus on the fabrication techniques used for the master molds, as well as the endothelial cell layer optimization. Having a tight endothelial cell layer is important to ensure that transport into and out of the brain is based on transcellular transport and not due to a leaky barrier. The first capillary model described includes a hydrogel-based extracellular matrix, and the second contains a planar membrane acting as a substrate for the endothelial cell barrier.

In addition, this work highlights improvements to a previously used tissue chamber that contains a cell-laden scaffold. The motivation for these improvements includes the fragility of the tissue chamber and only being able to perform in-line sampling from the circulating fluid within the

“blood” side, limiting the ability to perform in-line vessel transport studies. The fabrication of custom end-caps, to improve the tissue chamber stability, and the inclusion of sampling ports to the “brain” side are also described.

Lay Summary

Studying brain related diseases, such as Alzheimer's Disease has been a challenging task due to the inconvenience of sampling the brain environment, and the difficulties in developing human-like animal models to study the human physiology. These limitations lead to studying cellular behavior under different conditions in a 2-dimensional (2D) environment. The work presented here takes this 2D environment and adds the capability of incorporating flow onto the cell layer, thus better mimicking a brain blood vessel. This work describes the important considerations when transitioning to a flow-based cell culture environment, as well as the importance of improving system reliability before incorporating cells into the environment. This work will provide the designs of the microsystems that can be used for studying capillary and arteriole vessel physiology in a flow-based environment.

Preface

This research was funded and supervised by Dr. Karen Cheung and Dr. Cheryl Wellington. The original research idea was developed by Dr. Karen Cheung and Dr. Cheryl Wellington.

This work was conducted partially in the Center for Blood Research at the Life Sciences Center, and the Djavad Mowafaghian Center for Brain Health at the University of British Columbia. This research work and analysis of the research was conducted by Tiffany Cameron.

Contributions to Chapter 2 were made by Tanya Bennet and Tara Caffrey, who supervised and provided experimental planning help throughout. The chip design used in Chapter 2 is based off the chip designed and used by Tanya J. Bennet *et al.* (1). The image of the physical chip shown in Figure 3 has the same internal geometries as that used in the experiments described, although the chip in the image was developed by Jessica Hua, which has different PDMS layer thicknesses than the chips used in these experiments. This image is used as a visual representation of the 3 channels included in the chip.

Contributions to section 4.2.1 were made by Eric Lyall, who developed the tube-cutting apparatus. Contributions to section 3.2.3.2 were made by Elyn Rowe, who performed 50% of experimental planning and execution.

This research work led to the publication of a review article. T. Cameron, T. Bennet, E. Rowe, M. Anwer, C. Wellington, and K. Cheung, "Review of Design Considerations for Brain-on-a-Chip Models," *Micromachines*, vol. 12, no. 4, p. 441, Apr. 2021. Parts of this review are presented in

Chapter 1 of this thesis. I was involved with the review and editing of sections 1.4 and 1.6 and was responsible for the original writing of sections 1.1-1.3 and 1.7-1.10. Portions of figures throughout this thesis were created using Biorender.com.

Human Ethics were approved for this work, as per the UBC Ethics Board Certificate number: H13-02719 - TEBBB-Tissue engineered blood brain barrier: Development of a novel tissue engineered model to study Alzheimer's disease in vitro and H21-03401: In vitro models of the cerebrovasculature to study neurological disorders.

Table of Contents

List of Tables

List of Figures

List of Symbols

ß – beta

© - copyright

º - degrees

Q - flow rate

> - greater

μ - micron

π – pi (3.14159..)

r - radius

τ - shear stress

² - squared

η – viscosity

™ - Trademark (unregistered)

® - Registered trademark

List of Abbreviations

2D – Two dimensional

2.5D – Two and a half dimensional

3D – Three dimensional

Aß – Amyloid-beta

AD – Alzheimer's Disease

APOE – Apolipoprotein E

BBB – Blood-brain barrier

BMEC – Brain microvascular endothelial cell

BoC – Brain on a Chip

cAMP – Cyclic Adenosine monophosphate

DLP – Digital light processing

EC – Endothelial cell

ECM – Extracellular matrix

ELISA – Enzyme-linked immunosorbent assay

IPA – Isopropyl alcohol

iPSC – Induced pluripotent stem cell

HDL – High-density lipoprotein

NVU – Neurovascular unit

PC – Polycarbonate

PDMS - Polydimethylsiloxane

PET – Polyester

SLA - Stereolithography

TEER - Transendothelial electrical resistance

ZO-1 – Zonula-occludens-1

Acknowledgements

I would like to thank my supervisors, Dr. Karen Cheung and Dr. Cheryl Wellington for their dedication to collaborative research and their support throughout my program. I would also like to thank the members of my supervisory committee, Dr. Rizhi Wang and Dr. Sarah Hedtrich for providing feedback on my work throughout the duration of my program.

I would like to thank the University of British Columbia and the Canadian Institutes of Health Research for their financial contributions throughout my graduate program.

I would like to thank members of the Wellington lab and the Cheung lab for who I am extremely grateful to have met throughout my program, and for who I consider to be my dear friends. In the Wellington lab, I'd like to send my appreciation to Elyn Rowe, who acted as a role model for critical thinking and experimental rigor, Dr. Tara Caffrey, who had the patience to teach me many aspects of cell biology and experimental planning, Andrew Agbay for teaching me cell culture technique and answering many basic questions without hesitation or judgement, Dr. Jianjia Fan, who was always available to review my experiments and provide valuable feedback, Pantea Azadpur, for always providing moral support and a positive attitude, and Dr. Mehwish Anwer, with who I could always chat science. In the Cheung Lab, I'd like to extend my deepest appreciation to Tanya Bennet, who taught me many aspects of microfabrication and provided extensive support in the first year of my program, Jessica Hua and Avineet (Vinny) Randhawa who have always been there to troubleshoot with me during challenging times and providing moral support, Soroush Nasseri, who helped me on many occasions to troubleshoot technical difficulties, Eric Cheng, who was a valuable source for answering technical questions, Joseph Sadden, who

offered valuable suggestions during challenging times, and Dr. Samantha Grist, who provided valuable advice during confusing times.

Lastly, I'd like to send my deepest thanks to my family and friends, for their love and support throughout this journey.

Dedication

I’d like to dedicate my thesis to my family.

Chapter 1: Introduction

1.1 Motivation

In recent years, progress toward understanding human brain physiology and disease mechanisms has been advanced using animal models, and *in vitro* studies. The most common animal models are rodents, which are either studied as a whole animal or through use of primary cells harvested for *in vitro* studies. Mouse models are particularly appealing due to their low cost and the repertoire of genetically engineered strains for studying disease (2). While there are efforts to "humanize" mouse models to make them more relevant to study human disease, a major limitation is that rodents do not naturally develop some of the diseases seen in humans, and thus they are unable to recapitulate the complex series of events leading to pathologies such as Alzheimer's Disease (AD). The human and murine brain also differ considerably in the proportion of gray:white matter, regional organization and gene expression (3). The species-based limitations that accompany animal models have led to the widespread use of human-based *in vitro* models for exploring disease mechanisms and therapeutic development.

Human brain tissues can be modeled *in vitro* using organoids, where human induced pluripotent stem cells (iPSC) or embryonic cells are differentiated into neural cell types that mimic the brain physiology in a 3D structure (4). Neural organoids have become common tools for researching brain development and disease, with a focus on either localized regions or the complex interactions that occur between brain regions (5). Unfortunately, using organoids for late-stage disease modelling is limited by nutrient and oxygen diffusion into the 3D structure, and incorporating functional vasculature into organoids is an ongoing area of exploration (6). These limitations have influenced *in vitro* models to move towards a more controlled microenvironment such as brain-

on-chip (BoC) models, where brain cells can be patterned to resemble the brain architecture, and nutrients can be circulated throughout a microfluidic channel to mimic vascularization.

Transitioning from a relatively simple 2D monolayer culture - supported by widely available liquid handling and imaging systems - to a 3D microfluidic BoC model, will be more labor-intensive and costly. However, 3D models are capable of recapitulating important aspects of physiology, including physiological shear stress over endothelial cells – which is challenging to achieve with standard well plates or Transwells®, due to the large surface area of cell cultures - and the space for neuronal and astrocytic projections. Further, this development can be done with relatively common materials, as the ability to pattern complex structures using soft lithography enables microenvironments to be compatible with a flow system by incorporating channels and ports into elastomeric materials such as polydimethylsiloxane (PDMS) polymers (7).

Recent advances in the development of microfluidic BoC devices and biological research shed light on the importance of shear stress exerted on endothelial cells, substrate stiffness, and cell-to-cell contact for inducing the physiology that is observed *in vivo*. For example, BoC models have shown that shear stress exerted against brain microvascular endothelial cells (BMECs) plays a role in upregulating adherens and tight junction proteins (8), and modulating expression of blood-brain-barrier (BBB) markers such as claudin-5 and glucose transporter 1 (GLUT-1) (9). Several independent lines of evidence suggest that shear stress does not change BMEC morphology (10,11), but rather tightens the barrier; most often evaluated using trans-endothelial electrical resistance (TEER) and permeability assays (12). Additionally, recent 2D *in vitro* studies have demonstrated that substrate stiffness plays a role in BMEC tight junction integrity as well as

astrocyte and neuron morphology (13–15). Transwell® assays have also demonstrated the importance of cell-to-cell contact on BBB integrity, as several studies have shown that co-culture of BMEC with astrocytes and pericytes can improve TEER and permeability measures (16). Furthermore, *in vitro* models can be further established by including disease pathology into the microenvironment. For instance, to mimic AD, the model could include iPSC cells from AD patients, or a healthy BBB microenvironment could be spiked with recombinant proteins such as amyloid-beta (Aβ), to generate an *in vitro* model of AD.

1.2 In vitro models as a tool for studying Alzheimer's Disease

Studying diseases that are associated with the brain vasculature is a promising application for *in vitro* models since they can be modified with the contextual cues that accompany the diseased microenvironment. As AD is the leading form of dementia worldwide (17), and there is currently no cure, investigations using *in vitro* models could serve as tool for furthering the advancements of AD therapeutics. There have been limited therapeutic advances in the clearance of Aβ [one of the major neuropathological hallmarks of AD], and there is ongoing research to understand the mechanisms that underlie the vascular contributions to AD, which will hopefully lead to preventative treatment options. The strongest genetic risk factor, apolipoprotein (APOE), has detrimental effects when it contains the allele E4. APOE4, which is secreted in the brain by pericytes, astrocytes, neurons and microglia, is known to increase Aβ deposition in the vasculature, increase BBB breakdown and reduce vascular compliance (18).

1.3 Peripheral contributions to AD

There is also a second source of APOE, that is produced by peripheral macrophages and hepatocytes. The BBB prevents the peripheral and brain APOE from mixing, and the peripheral APOE is circulated on several lipoprotein subclasses including high-density lipoproteins (HDL) (19). As HDL is highly associated with protection from cardiovascular disease, which is also a major risk factor for AD, it has many properties that may be beneficial to the cerebrovascular, including reducing endothelial inflammation, promoting endothelial nitric oxide production and maintaining vascular elasticity (20). Additionally, APOA-1, the major HDL apolipoprotein, has been shown to reduce soluble brain Aβ40 and Aβ42 *in vivo* (21). These factors provided the groundwork for an *in vitro* human arteriole model to be developed, where HDL was circulated and was shown to promote clearance of Aβ through the reduction of collagen-I binding (22). This leads to the research question "will HDL promote Aβ clearance across a capillary vessel"?

1.4 Blood-brain barrier physiology

In this work, the functional unit of the BBB is considered to be a tri-culture of BMECs with pericytes and astrocytes, since these supporting cells are critical in maintaining the highly selective barrier *in vivo*, through many mechanisms (reviewed in (23)). Additionally, the neurovascular unit (NVU) is termed as a model consisting of BMEC, pericytes, astrocytes, and neurons. In the sub-sections below, the cell types associated with the BBB and the microenvironment are described, with a focus on the capillary. Furthermore, an overview of the different types of BoC are discussed, and their respective advances.

1.4.1 Endothelial cells

Brain endothelial cells line the inner walls of the cerebrovasculature and establish the highly selective barrier for entry into the brain. Single cell transcriptomics has demonstrated that these cells have a gradual phenotypic change along the transition from artery to capillary to vein (24), but most BoC models aim to recapitulate the capillary. Microfluidic chips, consisting of micro and nano scale geometries, often aim to recapitulate a capillary vessel since they are the primary region for nutrient and oxygen exchange within the brain, spanning ~400 miles (25); therefore, BMECs will be the focus of this section. When selecting BMECs for use in a BoC, they should express key markers seen *in vivo,* including endothelial cell-specific markers (platelet endothelial cell adhesion molecule-1 (PECAM-1), vascular endothelial (VE)-cadherin), tight-junction markers (claudin-5, occludin, ZO-1), and key transporters (GLUT1, P-glycoprotein, low density lipoprotein receptor-related protein 1 (LRP1) and major facilitator superfamily domain-containing protein 2a (MFSD2A)), in addition to their ability to form a confluent monolayer with a tight barrier.

1.4.2 Pericytes

Pericytes are mural cells embedded in the basement membrane of microvasculature. The cerebrovascular has significantly higher pericyte coverage than peripheral vessels (26,27), which underscores their functional importance in the brain. Over the last decade, pericytes have gained considerable attention for their critical role in maintaining BBB integrity (26,28), as it has also been shown that increases in BBB permeability with aging can be traced to pericyte loss (29). *In vivo*, pericytes guide astrocytic end feet and mediate their polarization (30), as well as induce specific transporter (Mfsd2a) expression in BMECs to promote a selective barrier phenotype (31). The reinforcing effect of pericytes on *in vitro* BBB integrity has also been observed by many

groups with various cell sources (32–35). The interaction between pericytes and BMEC is likely very complex, as Yamazaki *et al.* recently showed that pericyte genotypes can influence BMEC barrier integrity by altering their secreted ECM (36). These lines of evidence showcase the critical interaction among pericytes, astrocytes, and endothelial cells in the BBB. In addition to their roles in preserving a functional BBB, pericytes regulate cerebral blood flow and capillary diameter (37–39) and are involved in the immune response (40,41) among other functions (reviewed in (42)). Importantly, the contribution of pericyte dysfunction to the neuropathological features of stroke and AD is being increasingly recognized (43). Therefore, a BoC model without pericytes will limit insights into physiological and pathological functionality of the BBB, and effectively, the NVU.

1.4.3 Astrocytes

Astrocytes - named after their star-shaped morphology - are the most abundant cell type in the brain. They play many critical functional roles, including reinforcement of the BBB (44,45), regulating cerebral blood flow (46,47), responding to inflammation (41), (48), (49) maintaining molecular homeostasis through regulating ion and pH balance, (47), (50), and supporting neurons by facilitating synaptic stability and plasticity (51,52). Astrocytes extend their endfeet to contact and ensheath cerebral vessels (53) and have classically been considered an essential component to the physical barrier of the BBB. However, a recent mouse study that removed endfeet from cerebral vessels using a laser found that the vessels did not become more permeable (54), suggesting that it is their effect over time on endothelial cells - likely through secreted factors that could be soluble or components of ECM (55), (56) - that reinforce the BBB. *In vitro,* astrocyte contact or non-contact co-culture with BMECs from various origins has been shown to increase

tight and adherens junction gene expression and global permeability measures (57), (58–62) further illustrating that astrocyte cross-talk with endothelial cells is critical for BBB physiology.

To validate the astrocyte identity, the most common marker is glial fibrillary acidic protein (GFAP), which is the major intermediate filament protein in astrocytes that is upregulated when they are in a reactive state. However, GFAP is not expressed in all mature human astrocytes (63,64), therefore a panel of additional astrocyte markers including S100-beta, and N-myc downstream regulated gene 2 (NDRG2) (65,66) is recommended to confirm astrocyte identity prior to use.

1.5 Basement membrane

The cerebrovascular basement membrane (BM) is a specialized ECM secreted from endothelial cells, astrocytes, and pericytes that serves as a barrier between the endothelium and the brain parenchyma. At the level of the capillary, the ECM from each individual cell type is indistinguishable, while at other points along the vasculature (i.e. artery, post-capillary venule), there is more of a separation between endothelial and astrocytic ECM, either by layers of smooth muscle cells, or the perivascular space. Five key proteins make up the cerebrovascular BM: collagen-IV, laminins, nidogens, heparan sulfate proteoglycans (HSPGs), and fibronectin, but there are several other glycoproteins and soluble factors including growth factors, embedded within (reviewed in (67,68)). Importantly, laminin has three variable chains - making 16 possible isoforms - but only five have been detected in the cerebrovascular BM: laminin-111, -211, -411, -511, and 421 (66,69,70). In most cerebrovascular vessels, the endothelial BM consists of laminin -411 and -511 whereas, in the arterial endothelial BM, laminin-511 is predominantly expressed (71). Self-assembly of the BM begins with the laminins forming a sheet, followed by the binding

of nidogens and HSPGs, and then the binding of a collagen-IV network to the nidogens in order to stabilize the overall structure (72,73). To our knowledge, there is no consensus on the optimal ECM for use with primary BMEC. In a 2013 study, primary HBMECs in monoculture did not have a significantly higher TEER when cultured on a collagen-IV/fibronectin (80 μg/cm^2, 20 μg/cm^2) or Matrigel® (80μg/cm^2) coating compared to collagen-I (10 μg/cm^2) (74). Recently, a more comprehensive analysis on culture conditions of HBMEC has been done by Gray *et al.* who have explored stiffness, coatings, and additional media supplements to optimize mature tight junction expression. They tested a series of coatings, including: collagen-I (100 μg/mL), fibronectin (100 μg/mL), collagen-IV (100 μg/mL), laminin (2 μg/cm^2), and 0.4% thiol-modified hyaluron: 0.4% thiol-modified gelatin, with some combinations of the mentioned coatings, and they quantified tight junction phenotype (continuous, punctate, or perpendicular) (75). They found that the fibronectin coating marginally induced the greatest mature tight junction coverage compared to the other coatings, which is aligned with previous studies using porcine BMECs that demonstrated the importance of fibronectin, collagen-IV and laminin for *in vitro* barrier formation (76,77).

1.6 Nutrient supply

The NVU utilizes passive diffusion as well as selective and active transport to provide cells with the molecules (O_2), nutrients, ions and macromolecules (i.e. glucose) essential for neural function (78). Replicating the transport of these components across the microvasculature is important and can be accomplished through microfluidic platforms. The flow within these platforms is laminar (diffusion limited) and often controlled by pump based systems mimicking the passive diffusion of hydrophobic molecules across the brain endothelium (79). These systems also provide the

opportunity to replicate the microvascular wall shear stress present in the brain vasculature. The shear stress experienced *in vivo* is known to increase endothelial gene expression and barrier function (10,80); therefore, replication is important to create a BBB that restricts the diffusion of large hydrophilic molecules and solutes in the circulating blood from non selectively crossing into the cerebrospinal fluid.

1.7 Shear stress

The major initial considerations for BoC modeling include determining the region of interest within the brain and the corresponding vascular shear stress in that region. In the vascular network, the pulsatile flow that is seen in arteries, and that is driven by the cardiac cycle, is dampened by the cerebral arterial compliance and the cerebrovascular resistance, leading to steady blood flow in the capillaries and a mean wall shear stress of 1-6 dyne/cm^2 (81,82). The location of interest within the vascular network influences the BoC geometry, and the pump specifications (syringe or peristaltic) needed to incorporate flow into the system. To decide on flow rate and BoC dimensions, the appropriate shear stress equation should be used. For instance, for a rigid, uniform, cylindrical vessel, with laminar flow and incompressible, Newtonian fluid, the shear stress ($\boldsymbol{\tau}$) at the vessel wall can be derived from Poisseuille's law to become: $\boldsymbol{\tau} = 4Q*\boldsymbol{\eta}/\boldsymbol{\pi}*r^3$ (1). Where Q is the flow rate, $\boldsymbol{\eta}$ is the viscosity, and r is the radius of the vessel (Figure 1).

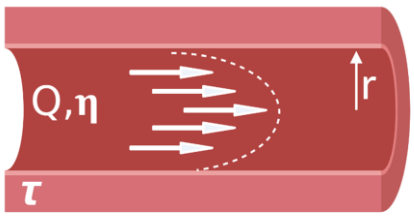

Figure 1: Parabolic shear stress profile in a blood vessel.

For example, to achieve a capillary-like shear stress of 1 dyne/cm^2 (83) and using sacrificial molding techniques to form a lumen with a radius of 100 μm, and standard cell media composition, Dulbecco's Modified Eagle Medium (DMEM) supplemented with 10% fetal bovine serum (FBS), which has a viscosity of ~0.93 mPa*s (84), then an approximate flow rate of 304 μL/hr would be required.

1.8 Previous BoC *in vitro* models

1.8.1 Fabrication techniques for *in vitro* models

During the prototyping stage, microfluidic chips are often fabricated using PDMS. PDMS is a transparent, biocompatible, oxygen-permeable polymer that can be easily molded into high resolution geometries (7). Creating a negative mold pattern is often performed using photolithography with a UV-sensitive material; patterning the silicon wafer with high resolution features in the micron range (85). More recently, lower cost, 3D printed molds have been used to fabricate geometries in the range of hundreds of microns (86).

1.8.2 2-dimensional models

Planar cell layers (2D) (Figure 2) are amenable to simple fabrication processes and are the easiest transition from a static 2D model. The design of a 2D microfluidic BoC typically includes two compartments, separated by a permeable membrane permitting cell-cell interaction, where at least one compartment acts as a flow channel to mimic vascular blood flow (12,87). Commonly used membrane materials include polycarbonate (PC), polyester (PET) and PDMS. In previous 2D BoC microfluidic models, PET and PC membranes were cut out of Transwell® inserts to use in microfluidic BoC (88). More recently, commercially available track-etched PET and PC A4 sheets

have been used (89) (90). To bond porous membranes to PDMS to obtain a leak-free channel, spin-coating PDMS (91), aminosilanization (92), or custom bonding procedures (93) may need to be performed. Furthermore, porous membranes such as PDMS will need further treatment to achieve the hydrophilicity required for adherence of ECM coatings (94). The pore size and thickness of the porous membrane should be selected based on the application, as contact of astrocytes and pericytes with the endothelial cell monolayer will influence BBB function (95), thus larger pore sizes (~3μm) should be considered to enable contact and increase fidelity to the native BBB anatomy. Commercially available microfluidic chip options such as the Human Emulation System® use a PDMS chip with 7.0 μm pore size in the membrane separating the channels (96). Another important consideration in a 2D model is the ECM coating used on the membrane to mimic the microenvironment of the human brain basement membrane. Recent studies have explored the effect of ECM composition on endothelial cell tight junction properties (97), as well as permeability in Transwell® inserts (98). However, there are limited investigations into ECM coatings appropriate for co-culture and tri-cultures in 2D environments that incorporate flow. Further exploration into ECM coatings used for BBB models will strengthen the robustness of 2D BoC models and potentially provide reliable environments to establish *in-vivo*-like cellular functions and gene expression.

1.8.3 2.5-dimensional models

In this thesis the term 2.5D model (Figure 2) is used to describe endothelial cells forming a flat 2D monolayer around a rectangular channel that contains a 3D matrix (99). 2.5D models are often used to recapitulate the architecture of the brain parenchyma by using a parallel channel design containing a hydrogel in one channel and flow across endothelial cells in the other channel. This

design uses pillars to create distinctions between channels, so that a hydrogel can be flowed into the channel and cured using thermal gelation, photocrosslinking or chemical crosslinking methods. A 2.5D design allows brain cells to migrate towards the endothelium through a hydrogel to provide direct cell-to-cell contact as an artificial membrane is not required (32). Having a planar 2.5D model will also improve imaging, since the media supply is parallel to the cells, compared to underneath and on top of the cells in 2D BoC models, which increases the working distance from the microscope focal point and may require imaging through additional layers of PDMS. Adriani *et al.* used a 2.5D model to embed primary rat astrocytes, and neurons in a collagen-I hydrogel using microscale trapezoidal PDMS structures that acted as phase-guides to create a hydrogel network along their flow channel (100). The commercially-available Mimetas Organoplate® platform also enables astrocytes and pericytes to be embedded into a collagen-I hydrogel, and endothelial cells to be seeded adjacent to the gel, and bi-directional flow is achieved using a rocking plate (101). Yoojin *et al.* developed a microfluidic chip with five parallel channels to study BBB dysfunction in AD (102). The use of collagen-I as a hydrogel has been largely investigated based on its structural integrity when gelled at a high concentration (>4 mg/mL). However, collagen-I is not found in the brain microvascular ECM, therefore, there is a need for a hydrogel that can maintain its form while in a gelled state. Some 2.5D models have used a fibrin-based gel that was able to support angiogenic behaviour (103), with and without interstitial flow (104). Moving away from collagen-I based 2.5D models will enable a more physiologically-relevant brain compartment, where further insight can be gained into the functionality of neurons, mural cells, and glia.

1.8.4 3-dimensional models

A 3D BoC (Figure 2) consists of a 3D matrix completely surrounding a perfusable circular cross-section of the endothelial cell layer. Several methods can be used to develop BoC with a circular cross section, including using a needle as a sacrificial mold within a hydrogel (41), (32,105–108) and using gravity-driven pressure to displace the hydrogel, also known as viscous fingering (109). Notably, there are recent 3D BoC models that contain immortalized or primary endothelial cells (41,105,107–111), pericytes (41,107,109) and astrocytes (41,105,108–110), and some progress is being made in including iPSC-derived cells in 3D BoC devices (106,112).

One of the major challenges with creating 3D BoC is the ability to select a hydrogel that is sufficiently mechanically stable to withstand perfusion while also providing a physiologically relevant ECM for cell growth. As in 2.5D systems, collagen-I is also commonly used as an ECM that encapsulates either astrocytes or pericytes in a 3D BoC architecture (41,109,110,113). Recent advancement by Seo *et al.* demonstrated growth of a mixed population of NVU-composing cells, such as pericytes, astrocytes, microglia, oligodendrocytes, neurons and neural stem cells into a collagen matrix that was then seeded with hCMEC/D3s and perfused the lumen for 5 days (114). A mixed matrix of collagen-I, Matrigel® and hyaluronic acid that supports astrocyte growth in 3D and endothelial cell growth on the inner lumen has also been developed (105,108). Studies on mechanically stable hydrogels other than collagen-I that can support brain cells are of high interest. For instance, human umbilical vein endothelial cells (HUVECs) and brain pericytes were successfully cultured in a fibrinogen matrix that could withstand perfusion for up to 7 days (107).

To identify viable options for hydrogel-based ECM for BoC devices that are suitable to represent the NVU, knowledge gained from other *in vitro* modeling fields should be considered when developing BoC models. For example, there have been advances in angiogenic brain models that use biocompatible hydrogels to culture combinations of iPSC-derived endothelial cells, astrocytes, pericytes, microglia, and neurons in 3D (115,116). In addition, Arulmoli *et al.* have demonstrated mechanical compatibility and biocompatibility of a salmon fibrin/hyaluronic acid/laminin hydrogel that could support iPSC-derived neurons and was in the brain stiffness range (117). Furthermore, O'Grady *et al*. developed a gelatin-based, N-cadherin hydrogel that supported significant outgrowth for cultured neurons compared to conventional biomaterials such as Matrigel®, and had the mechanical stability to form a lumen (118). Geoffrey *et al.* have recently reported the mechanical properties of hydrogels used in NVU development (119), which will allow investigators to understand the mechanical characteristics of hydrogels before developing 3D BBB models.

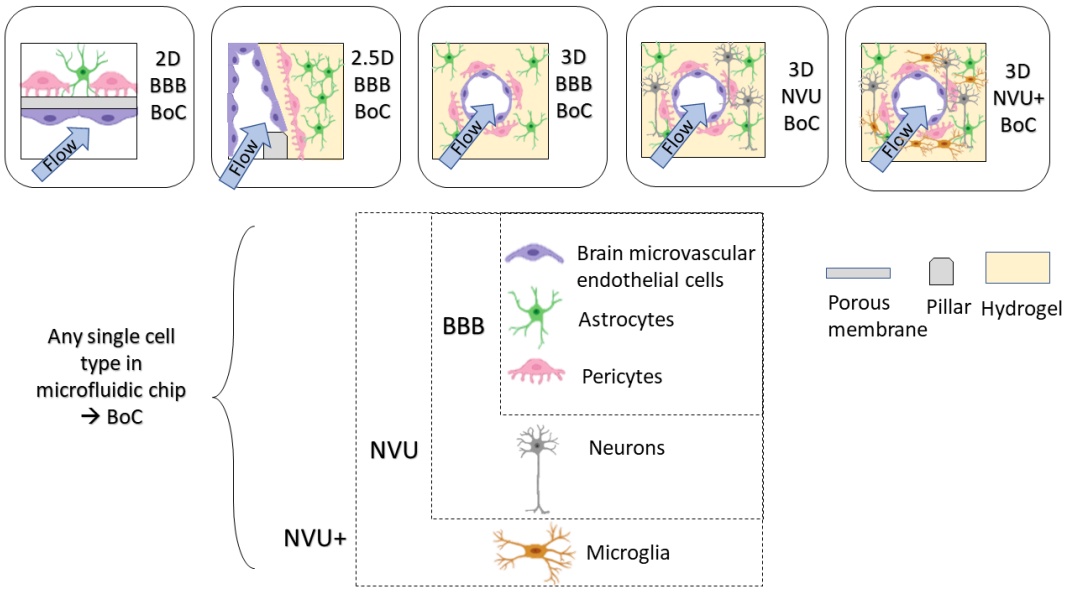

Figure 2: Schematic of the selected terminology to represent 2D, 2.5D, 3D BBB and NVU *in vitro* models. The 2D BBB consists of a planar membrane, the 2.5D BBB contains a hydrogel separated by a pillar, the 3D BBB, NVU and NVU+ models have a circular geometry.

1.9 Thesis Objectives

The main objective of this thesis is to demonstrate the steps taken to develop a microfluidic chip that is applicable for studying AD pathology. The model should reflect a healthy vasculature, and permit the inclusion of AD pathological hallmarks, such as amyloid plaques, and allow for the circulation of potential therapeutic factors, such as HDL. In addition, this thesis describes improvements to a previously used tissue chamber that was used for studying AD pathology. Overall, this thesis highlights the steps taken to establish *in vitro* vascular models for applications in AD.

1.10 Thesis Organization

The structure of this thesis follows the timeline of the experiments performed. This thesis starts with the conceptualization of a 3D hydrogel-based microfluidic chip that is explored to identify its compatibility with astrocytes and endothelial cells. Then, it leads into a second design that removes the complexity of a hydrogel and focuses on improving the robustness of the fabrication process of the physical microfluidic chip, as well as preliminary efforts to develop an endothelial cell monolayer. Lastly, tissue chamber improvements are presented that reveal the importance of stability with *in vitro* models, as well as the challenges and considerations that are associated with material selection for brain vasculature systems. Finally, a conclusion is presented that summarizes the key findings, as well as future directions for each model.

Chapter 2: 3D BBB chip model development

2.1 Introduction

To establish a microenvironment that mimics an *in vivo* capillary, a 3D vascular model was conceptualized. The requirements for this model were that the model mimic capillary anatomy with a circular geometry surrounded by ECs, with a fluid exerting a shear stress between 1-6 dyne/cm^2 (82) and an ECM with stiffness of 1-3 kPa (120). Additionally, the model should include direct cell-to-cell contact with astrocytes, pericytes and neurons. Ideally, this model would include all iPSC-derived cells that are genetically consistent, for example, either APOE 3/3 or APOE 4/4 to study apoE isoform effects on vascular physiology. The model should be oxygen permeable to allow proper gas exchange and be made of transparent material to enable continuous live cell monitoring. This model should also include in-line sampling of both the blood and brain side of the BBB to allow for quantitative measurements via ELISAs.

2.2 Methods

A PDMS-based microfluidic chip was designed that would permit all the requirements listed above to be met. This chip (Figure 3) includes two channels that have a 1 mm x 1 mm cross section separated by a porous 0.4 μm PET Transwell® membrane (Corning, cat. no. 3450). The top channel is meant for media exchange to support the brain cells (astrocytes, pericytes, neurons) within the device. The bottom channel contains a gelatin-methacrylate (GelMA) hydrogel that provides a structure for supporting brain cells within the hydrogel and blood cells on the surface of a hollow lumen within the hydrogel. This lumen is then perfused with media to provide the shear stress needed to encourage endothelial cell gene expression.

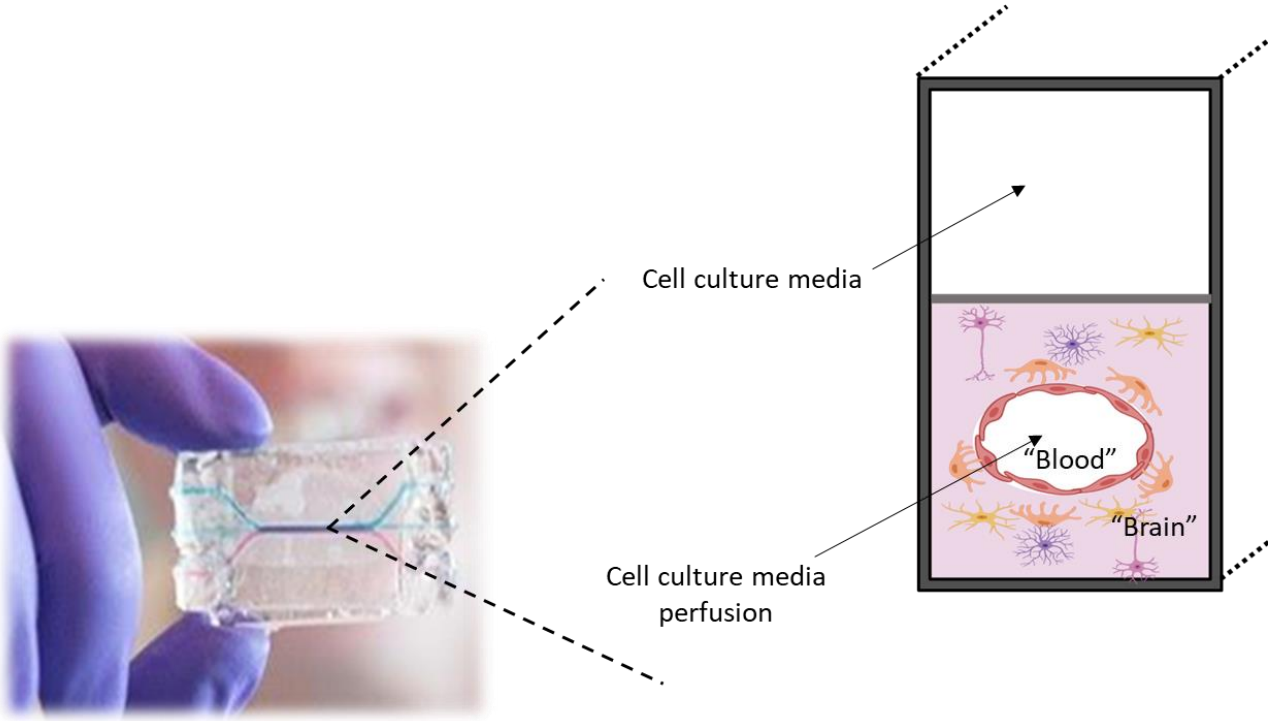

Figure 3: 3D BBB chip physical representation (left) and conceptualized design (right).

2.2.1 Microfluidic chip fabrication

Negative molds were designed using computer-aided design (CAD) software (Solidworks 2020, CMC Microsystems). Then, the parts were exported to STL format for uploading onto the PreForm software (Version 3.12.2, FormLabs). A proprietary clear resin (FormLabs, cat. no. RS-F2-GPCL-04) and a selected printing resolution of 25 µm were used. The parts were oriented on the build platform with a 45º angle and with as little supports on the feature side of the print as possible. Once printed, the parts were removed from the build platform and post-processed as per the manufacturer's recommendations. Briefly, the parts were added to an initial isopropyl alcohol (IPA) bath for 5-10 minutes, then transferred to a second IPA bath for another 5 minutes. The parts were left to dry overnight in a fume hood and UV-cured on both sides for 30 minutes at 60ºC (FormCure, Formlabs, cat. no. FH-CU-01). Two 22G (McMaster-Carr) needles and a 25G needle

(McMaster-Carr) were inserted into the mold to provide an inlet and outlet for the bottom and top channels, and to serve as a guide for the lumen formation (Figure 4). Then, a 10:1 mixture of PDMS and a crosslinking agent (Dow Sylgard® 184 Silicon Elastomer) was mixed in a THINKY MIXER at 2100 RPM (Thinky, cat. no. ARE 310) for 2 minutes. The PDMS mixture was added to the molds and put into a desiccator for 30 minutes before transferring the molds to cure in a 50ºC oven for at least 4 hours. Then, the PDMS layers were removed from the molds using an exacto-knife and the dust was removed using Scotch™ tape and compressed air. Then, the molds were placed on a taped glass slide and the PET membrane was removed from the Transwell® insert and cut in half. Using tweezers, the membrane was carefully set into position to cover the channel. The two layers of PDMS were oxygen plasma treated (Harrick plasma cleaner) at <600 mTorr for 1 minute before manually aligning the channels and compressing the PDMS layers together for approximately 30 seconds. The plasma bonded PDMS layers were then transferred to a 65ºC oven for at least 2 hours to complete the bonding procedure.

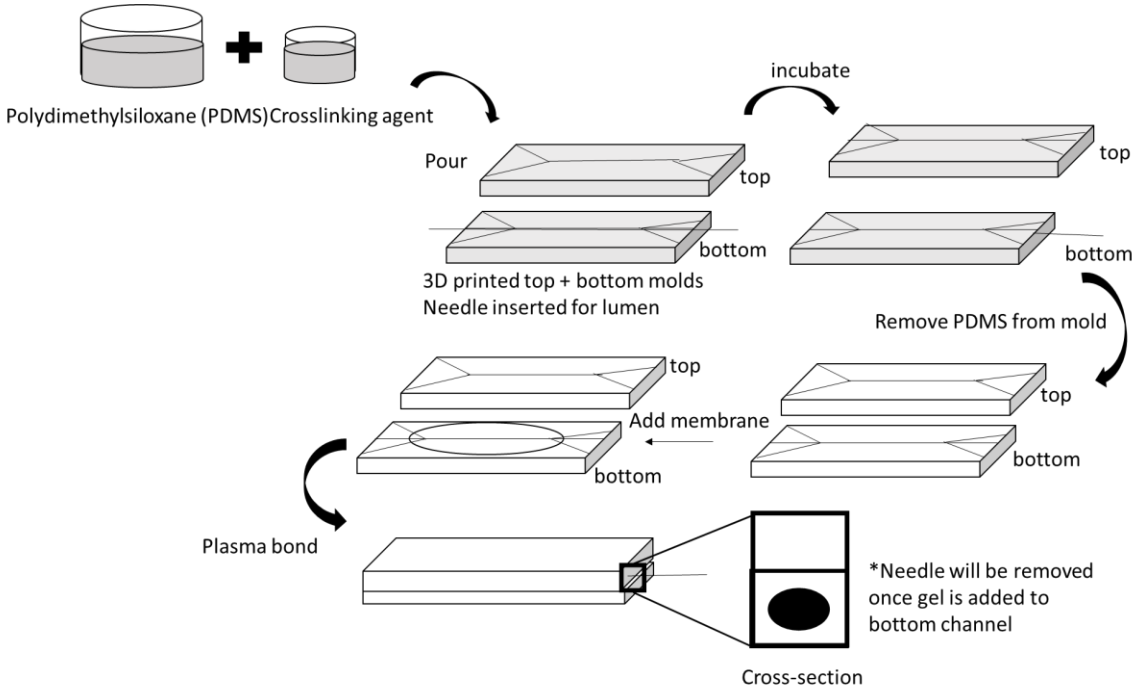

Figure 4: A simplified schematic of the chip fabrication procedure for creating a PDMS chip that contains a sacrificial needle guide for forming a lumen.

2.2.2 Hydrogel formation

GelMA (Cellink, cat. no. VL3501020510) was made as per the manufacturer's recommendations. Briefly, 12% w/v methacylated gelatin in astrocyte culture medium was combined and stirred on a hot plate for 30 minutes at 45ºC. Then, 1.2% v/v Lithium phenyl-2,4,6-trimethylbenzoylphosphinate (LAP) was combined with astrocyte medium and sterile filtered before combining with the GelMA. The mixture was stirred on the hot plate for 15 minutes at 70ºC. The prepared hydrogel was then transferred to a falcon tube and wrapped in aluminum foil for storage at 4ºC. To create 6% w/v GelMA, the solution was diluted with the same media as used in the initial batch. Additionally, the second hydrogel, Matrigel™ Basement Membrane Matrix (Corning, cat. no. C354234), was handled on ice and either used as provided by the

manufacturer recommendations or was transferred to the 12% GelMA solution to make the third hydrogel. This method was previously developed by Bennet *et al.* (1). Briefly, the solution was put into an ultrasonic cleaner (Branson, model 2100) at 40 kHz and 37ºC for 45 minutes for allow for dispersion of the Matrigel™ within the GelMA. Finally, the GelMA containing Matrigel™ hydrogel was stored at 4ºC until ready to use (later referred to as 12% w/v GelMA: Matrigel™).

2.2.3 Cell culture

In well plate: Performing experiments in a well plate prior to moving to the microfluidic chip allows for experimental variables to be narrowed down before moving to in-chip experiments. In this preliminary experiment (Figure 5), the goal was to identify one hydrogel to test within the chip.

Tandem dimer tomato (tdTomato) – labelled astrocytes (source: Julia TCW, clone number: TCW2E33-2E3-4 Ast) (121,122) were cultured with astrocyte medium (ScienCell, cat. no. 1801) in a plastic clear, 96-well plate in different hydrogel conditions to identify a single hydrogel to use in chip. Astrocytes were suspended at a density of 0.01 million cells/mL into the three previously described hydrogels (section 2.2.2). The astrocytes were cultured for 4 days with media exchanges every second day.

Human brain microvascular endothelial cells (HBMECs) (Lonza, lot no. 376.01.03.01.2F), between passage 6-10 and human umbilical vein endothelial cells (HUVECs) (isolated in house from umbilical cords from Children's hospital, line PM 321), and iPSC brain microvascular endothelial cells (iBMECs) (IPSC line: Haakon Nygaard ISOAPP, cultured using a previously

published protocol (123)), were seeded into a 96-well plate on top of 6% w/v GelMA with 0.6 v/v % LAP with or without a 0.4 mg/ml collagen IV (Sigma, cat. no. c5533) and 0.1 mg/ml fibronectin (Sigma, cat. no. F1141) at a seeding density of 10,000 cells/well. HBMECs and HUVECs were cultured with endothelial cell growth media (EGM-2) (Lonza, cat. no. CC-3162) with 2% v/v fetal bovine serum (FBS) with and without 10 mM Y27632 rock-inhibitor. IBMECs were cultured with human Endothelial Serum Free media (hESFM) (Fisher Scientific, cat. no. 50-104-8418) with 200x B27 supplement (ThermoFisher, cat. no. 17504-044) with and without 10 mM Y27632 rock-inhibitor. Media exchanges were performed every second day. A LIVE/DEAD™ viability assay kit (ThermoFisher Scientific, cat. no. L-3224) was used as per the manufacturers' recommendations to examine the viability of the endothelial cells on day 6.

In chip: IPSC astrocytes expressing tdTomato (source: Julia TCW, clone number: TCW2E33-2E3-4 Ast) were used to visualize cells throughout the experiment. Astrocytes were resuspended at 3 million cells/mL into the 6% w/v GelMA hydrogel and loaded into a 1 mL syringe and inserted into the chip inlet tubing. The chip was put under a UV light with a wavelength of 365 nm and an intensity of 10-20 mW/cm^2 for 30 seconds on both sides to ensure crosslinking of the GelMA. Once the GelMA was crosslinked, a sacrificial 200 μm acupuncture needle (TeWa, cat. no. CJ 2050) was manually removed and the ports were closed off with 25G needles (Mcmaster-carr). The cells were cultured with a flow of 60 μl/hr through the top channel of the chip for 6 days.

2.2.4 Imaging

The 96-well plate and chips were imaged using an inverted brightfield and epi-fluorescence microscope (Nikon TE-2000-U) with an exposure rate of 250 ms.

2.3 Results

The main objective of the well plate experiment was to identify a hydrogel choice that would be suitable for use within the chip. Unfortunately, Matrigel™ on its own does not have the mechanical characteristics (modulus of elasticity ~400 Pa (124)) to hold a lumen shape, as demonstrated by O'Grady *et al.* (supplemental information, Figure S1) (118); therefore, the main objective was to determine whether 6% w/v GelMA or 12% w/v GelMA: Matrigel™ were suitable for use within the microfluidic chip. Matrigel™ was originally used as a positive control since it is widely used in central nervous system applications. The goal was to identify which of the two hydrogels resulted in astrocyte end-feet projections like that seen in the Matrigel™ condition. It was observed that astrocytes cultured for 6 days in a 6% w/v GelMA condition had more resemblance to astrocyte projections occurring compared to a 12% w/v GelMA:Matrigel™ condition (Figure 5). The lack of astrocyte projections seen in the 12% w/v GelMA:Matrigel™ identified the condition as an unfavorable hydrogel for culturing astrocytes.

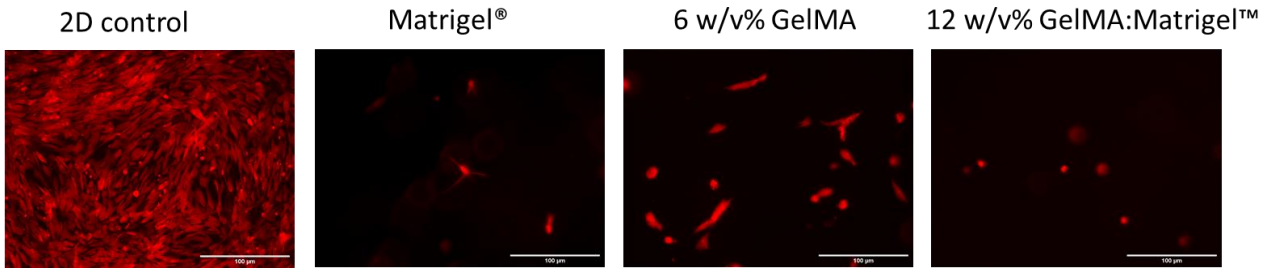

Figure 5: Epi-fluorescent images of astrocytes expressing tdTomato are shown in 2D, suspended in Matrigel™, 6% w/v GelMA, 12% w/v GelMA:Matrigel™. Scale bar is 100 µm.

The 6% w/v GelMA was then selected to be used within the chip. To identify if the 6% w/v GelMA was suitable for using within the chip. The mechanical stability of the selected concentration was then investigated to see if it allowed for a lumen to be formed. In Figure 6, I demonstrate the ability to create a lumen by removing a sacrificial needle after UV crosslinking the 6% w/v GelMA for 1 minute.

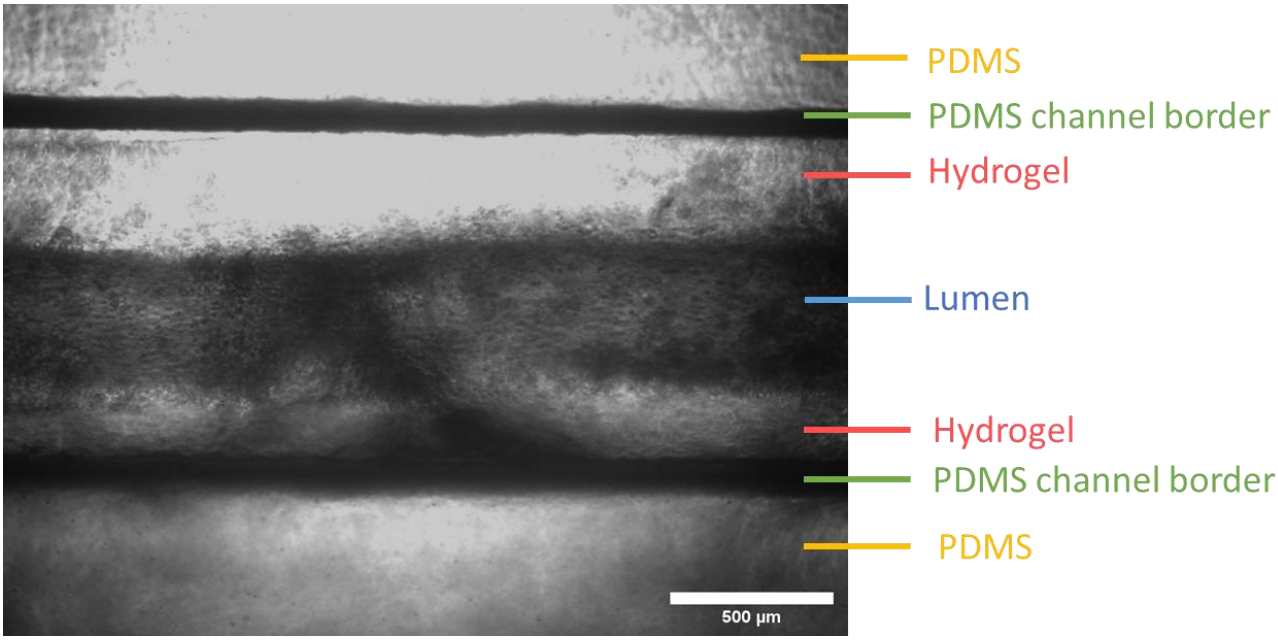

Figure 6: Representative image of the lumen formation in the hydrogel. Image taken with brightfield fluorescence. Scale bar 500 µm.

Then, to investigate if the chip provided a favorable environment for astrocyte growth, the tdTomato astrocytes were seeded into the chip. The goals of the experiment were as follows: i) to determine if the cells can be visualized within the chip, ii) to determine if the cells remain in the gel while applying a flow of 60 µl/hr through the top channel iii) and to determine if the

astrocyte projections are equal or more prominent while in a flow-based environment. In Figure 7, astrocytes are present in the chips, and they are visualized at three regions of interest (ROI) using epi-fluorescence.

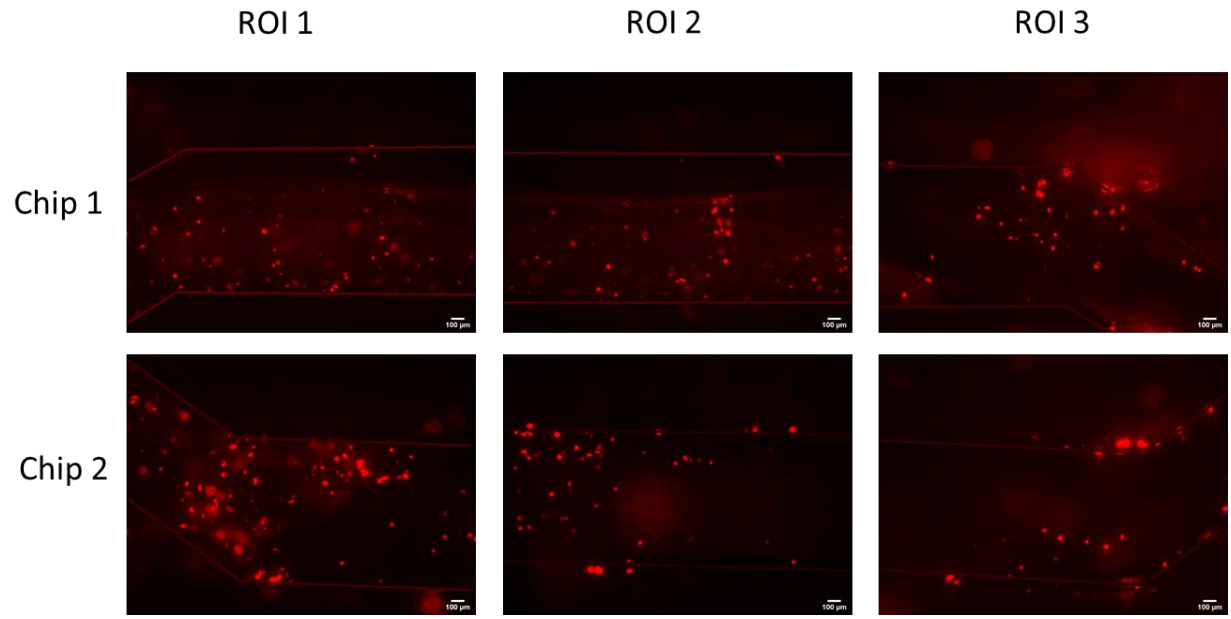

Figure 7: Epi-fluorescent images of astrocytes expressing tdTomato seeded into 6% w/v GelMA. Red lines outline the borders of the channel. Scale bar is 100 µm. Images are taken at three regions of interest (ROI).

The outcome of this experiment identified that i) it was possible to visualize the astrocytes while they are in the chip, ii) the astrocytes remained in the hydrogel after being exposed to a flow of 60 µl/hr for 6 days, and iii) the astrocytes did not have a healthy morphology, as evidenced by the lack of astrocyte end-feet projections. These findings suggest 6% w/v GelMA has potential to become a suitable base material for performing 3D hydrogel-based BoC experiments; although to provide a microenvironment that is optimal for astrocyte health, the hydrogel components will

need to be further optimized. Future experiments should confirm that astrocytes in 6% w/v GelMA should not be inflamed compared to astrocytes grown under standard 2D conditions.

In addition, the compatibility of 6% w/v GelMA with different endothelial cell sources was investigated. This step was required to move forward with a co-culture containing astrocytes suspended in GelMA and endothelial cells lining the lumen. HBMECs, HUVECs and iBMECs were seeded on top of 6% w/v GelMA in a 96-well plate and the growth of the endothelial cells was investigated. For the experimental outcome to be considered a success, the endothelial cells would need to adhere to the 6% w/v GelMA and they would need to proliferate and have the majority of the cells be alive after 6 days in culture. Four experimental runs were performed, and for the first and second experimental run, the endothelial cells were seeded on the 6% w/v GelMA without a coating and no additional components added to the culture media (EGM-2, 2% FBS). After observing limited success of the attachment and growth of the HUVECs, HBMECs and iBMECs, rock-inhibitor was added to the media for the first 48 hours during the experiment to promote adhesion, proliferation and prevent apoptosis (125). Additionally, to further promote endothelial cell attachment, a single coating condition (0.4 mg/ml collagen IV, 0.1 mg/ml fibronectin) was tested. The conditions were imaged using brightfield or epifluorescence and their outcome was noted (Figure 8). A red color was given to the sample well if the cells did not attach to the 6% w/v GelMA, or if the majority of the cells were deemed dead via the LIVE/DEAD™ assay, a half green - half red color was given if there were both alive and dead cells within the well, and a green color was given to the successful samples, which indicates that the majority of the cells adhered, proliferated and remained alive at the end of the 6 day timepoint. Further representative images are shown in Appendix A.

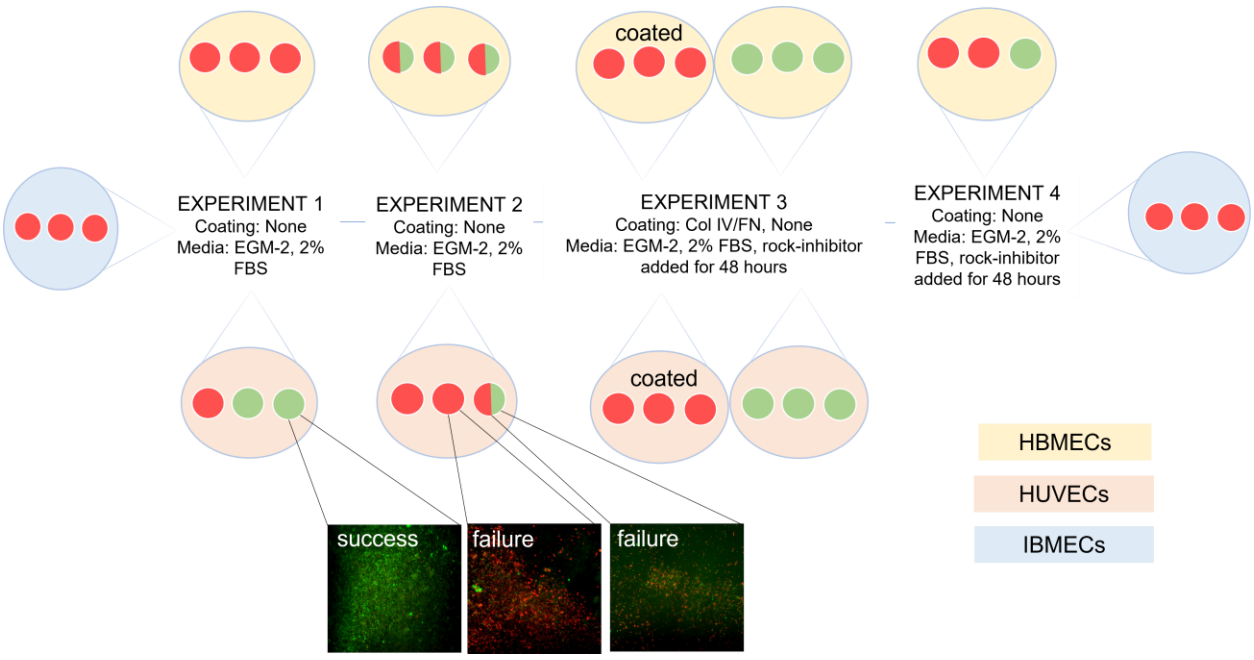

Figure 8: Experimental outcomes of endothelial cells seeded on 6% w/v GelMA. A red color was given to the sample well if the HUVECs, HBMECs or iBMECs did not attach to the GelMA, or if the majority of the cells were deemed dead via the LIVE/DEAD™ assay, a half green - half red color was given if there were both alive and dead cells within the well, and a green color was given to the successful samples, which indicates that the majority of the cells adhered, proliferated and remained alive at the end of the 6 day timepoint

Overall, there was a low success rate of the HBMECs (4/15 wells), HUVECs (5/12 wells), and iBMECs (0/6 wells) when seeded on 6% w/v GelMA (Table 1).

Table 1: Success rate of experiments performed with HUVECs and HBMECs seeded on 6% w/v GelMA.

Success	HBMEC	HUVEC	iBMECs
Rate (# of wells)	4/15	5/12	0/6

The outcomes of the experiments presented above indicate that 6% w/v GelMA has some potential to become a suitable material for providing the mechanical stability needed for forming a lumen; although, its compatibility with iPSC astrocytes, HUVECs, HBMECs, and iBMECs is not sufficient. These findings have shown that more optimization of the extracellular matrix composition is needed before a functional BBB can be formed.

2.4 Discussion

The previously described 3D BBB *in vitro* model has many benefits to the conceptualized design such as in-line visualizing, and sampling of both the blood and brain side of the BBB. Additionally, this design incorporates a 3D ECM which can provide a stiffness in the kPa range. Preliminary results show that a lumen can be formed using this platform, and that cells can be suspended into the hydrogel for multiple days. Due to the variability of the growth of the HBMECs, HUVECs and iBMECs and the lack of astrocyte projections when cultured with the 6% w/v GelMA, extensive optimization would be required at this point. In this work, there are many variables to consider for optimizing the platform. Recommended next steps include starting with the optimization of the endothelial cells, as these cells can provide a baseline barrier for the BBB. Then, additional cell types can be added to the system, and their performance can be compared to the baseline BBB. To optimize the hydrogel for including multiple cell types, it will require adding additional aspects to

the microenvironment, such as relevant central nervous system (CNS) proteins to the hydrogel or media and tuning the stiffness of the hydrogel to ensure there is no inflammatory response from the cells within the system. It will be vital to demonstrate that these materials do not results in cellular inflammatory pathways.

Limitations of the data gathered include the small experimental replicates, and it is advisable to reproduce these results with three experimental replicates to have a conclusive outlook on the work produced.

Chapter 3: Development of a planar 2D microfluidic chip for studying AD

3.1 Introduction

To facilitate the study of the effect that circulating factors has on the transport of amyloid-beta through a capillary BBB, a simplified model was developed. The use of a 2D model compared to a 3D model removes the complexity of the hydrogel component, allowing for cells to be seeded directly onto an ECM-coated membrane, thus by-passing the requirement for a substrate with the mechanical integrity to form a lumen while also supporting cell survival. The 2D BoC model was conceptualized to have a "blood" compartment that is able to be perfused with media and a static "brain" compartment that can be sampled throughout the experiment. Having the ability to visualize cells in-line allows for investigating effects of compounds on cell morphology and recovery. Additionally, having a perfusable "blood" environment allows for mimicking physiological flow, as well as provides the opportunities to circulate factors, such as HDL, within the "blood" compartment and studying the effects on the cells present.

3.2 Methods

3.2.1 Structure of microfluidic chip

The microfluidic device consists of two layers of PDMS that are separated by a porous, transparent polyester membrane with a pore size of 0.4 µm, a porosity of 2.0×10^6 cm^2 and a thickness of 12 µm (it4ip, cat. no. 200M12/620N403/47). The porous membrane allows for astrocytes and pericytes to be seeded on the top of the membrane and endothelial cells to be seeded on the bottom of the membrane. This structure of microfluidic chip allows for cell-to-cell interactions between the "blood" and "brain" cells as well as the ability to apply physiological shear stress on the endothelial cell layer. Three designs of microfluidic chips have been made, with the main

difference being the dimensions of the top reservoir that acts as the "brain" compartment, the positioning of the inlet and outlet ports, and the sealing method used for the ports (Figure 9). There are also variation in the width of the PDMS chips, as Design #3 is slightly smaller in width than the other two designs, to facilitate a faster mold fabrication process. This alteration does not impact the cellular microenvironment, since all three designs have the same bottom channel size and membrane surface area in contact with the endothelial cells.

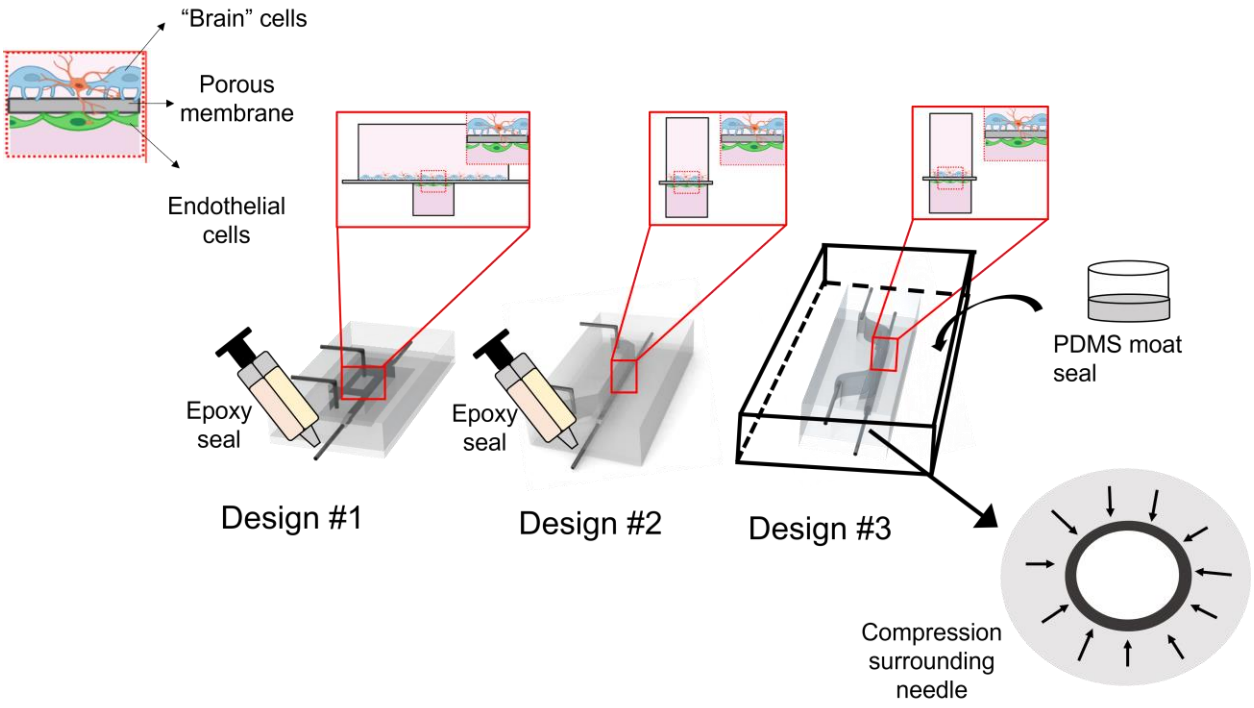

Figure 9: Three designs of 2D planar microfluidic chips are shown above. This figure illustrates the main differences between each microfluidic chip being the top channel, the inlet and outlet port positioning and the sealing method.

3.2.1.1 Design #1: Large top reservoir with top ports

For Design #1 (Figure 9), the top PDMS layer contains a static 10 mm x 18 mm x 5 mm reservoir that acts as the "brain" side of the BBB and the bottom PDMS layer contains a perfusable 1 mm x 1 mm x 18 mm channel that acts as the "blood" side of the BBB. The "blood" channel inlets are made with ½" 22G straight needles, and the "brain" reservoir ports are made with 90º bent ½" 22G needles (McMaster-Carr). The holes for these ports are made using a 0.75 mm biopsy punch (Ted Pella, Inc. cat. no. 15115-2). The ports are sealed to the PDMS chip using 5-minute epoxy (LePage).

3.2.1.2 Design #2: Small top reservoir with top ports

Design #2 (Figure 9) includes a static top reservoir with a width of 1 mm, a length of 18 mm (straight), (5mm slanted), and a height of 5 mm with the inlet and outlet ports inserted from the top layer of PDMS using a biopsy punch of 0.75 mm (Ted Pella, Inc.). The needles used for the top channel ports are ½" 22G 90º bent needles, and the needles for the "blood" channel are ½" 22G straight needles (McMaster-Carr). The ports are sealed to the PDMS chip using 5-minute epoxy (LePage).

3.2.1.3 Design #3: Small top reservoir with side ports

Design #3 (Figure 9) includes a static top reservoir of 1 mm width, 18 mm length (straight), (5 mm slanted) and the inlet and outlet are inserted from the side of the PDMS. The needles used for the top channel ports are ½" 22G straight needles, and the needles for the "blood" channel are ½" 22G straight needles (McMaster-Carr). The ports are sealed using a PDMS moat.

3.2.2 Fabrication of microfluidic chips

To develop the designs mentioned above, molds would need to be available for producing the top and bottom layers. There are limitations in commercially available 2D microfluidic chip designs that have a perfusable blood and brain compartment. For instance, the Human Emulation System®'s S1 chip uses cell seeding volumes as low as 10-20 μL which would challenge the ability to perform multi-day media exchanges in the top compartment since the permeability of PDMS allows for evaporation (126). In addition, commercially available 2D microfluidic chip options have expensive start-up and consumables costs (Emulate®'s S1 chip is $238/chip (as of April 2021 via email confirmation from Emulate® representative)) and are limited by their set chip geometry. Additionally, traditional microfluidic mold manufacturing methods, such as photolithography, is challenging to achieve the required depth for the static "brain" media reservoir, which would be included in the mold for the top layer of PDMS. For these reasons, it was decided that going forward with in-house mold fabrication techniques would be the best option. In the sections below, mold fabrication techniques are described for each chip design.

3.2.2.1 Design #1: Fabrication of mold

For Design #1, to fabricate the geometries required for the top and bottom layers of PDMS, a three-dimensional (3D) stereolithography (SLA) printer (Formlabs, Form2) was used (Figure 10). Computer-animated design (CAD) software (Solidworks, CMC Microsystems) was used to design the parts, then they were transferred to a slicing software (Preform, Version 3.12.2, FormLabs) to be transferred to the 3D printer. When uploading to the printer, a resolution of 25 μm and clear resin was selected. The 3D printed molds were removed from the print bed and post-processed as per the manufacturer's protocols. Briefly, the parts were immersed in an IPA bath for 5-

10 minutes, then left to dry. Finally, the parts were cured under ultraviolet (UV) light (Form Cure, Formlabs) for 30 minutes at 60ºC.

3.2.2.1.1 Optimization of SLA post-processing procedure

Soft lithography is often used to produce PDMS layers that are able to bond irreversibly to each other under oxygen plasma (127). In this case, the SLA printer was used to make the molds that would be used for casting PDMS. Unfortunately, the PDMS layers produced in this way had a rough surface finish that would not allow for repeatable bonding of two PDMS pieces. Therefore, to improve the repeatability of PDMS-PDMS bonding using the SLA molds, attempts were made to optimize the post-processing procedure of the SLA printed molds (Table 2). Unfortunately, out of the conditions tested, none resulted in a smooth surface finish that would be optimal for successful bonding of the PDMS layers.

Table 2: Additional post-processing steps taken to attempt to optimize the printed parts. A qualitative surface finish is described, based on visual observation of the casted PDMS layers.

Post-processing/cleaning conditions	Surface Finish
IPA dip 2 mins + dry print, PDMS cure overnight	rough
Scrub print with soap + let soap dry, PDMS cure overnight	rough
Soak in soap with 70% ethanol 30 mins, PDMS cure 2 hrs	rough
Soak in soap with 70% ethanol 1.5 hrs, chip cure overnight	rough
No wash, PDMS cure 2 hrs	rough

3.2.2.2 Design #2: Fabrication of mold

For Design #2, similar fabrication steps were taken as seen above in section 3.2.2.1 except an additional step was taken. After the post-processing of the SLA-printed molds, an acrylic base was added to the base of the molds (Figure 10). The molds were made to have features that were extruded to offset an acrylic piece. Acrylic (Mcmaster-Carr) was laser-cut using a CO_2 laser (VersaLASER®) and the shape for the acrylic-cut was made using a CAD software (SolidWorks, CMC Microsystems). The DXF part was transferred to another CAD software (AutoCAD, student edition, 2020) for changing the line widths of the parts and making it color-coated to be compatible with uploading to the laser-cutting software. Within the laser-cutter parameters, a power setting of 40-50% and a speed of 15-25% was used. Each acrylic cut needed approximately 15 rounds to completely cut through the acrylic piece. Then, the acrylic was manually pressed into the 3D printed mold, and PDMS was casted. PDMS was left to cure for 1-2 days to compensate for some PDMS that leaked underneath the acrylic and needed time to cure. The acrylic layer resulted in a smooth PDMS surface finish that allowed for the PDMS replicates to be irreversibly bonded under oxygen plasma. This method has the limitation of not affecting the extruded features surface finish, therefore the PDMS channels were still rough, resulting in difficulties while imaging. Additional limitations include the ability for the acrylic to fit perfectly against the extrusion, as the molds and acrylic can be imperfect due to resolution limitations, therefore, between the intersection of acrylic and 3D printed mold, there can be micro extrusions of PDMS where the channel is located.

3.2.2.3 Design #3: Fabrication of mold

For Design #3, a digital light processing (DLP) printer (Creative CadWorks, version M50) was used with PDMS master mold resin (Creative CadWorks) to produce 3D printed molds. Since the resin in a DLP printer is cured layer-by-layer using a light projector and not point-by-point using a laser beam, like with the previously used SLA printer, it is expected to provide a better surface finish. In addition, the printer used in this work was made specifically for PDMS casting, as the PDMS master mold resin is made with methacrylated monomers and oligomers and the light engine is optimized for this resin, allowing for an excellent surface finish (128). For Design #3, a CAD (Solidworks, CMC Microsystems) part was produced and the STL file was imported to the Utility software (version 6.3.0.t3, Creative CadWorks) to convert it to a .3DP file. The file was then uploaded to the DLP printer with a z-resolution selection of 30 μm, and the part was laid flat on the print bed, with the feature side facing upwards. After printing, the print was then rinsed in a 99% IPA bath for 20 minutes, air dried, then rinsed again in an IPA bath for 20 minutes. Then, it was air-dried again with compressed air and it was put into a UV chamber (Formcure, Formlabs) for 40-60 minutes at room temperature with the features side facing up and flipped and UV cured for 20 minutes with the feature side facing down. This DLP printed molds result in a PDMS layer that is transparent and has a smooth surface finish (Figure 10).

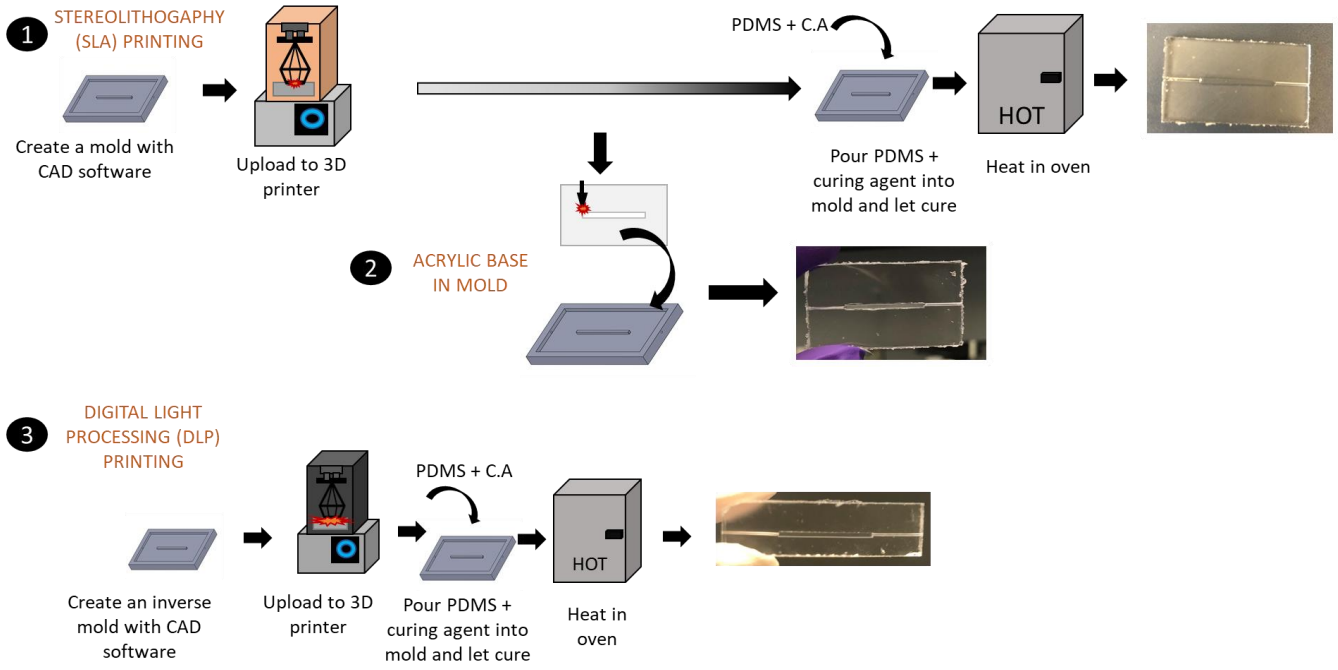

Figure 10: Illustrative diagram showing the fabrication process involved with each chip design used. Design #1 uses an SLA printer to make the molds. Design #2 uses an acrylic base within the SLA printed molds to form the final mold and Design #3 uses a DLP printer to make the molds. Each mold is then casted with PDMS and put under heat until the PDMS is cured. The final images of each PDMS layer from each mold fabrication method is shown.

3.2.3 Experimental procedure

3.2.3.1 Cell culture

HBMECs (Lonza, lot# 376.01.03.01.2F) were thawed from passage 6 and used between passage 6-9. HBMECs were cultured onto fibronectin-coated plates and passaged at 80% confluency. Cells were lifted using 0.05% trypsin and cultured with EGM-2 bullet kit containing 2% v/v FBS (Lonza, cat. no. CC-3162).

3.2.3.2 Chip sterilization, coating and seeding

To develop an endothelial cell barrier within the microfluidic chip, there are preparation steps that are required. These steps include sterilization and ECM-coating. A 1 mL syringe with a 22G dispensing tip was inserted into chip tubing to perform all liquid exchanges. For each design, a 10 minute 70% ethanol rinse, followed by two PBS washes, and an overnight equilibration using EGM-2 media was used to prepare the chips for ECM-coating. Then, a coating of 0.4 mg/mL collagen IV (Sigma Aldrich, cat. no. c5533), 0.1 mg/mL fibronectin (Sigma Aldrich, cat. no. F1141), and 0.1 mg/mL laminin (Sigma Aldrich, cat. no. L2020) was applied the day after equilibration and left overnight in the fridge. Lastly, the chip was washed twice with PBS to ensure there was no acid leftover from the collagen IV coating. Then, cells were seeded into the chip at a density of 5 million cells/mL and then attached to a pump for 5-7 days to allow for perfusion through the endothelial channel. Due to some systematic challenges associated with having physiological shear stress (~1 dyne/cm^2) by using a peristaltic pump (further described in section 3.3.2), some experiments were carried out with a syringe pump, resulting in non-physiological shear stress values within the channel (~0.001 dyne/cm^2) due to the inability to recirculated the media at high flow rates (Appendix B). The top reservoir media was exchanged every two days.

3.2.3.3 Immunocytochemistry and staining

HBMECs were stained to visualize f-actin, nuclei and tight junction zonula-occludens (ZO-1). All staining was performed in-chip. A 1 mL syringe with a 22G dispensing tip was inserted into the chip tubing to perform all liquid exchanges.

For ZO-1 staining, HBMECs were washed 3 times and fixed with 4% paraformaldehyde in PBS and left at room temperature for 15 minutes. Samples were washed twice with PBS for 10 minutes. Samples were blocked in PBS with 2% bovine serum albumin (BSA) and 5% normal donkey serum (NDS) for one hour at room temperature. Samples were incubated with primary antibody ZO-1, mouse, (Thermo, cat. no. 33-9100) at a 1:100 dilution overnight at 4ºC. Samples were washed 3x5 minutes with PBS. Samples were incubated with the secondary antibody Alexa Fluor 647, donkey anti-mouse (Invitrogen, cat. no. A31571) at a 1:500 dilution for one hour at room temperature. Samples were washed 3x5 minutes in PBS.

For f-actin staining, samples were fixed, using the method described above and staining was performed after or in lieu of tight-junction staining. After washing the fixative 2x5 mins with PBS, samples were incubated with the dimethyl sulfoxide (DMSO) stock solution at a 1:400 dilution in PBS for 1 hour at room temperature. Samples were left in a dark, covered container to prevent photobleaching and evaporation while staining. Then, samples are washed 2x5mins with PBS.
For nuclei staining, cells were either stained live or fixed, with Hoechst (Thermofisher Scientific, cat. no. H3570) at a 1:1000 dilution in EGM-2 or PBS. Live cells were washed with EGM-2 and fixed cells were washed 2x5 minutes with PBS.

Chips were disassembled using an Exacto knife and pliers, and the membrane was removed and placed onto a glass slide with tweezers. The membrane was placed with the cell side facing upwards. ProLong® gold Anti-Fade containing 4′,6-diamidino-2-phenylindole (DAPI) was used to mount the membrane and a cover slip was placed onto the membrane. The edges of the coverslip

were sealed using clear nail polish to prevent evaporation. The mounted samples were stored at 4ºC.

3.2.3.4 Epi-fluorescent imaging

Images were taken on an inverted microscope (Zeiss, Observer.Z1) with a numerical aperture of 0.55 and working distance of 26mm. Auto exposures were taken of the samples.

3.2.3.5 Permeability assay

Permeability assays were performed on chips (data not shown due to chip failures). To perform permeability assays, 4 kDa Fluorescein isothiocyanate–Carboxymethyl (FITC) – dextran was inputted into the chips at a 250 μg/mL starting concentration. The tubing lines were primed with FITC-dextran before starting the pump, and the system was left for 1 hour to allow for diffusion into the top reservoir. After the timepoints, media was taken from both the bottom channel and the top channel using a syringe and inputted into a black, round bottom 96-well plate for reading on a plate reader. A standard curve was made for each test. In future experiments, the data can be analyzed based on the assumptions that i) the concentration of FITC-dextran in the input channel is constant, ii) transport from the top reservoir to the bottom channel is negligible and iii) transport is dominated by passive diffusion. To gain a blood-brain barrier permeability (P_{app}) value, the following equations (2), (3) can be used (129).

$$P_{app} = \frac{V_{top}C_{top}}{AC_{bot}t}, when\ t \ll \frac{V_{top}}{AP_{app}} \quad (2)$$

$$\frac{1}{P_{app}} = \frac{1}{P_{BBB}} + \frac{1}{P_M} \quad (3)$$

Where P_{app} is the apparent permeability (cm/s), V_{top} is the volume of the top reservoir, C_{top} and C_{bot} are the measured solute concentrations in the top and bottom channel, A is the endothelial area and t is the time of perfusion. Finally, the permeability of the membrane (P_M) can be calculated using the P_{app} formula (2), and by using blank chips that do not contain cells, but only the coating. Finally, the permeability of the BBB (P_{BBB}) can be calculated based on the permeability of the cell layer on the membrane with the coating and the permeability of just the membrane with coating.

3.2.3.6 Tight junction maturity analysis

Understanding the tight junction morphology allows for a localized understanding of the endothelial barrier integrity. As neurodegenerative diseases have been known to have a disrupted barrier, accompanied by unregulated transport, understanding that parameters that allow for a healthy or unhealthy barrier are of utmost importance. One strategy is to label the immunostained tight-junctions into a descriptive category based on the state of the tight junctions. For this reason, labelling the tight junction maturity can be used to distinguish mature (continuous) and immature (discontinuous) junctions – relating to a healthy vs. unhealthy barrier. Investigations have been made into what environmental factors contribute to endothelial cell mature junctions, such as coatings and gels to use on Transwell® inserts, as well as the inclusion or exclusion of factors into the media, such as cyclic adenosine monophosphate (cAMP), and rock-inhibitor (75).

For the purpose of this work, the maturity of tight junctions was not analyzed due to the low experimental replicates ran; although, since this software is such an important feature when studying the endothelium integrity, I have included a description and a simplified example figure to demonstrate how to use the JAnaP below (Figure 11). The example image represents HBMECs

seeded on a membrane with a coating of collagen IV and fibronectin (further described in section 3.2.3.8) and stained for ZO-1. This image is used to demonstrate the processing steps required to classify the cell tight junctions.

To analyze the maturity of tight junctions, the Junction Analyzer Program (JAnaP) developed and shared publicly by Gray *et al.* may be used (75). There is a detailed protocol available online, at the StrokaLab Github page (https://github.com/StrokaLab/JAnaP). Briefly, endothelial cells can be fixed and stained for tight junctions as per the antibody manufacturers recommendations. An epi-fluorescence microscope with an image processing software can be used to acquire images. Images need to be captured with a 1024 x 1024 pixel resolution and the TIFF files can be uploaded to the junction analyzer program for analysis. A labelling convention in the form of: Date_condition_fluourescentchannels_excitation_magnification_sample# is recommended. Images should be taken with at least 40x magnification. Batch image brightness can be increased using ImageJ software before uploading to the JAnaP. Images can be inputted into the JAnaP and outlining (waypointing) of cell tight junctions can be performed manually. Three cells per image sample is recommended to be outlined and three experimental replicates should be run. The provided Jupyter notebook by JAnaP allows for custom manual thresholding of the samples to decipher tight junction morphology. Finally, the output of the JAnaP provides the individually lined cell information. Continuous, punctate and perpendicular junctions can then be automatically outputted to a spreadsheet where each outline is characterized by its path length and thickness (Figure 11).

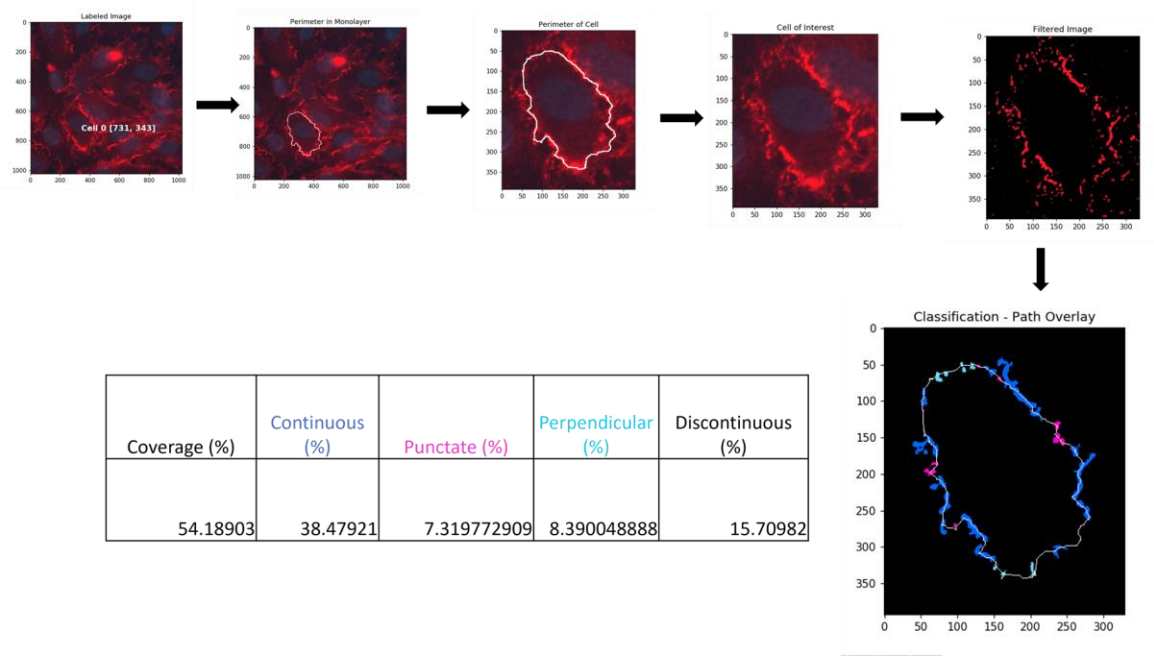

Coverage (%)	Continuous (%)	Punctate (%)	Perpendicular (%)	Discontinuous (%)
54.18903	38.47921	7.319772909	8.390048888	15.70982

Figure 11: Example figure to illustrate the steps taken to classify tight junctions using the Junction Analyzer Program. Left to right: A cell is manually waypointed, by outlining the border of the cell, then the image is manually thresholded to remove background fluorescence, and finally, the waypointed image is automatically processed by the JAnaP to identify the percent of the waypointed area that is covered by tight junctions (coverage (%)), and the percent of the waypointed area that have continuous (continuous (%)), punctate (punctate (%)) and perpendicular (perpendicular (%)) tight junctions.

3.2.3.7 PDMS Bonding performance

To identify the bonding performance of the PDMS-PDMS bonds, first, a visual inspection was made, to ensure all areas of the chip were transparent, then a leak-test was performed by manually pushing food-colored dyed PBS through tubing attached to the chip (Figure 12). If the liquid was confined to the channel, then the chip was deemed bonded, and acceptable to use for an experiment.

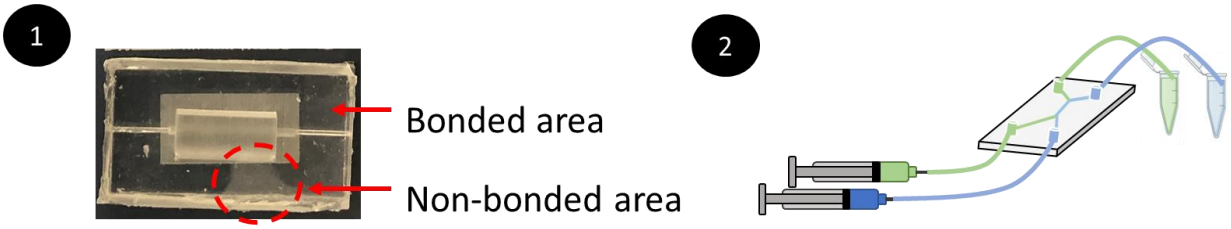

Figure 12: Two ways to test chip performance before using the chips for an experiment. 1) Observing the transparency of the chip after plasma bonding, 2) performing a manual leak test by inserting liquid through each channel.

3.2.3.8 Selecting an ECM

To select an ECM composition to use within the BBB chip, a series of ECM materials were selected and tested on the PET membrane. Since the basement membrane mainly consists of fibronectin, laminin and collagen IV, a panel of combinations was tested. In addition, Matrigel™ (Corning, cat. no. 354234) was used, as it is often used for neurovascular *in vitro* assays. Collagens I and IV (Sigma cat. no. C3867, C5533) were coated at 10 μg/cm^2, fibronectin (Sigma, cat. no. F1141) was coated at 2.5 μg/cm^2, laminin (Sigma, cat. no. L2020) was coated at 2 μg/cm^2 and Matrigel™ was coated at its original concentration. The coatings were added to the membrane for 2 hours at 37ºC and then the excess liquid was aspirated before HBMECs at passage 8 were seeded at a cell density of 100,000 cells/cm^2. Cells were cultured with EGM-2 (Lonza) for 5 days with media exchange every second day. The resultant cell morphology and tight junction presence were observed.

3.3 Results

3.3.1 Mold fabrication

Of the three mold fabrication techniques previously discussed in section 3.2.2, the best fabrication method for casting PDMS suitable for oxygen plasma bonding was determined to be using molds created by the DLP printer. The main attributes that make the DLP printer the most suitable for PDMS casting is the transparency of the resulting PDMS layer, the visually smooth surface finish, and the faithful reproduction from the mold master to the replicate. Limitations with the other two methods include the following. The PDMS layer casted from the SLA printed molds show that the PDMS layer is not transparent, and it contains a diagonal pattern on the surface of the layer, both indicating that the PDMS layer does not have a smooth surface finish that is sufficient for PDMS-PDMS bonding. Furthermore, using an acrylic base in the SLA printed mold results in a visually transparent PDMS surface on the areas in contact with the acrylic; although, there exists a rough surface finish on the channel due to the PDMS being in contact with the SLA printed part in that region. Additionally, this technique results in irregularities of the channel geometry where the acrylic is in contact with the printed part, leading to micro extrusions of PDMS being present, and ultimately leading to a non-flat membrane when assembling chips. A visual representation of the three resultant PDMS layers is shown in Figure 13.

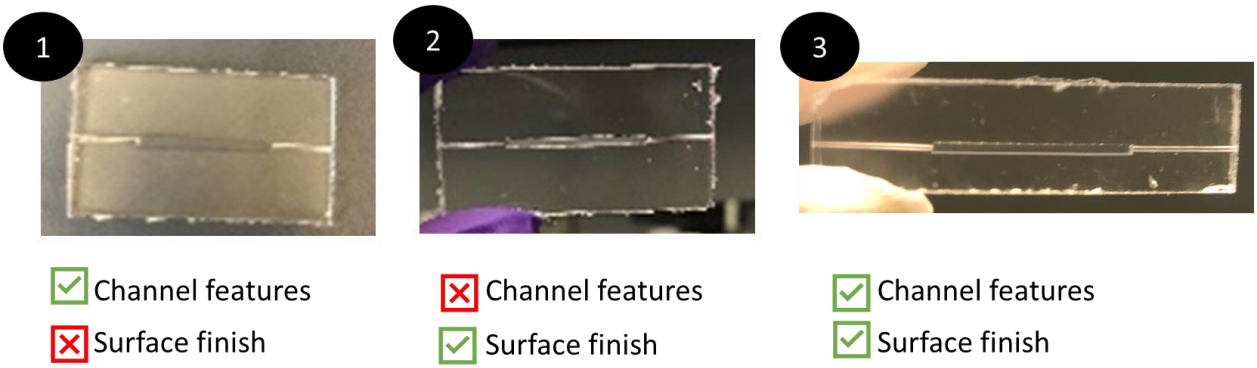

Figure 13: Visual comparison of the main outcomes of the different mold fabrication techniques. 1) the SLA printed mold produces a rough surface finish, 2) the acrylic base in the SLA printed mold produces irregularities at the channel, and 3) the DLP printed molds produce sufficient channel features and surface finish for PDMS bonding.

3.3.2 Optimization of experimental procedure

When performing experiments with Design #1, it was observed that the large size of the top reservoir resulted in a non-flat PET membrane that allowed for cells to be seep out of the bottom channel and under the membrane, onto the PDMS layer (Figure 14), indicating that there is a lack of compression on the outer sides of the membrane, resulting in the membrane not lying completely flat against the channel.

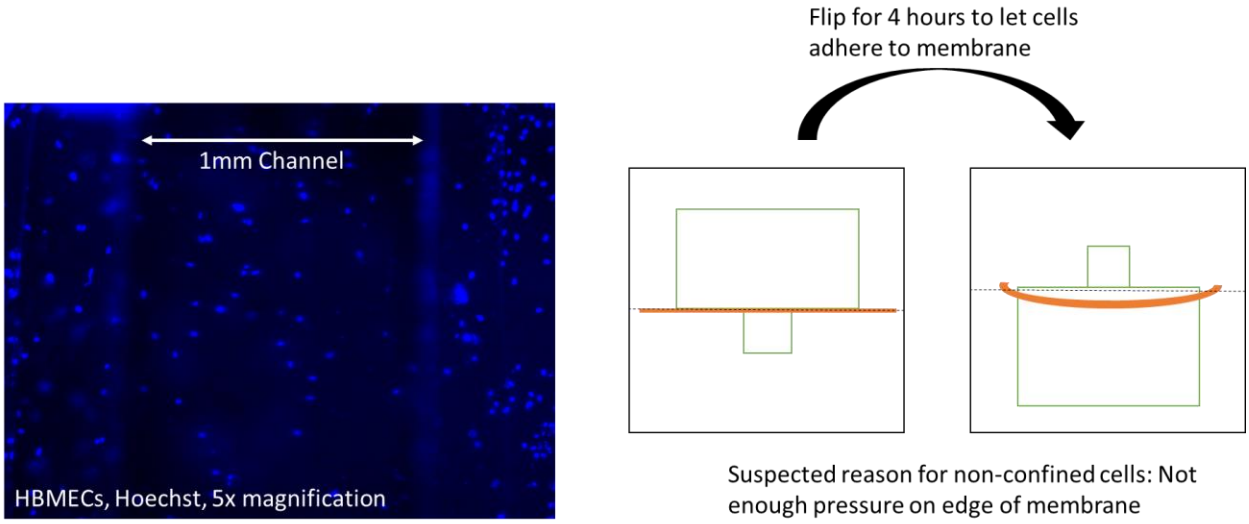

Figure 14: Representative image showing that the HBMECs that are stained with Hoechst (left) are not confined to the channel in Design #1. A visual depiction of the suspected reason for the non-confined cells is shown on the right.

This led to the decision to reduce the width of the top reservoir, to provide more compression on the PET membrane and increase the effect of the sandwiching of the PDMS-PDMS bond. This led to Design #2 and resulted in cells being confined to the bottom channel, as tested using readily-available, pre-labelled epithelial cells (donated by St. Paul's Hospital, Vancouver) expressing green fluorescent protein (GFP) (labelled using in-house lentiviral transduction) and seeded at 5 million cells/mL and let adhere for 4 hours. These images are taken while live cells are still within the chip. As seen in Figure 15, there is clearly a distinguished channel present; based on most of the cells being within the channel border. Therefore, it was evident that the new chip design with a smaller width top channel provided more compression on the membrane, ultimately confining cells to the channel.

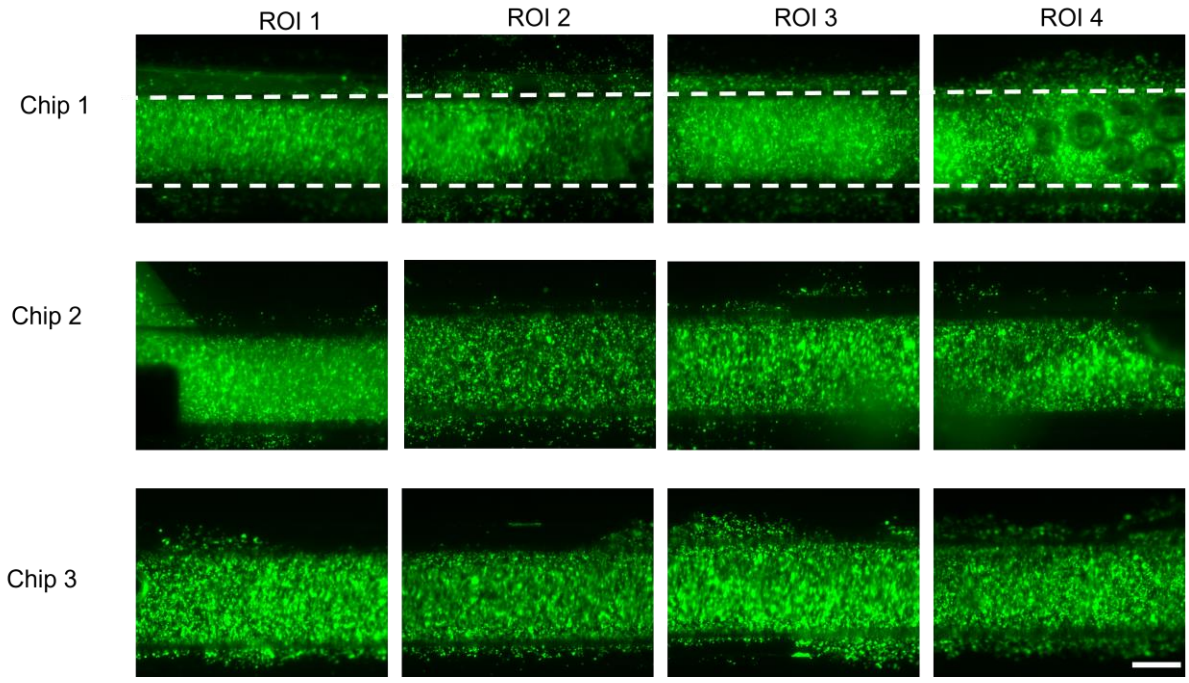

Figure 15: Epithelial cells expressing green fluorescent protein (GFP) are confined to the channel. The channel borders of chip 1 are outlined manually using white dotted lines. Scale bar is 500 µm.

Using Design #2, four experiments were carried out to completion, and many systematic errors occurred throughout these experiments. During these experiments, bubbles formed and became trapped in the top reservoir at the sharp edges in the reservoir channel, the epoxy that kept the inlet and outlet ports attached to the chip would come undone, the peristaltic pump tubing would rupture under pressure from the peristaltic pump cassettes, or the tubing would disconnect at the junction of the peristaltic pump tubing and the silicon tubing (Figure 16).

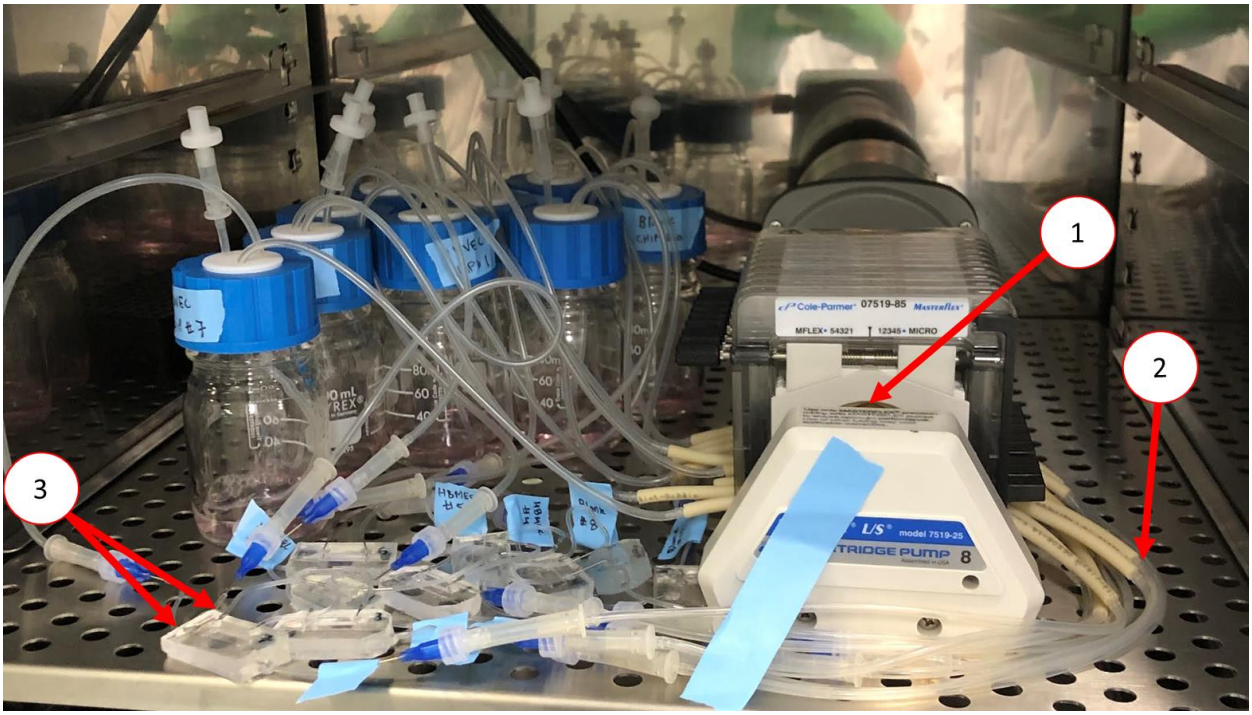

Figure 16: Failure modes seen while running multiple chip experiments. 1) Pump tubing ruptures under pressure from manually tightening cassette, 2) Connector between stiff and flexible tubing comes undone, 3) Inlet and outlet ports of the chip become disconnected.

This led to Design #3 and a new method of connecting the ports into the outlet of the chip, as well as using a syringe pump instead of a peristaltic pump for future experiments. A PDMS moat was used to secure the input and outlet ports to the microfluidic chip. Additionally, the inlet and outlet needle molds were made using a needle with a smaller outer diameter to allow for compression when inserting the needle ports (Figure 17). A detailed protocol for creating Design #3 PDMS chips is described in Appendix C.

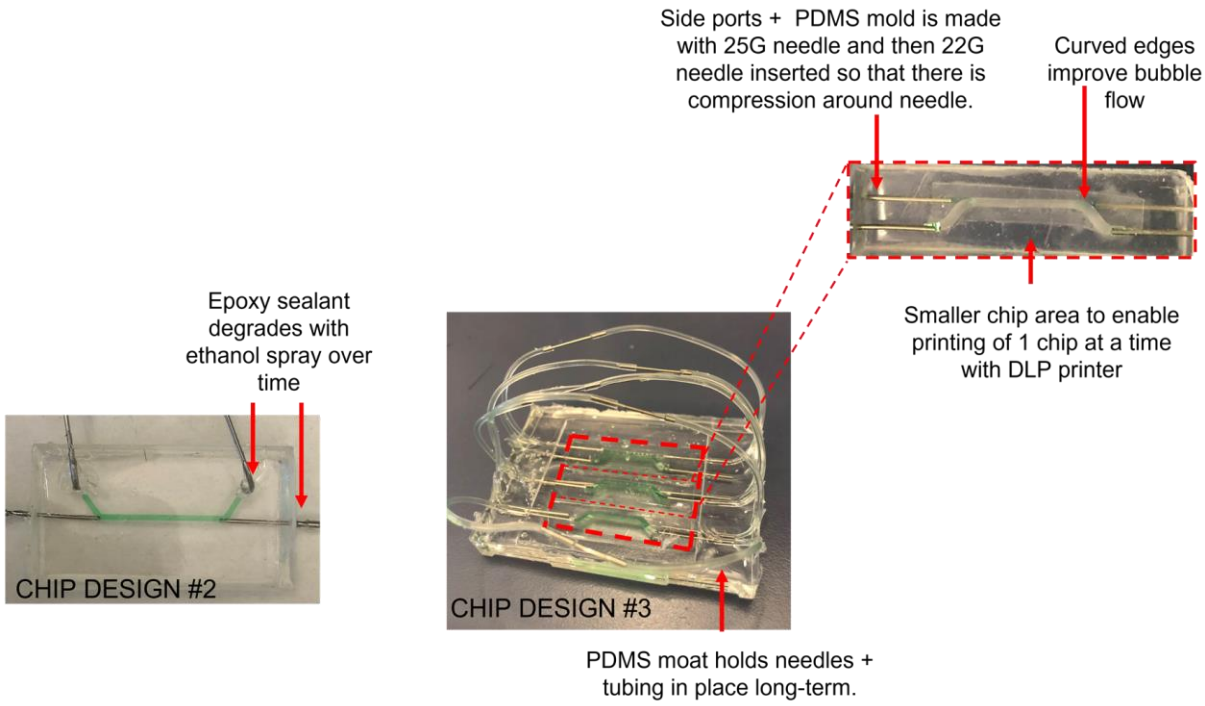

Figure 17: PDMS moat used to hold inlet and outlet ports in place. Comparison between two chips to show that the new Design #3 contains a PDMS moat and the side ports are made with smaller gauge needles.

The adjustment of creating a PDMS moat is beneficial because it embeds the needles and tubing into the PDMS, creating a robust and long-term solution to connecting macro-sized tubing to microenvironments. Additionally, the process takes about 1 day to allow for the PDMS to cure, this is slightly more time required than the epoxy sealing method. Additionally, having the PDMS moat allows for ethanol to be applied for disinfection of the chips without the consequence of delamination of the inlet and outlet ports. This is described in Table 3.

Table 3: Comparison of inlet/outlet port sealing methods.

Inlet/outlet port sealing	Pros	Cons
Epoxy seal	- Total application and cure time <1 hour.	- Epoxy delaminates upon contact with ethanol.
PDMS moat	- PDMS moat holds needles securely in place long-term.	- PDMS moat step takes ~1 day to form and cure.

3.3.3 Chip experiment performance

Chips were fabricated using the methods described above, resulting in the main design changes described below in Table 4.

Table 4: Comparison of the different design changes with each 2D planar chip design.

	Design #1	Design #2	Design #3
Fabrication of molds	SLA printer	SLA printer + acrylic base	DLP printer
Port inlet size	22G	22G	25G
Top reservoir shape	Sharp edges	Sharp edges	Smooth edges
Port sealing method	Epoxy	Epoxy	PDMS moat
Flow path	Recirculating, 1 dyne/cm^2	Recirculating, 1 dyne/cm^2	Unidirectional, 0.001 dyne/cm^2

Design #1 had the lowest success rate (12%) when performing the first step of the fabrication process, which is the bonding of the two PDMS layers. Based on observing the transparency and the leak testing of the bonded layers, it was determined that PDMS bonded with the SLA mold did not perform as well as those bonded with the acrylic base or the DLP mold, therefore they were not deemed as successful chips and could not be used for experimental runs due to their poor performance. The successfully bonded chips were then put through the sterilization process and

seeded with HBMECs and put under flow. After at least 5 days in culture and under flow, the remaining chips were examined to identify if they were still intact to be used for analyses. It was observed that many (69%) of Design #2 chips had experimental errors (Figure 16) and therefore were not considered viable chips. A breakdown of the chip success rate after 5 days in culture is shown in Figure 18 and it is evident that the chips with Design #3 using a DLP mold with a PDMS moat had the best success rate of 88% after testing 17 chips.

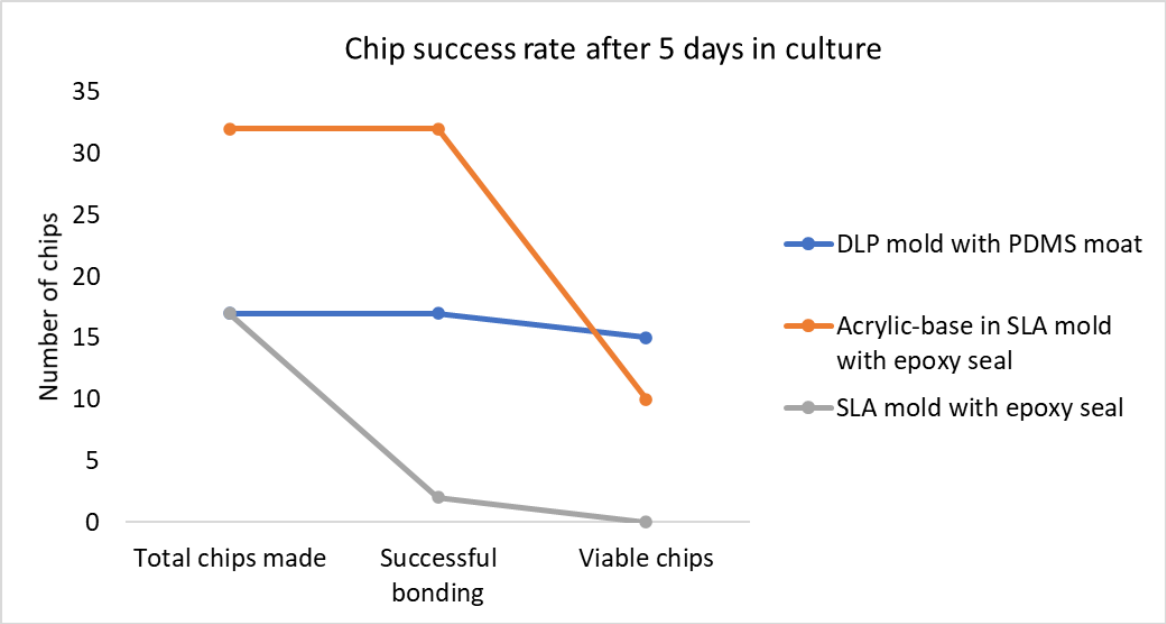

Figure 18: Chip success rate of DLP mold with PDMS moat, acrylic base in SLA mold with epoxy seal and SLA mold with epoxy seal.

3.3.4 ECM-coating selection

As seen in the panel of images in Figure 19, the no coating condition did not result in a uniform layer of HBMECs with cobblestone morphology. Additionally, the laminin condition was considered sub-par for establishing an HBMEC monolayer. As Matrigel™ is subject to have lot-

to-lot variability, it was deemed unacceptable to use as a coating. Additionally, since there were no visual indicators of a difference between the tight juncitons stained in the collagen IV/fibronectin, collagen IV, and collagenIV/laminin conditions, it was decided that a combination of all three ECM proteins would be a beneficial coating to use. Furthermore, the 2D BoC literature has previously used these ECMs (130,131); therefore, to ensure the best possible outcome, the literature concentrations were selected, for a final solution consisting of collagen IV (400 µg/mL), laminin (10 µg/mL) and fibronectin (100 µg/mL).

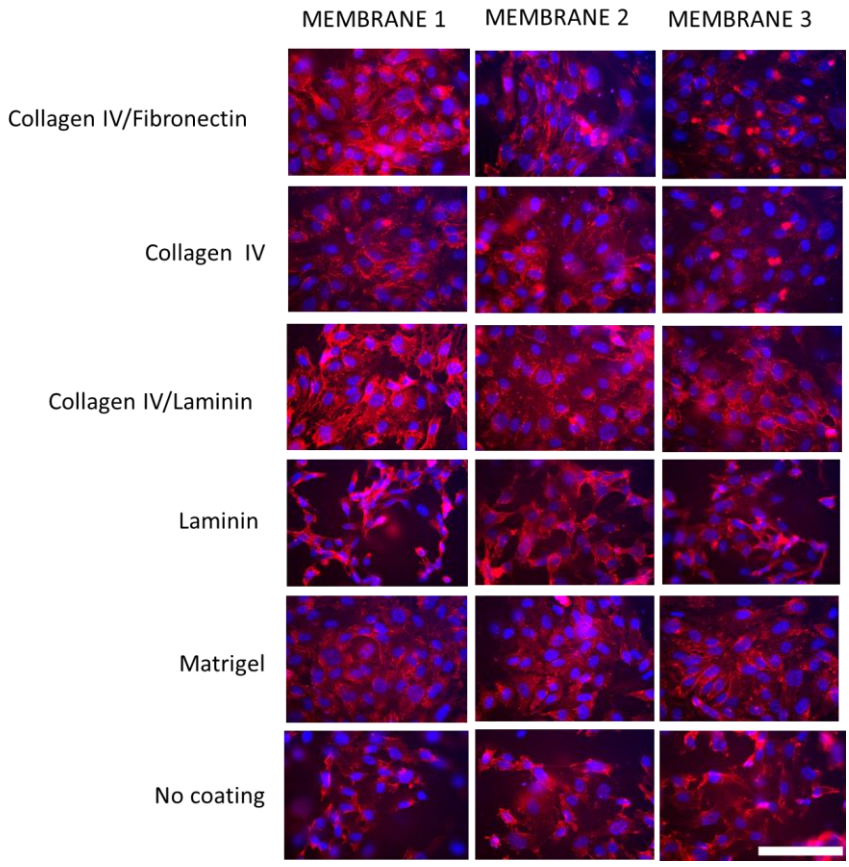

Figure 19: Representative image of HBMECs stained for nuclei (Hoechst) and tight junction protein ZO-1 (Alexa fluor 647) on PET membranes that has ECM coatings. Scale bar of 100 µm.

3.3.5 HBMEC monolayer

There was a low sample size of the chips that were deemed viable after the experiment and also contained cells. Design #2 had 11 viable chips and Design #3, had 8 viable chips. A confluent monolayer was characterized visually by assessing the coverage of the cells. Representative images of the confluent monolayer images are shown in Figure 20.

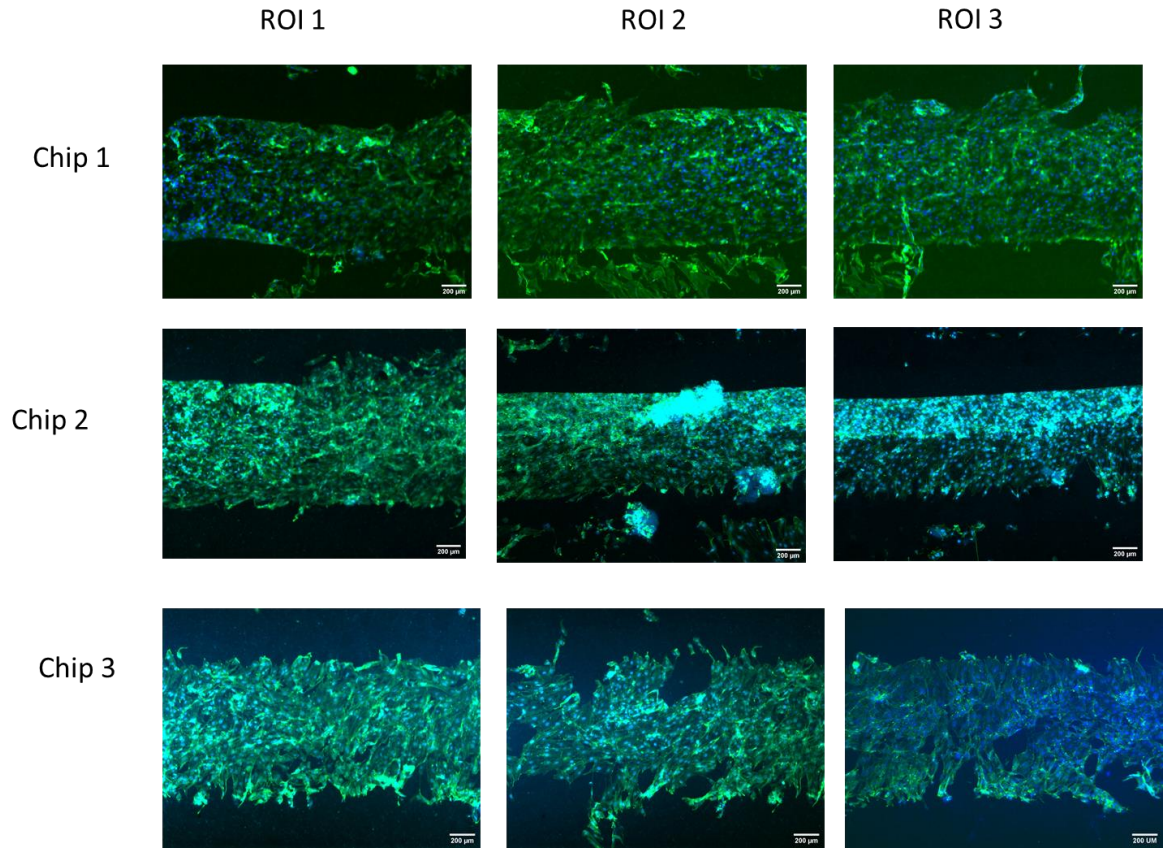

Figure 20: HBMECs adhered onto the PET membrane in the chip after 5 days in culture. Cells stained for F-actin to visualize cell coverage. These chips are a representation of a confluent monolayer. Scale bar 200µm.

The breakdown of chips with a confluent monolayer are shown in Figure 21. It was observed that the chip Design #3 produced a better success rate of 55% compared to Design #2 which had a success rate of 20% for obtaining a confluent monolayer; hypothetically due to the ease of use and the reduction of experimental errors that occurred.

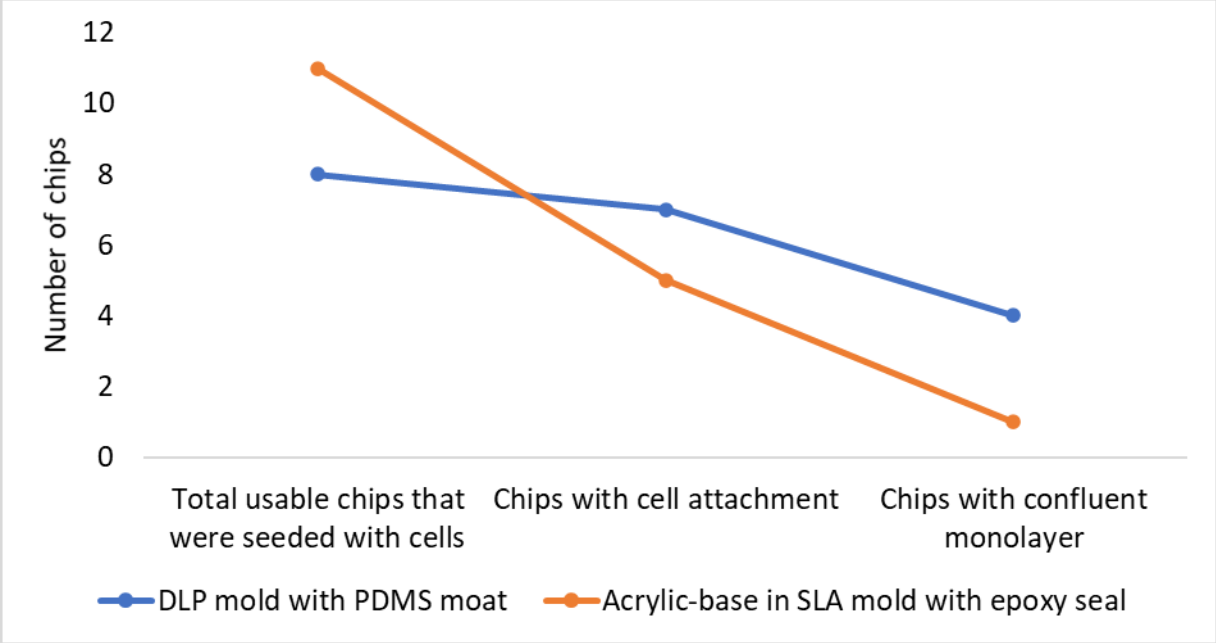

Figure 21: Number of chips with cell attachment and a confluent monolayer after 5 days in culture.

3.4 Discussion

The development of a 2D planar BBB chip was conceptualized and initial optimization experiments were performed. The design of the chip is tailored towards a BBB chip that can be seeded with cells on both sides of the membrane to form a barrier. The designs of the chips reflect the robustness of the fabrication process and the cell adherence and proliferation outcome. A table depicting the overall success rate (based on yield) of the chip designs, as well as possible failure modes between different check-points in the fabrication and experimental process are shown in

Table 5. Overall, the development of these chips using the fabrication methods previously described (section 3.2.2) demonstrated the best results when using the chips made with a DLP printed mold, 25G needle molds, curved top channel edges, and PDMS moat sealing. Overall, the Design #3 allowed for a chip fabrication success rate of 88% and the cell culture monolayer success rate of 57%.

Table 5: Success rate of chip designs and possible failure modes between the fabrication and experimental checkpoints.

Description		Yield			Common and suspected failure modes
		Design #1	Design #2	Design #3	
Sample size of chips between check-points 1-2		17	32	17	
Check-point 1	Successful PDMS-PDMS bonding based on complete transparency of PDMS pieces and manual leak test	12%	100%	100%	Design #1: Rough surface finish of molds. Design #2: N/A Design #3: N/A
Check-point 2	Viable chips at the end of the experiment	0%	31%	88%	Design #1: PDMS-PDMS leakage. Design #2: Ports connecting chip to peristaltic pump disconnecting at junction, chip inlet and outlet ports disconnecting from chip due to epoxy delamination. Chip bursting due to debris from peristaltic pump tubing occluding PDMS chip channel. Peristaltic pump tubing rupture while manually tightening cassettes. Design #3: Tubing connecting chip to peristaltic pump disconnecting. Tubing coming undone from needle on syringe that is dispensing media.
Sample size of chips between check-points 3-4		N/A	11	8	
Check-point 3	Chips with cell attachment	N/A	45%	88%	Design #1: N/A Design #2: Cell death due to edges in top channel allowing for bubbles to get trapped while introducing media to system. Cell death due to air bubbles forming in bottom channel once epoxy delaminates from PDMS allowing for air to be introduced to the internal features on the chip. Cell detachment due to uneven ECM coating. Design #3: Cell detachment due to uneven ECM coating.
Check-point 4	Chips with a confluent monolayer	N/A	20%	57%	Design #1: N/A Design #2: Washing and fixing steps and disassembly of chips caused cells to lift before mounting membranes onto glass slides. Cell detachment due to uneven ECM coating. Design #3: Washing and fixing steps and disassembly of chips caused cells to lift before mounting membranes onto glass slides. Cell detachment due to uneven ECM coating.

The current chip Design #3 is at a point that the physical microfluidic chip is robust and ready to use. Although, to prevent systematic errors during an experiment, future optimizations of the interface from the microfluidic chip to the pump can be investigated. This includes limiting the amount of handling that is needed to attach the microfluidic chip to the pump, as well as ensuring that throughout the experiment, there is no manipulation of the tubing, which can result in disconnection of the tubing from the syringe.

After optimization of the physical system is complete, more effort is needed to optimize the cell culture environment. Previously reported values for an organ-on-a-chip platform that was used with epithelial cells produced a success rate of ~70% for microfluidic cell culture (132); therefore, that should be the yield% goal of future optimizations. The cellular optimization should be quantified using functional assays such as a permeability assay (described in section 3.2.3.5) and tight-junction maturity should be classified (described in section 3.2.3.6). Suggestions for optimizing the cell culture environment are further described below in section 5.1.1.2.

Limitations of the experiments reported in this work include that the low experimental replicates involved with using cells. This is a consequence of the robustness of the chips, and the challenges that come with developing the physical model as well as the cellular model in parallel.

Chapter 4: Optimization of a tissue chamber

4.1 Introduction

This platform was originally designed by Robert *et al.*(22), who developed a bioreactor system (Figure 22) to perfuse an arteriole scaffold seeded with endothelial cells, smooth muscle cells and astrocytes. The bioreactor system uses a combination of tubing and connectors to develop a recirculating system to study artery pathology. The system consists of a medium bottle allowing for gas exchange through a 0.22 μm filter, a tubing line that allows for media flow using a peristaltic pump. The seeded scaffold is submerged in a nutrient rich aqueous environment to allow for nutrient supply from both the perfused vasculature and from surrounding of the scaffold. The area that the seeded scaffold sits within the system is known as the tissue chamber and the purpose of this work is to demonstrate design changes that were made to make this aspect of the system more robust. Additionally, as bubble formation within the tissue chamber was seen as an issue while testing the modified designs, an investigation into bubble formation under different conditions is described.

4.1.1 Previous tissue chamber design

The previous bioreactor system (Figure 22) consists of a tissue chamber that is made from a flexible 3/8" ID silicon tubing (Fisher Scientific, cat. no. 14-179-118) that is connected to a circulation loop via male luer to 1/16" barb ports (Nordson Medical, cat. no. MLSL004-6005). The 1/16" ports connect to a 1mm thick Biofelt® non-woven polyglycolic acid (PGA) scaffold (Confluent Medical Technologies) that is dip-coated with 1.75% polycaprolactone (PCL) (Sigma, cat. no. 440744) and tetrahydrofuran (THF) (Sigma, cat. no. 401757) solution and once it dries, it is coated again with a 10% PCL/THF solution. The scaffold is the left to dry before being sterilized

by a 30 minute 70% ethanol bath and washed 3 times with PBS. Then, the scaffold is seeded with endothelial cells, smooth muscle cells and astrocytes. Each experimental run consists of 12-16 independent scaffolds and lasts 21 days.

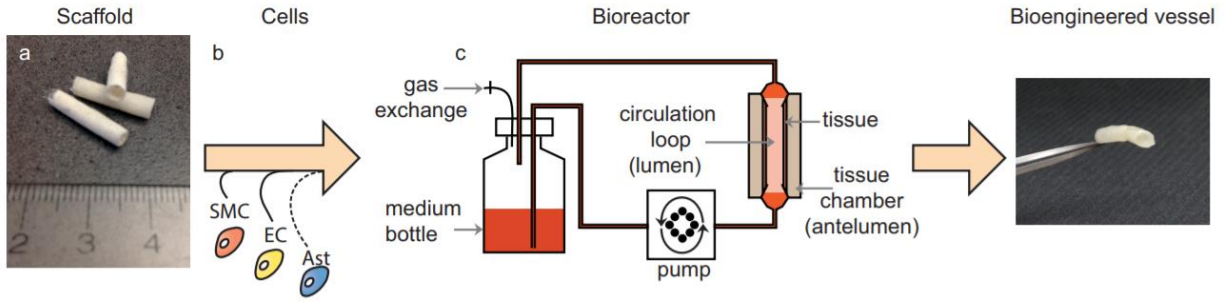

Figure 22: Schematic of previous bioreactor system. Image taken from (22). The scaffold (a) is seeded with endothelial cells, smooth muscle cells and astrocytes (b) and put into the bioreactor system (c) where the bioengineered vessel is cultured.

Limitations in the previous design consists of the inability to sample the antelumen compartment of the tissue chamber throughout the experiment, the instability of the tissue chamber once it is connected to the pump tubing and the overall space constraints that are within the incubator (Figure 23).

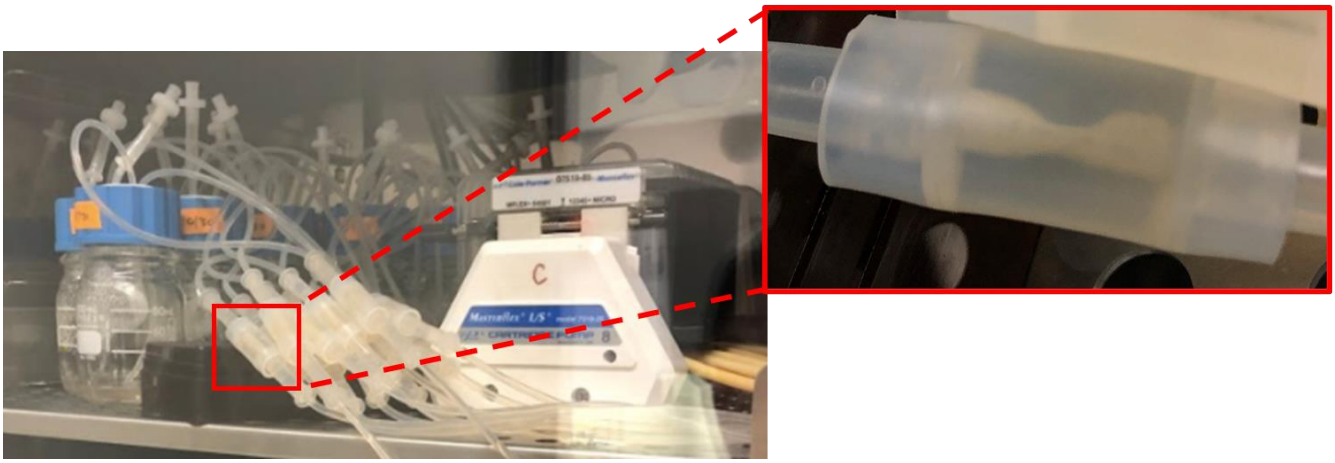

Figure 23: Representative image of the manipulation of the scaffold based on tubing movement. The fragility of the scaffold is the motivation behind the need for a more stable tissue chamber.

4.2 Methods

4.2.1 Fabrication of new tissue chamber

To improve the robustness of the current bioreactor system, a few changes in the design of the bioreactor have been made. The previous pressure-fitting ports have been switched to threaded ports (Nordson Medical, cat. no. PMS230-210-1), and custom-made, 3D printed pressure-fitting end-caps have been added to ensure the ports are aligned, resulting in consistent scaffold placement within the bioreactor system. A custom-made tube-cutting apparatus is used to ensure the distance between the ports is consistent. In addition, luer-lock sampling ports (Nordson Medical, cat. nos. FTLL004-1, MTLLP-1) have been added to the tissue chamber tubing, which offers the ability to do sampling or media changes throughout an experiment. These changes results in a price per bioreactor increase from $10.50 to $16.30 (Appendix D). The main attribute to this price increase is the cost of end-caps, which haven't been tested for long-term use or autoclave cycling; therefore, they've been estimated to last only 6 bioreactor runs before warping or cracks occurs. The tubing

is ½” ID and 11/16” OD silicone tubing (Cole Parmer, cat. no. RK-95802-22). The main differences between the two designs are the end-cap design and material selected. The first design of the modified tissue chamber (Figure 24) includes end-caps that had an external diameter of 12.7 mm and a length of 6 mm and were designed to be made of polypropylene. Polypropylene was chosen due to the low protein absorption capabilities (133) and because the future use of these tissue chambers could include testing amyloid plaque transport which is a major concern in AD research.

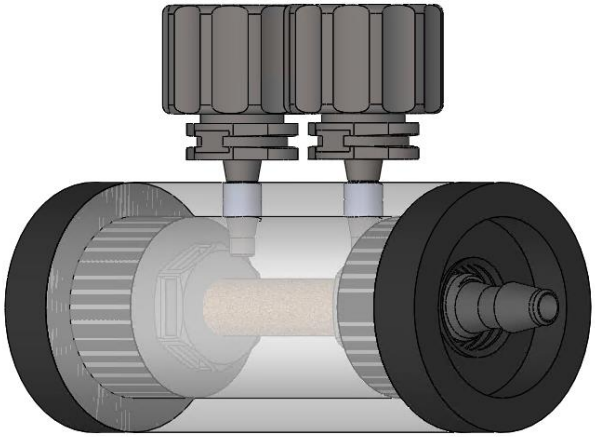

Figure 24: Tissue chamber Design #1 with end-caps, threaded ports and luer-lock sampling ports.

The second tissue chamber design (Figure 25) includes a larger end-cap outer diameter of 14 mm and an increased length of 10 mm, and the end-caps are 3D printed out of biomedical clear resin (Formlabs) which allows for a resolution of 100 μm to be used while 3D printing. These end-caps were printed on a FormLabs 3 printer, and consideration was made to reduce supports on the surface in contact with the threaded port to ensure tight sealing.

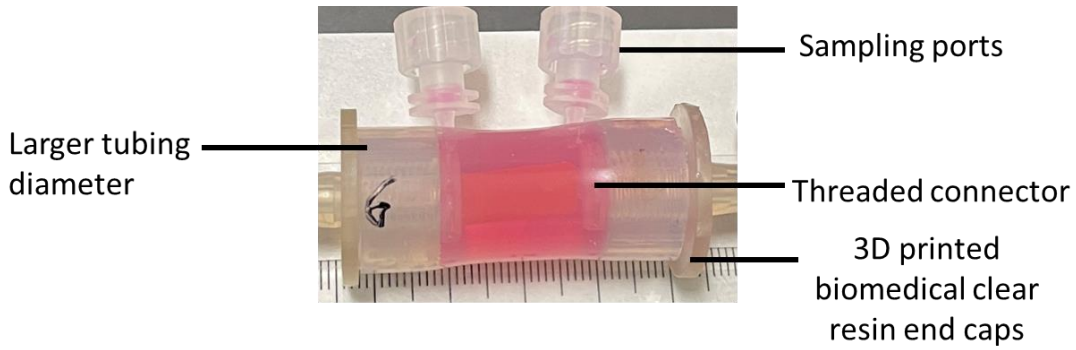

Figure 25: Tissue chamber Design #2, with indications of main design features.

4.2.2 Bioreactor system changes

Falcon tube caps were 3D printed using biomedical clear resin and used as a media reservoir (Figure 26). These caps allow for each run to have sterile, clean, media reservoirs, and reduce the risk of contamination and debris from entering the scaffold.

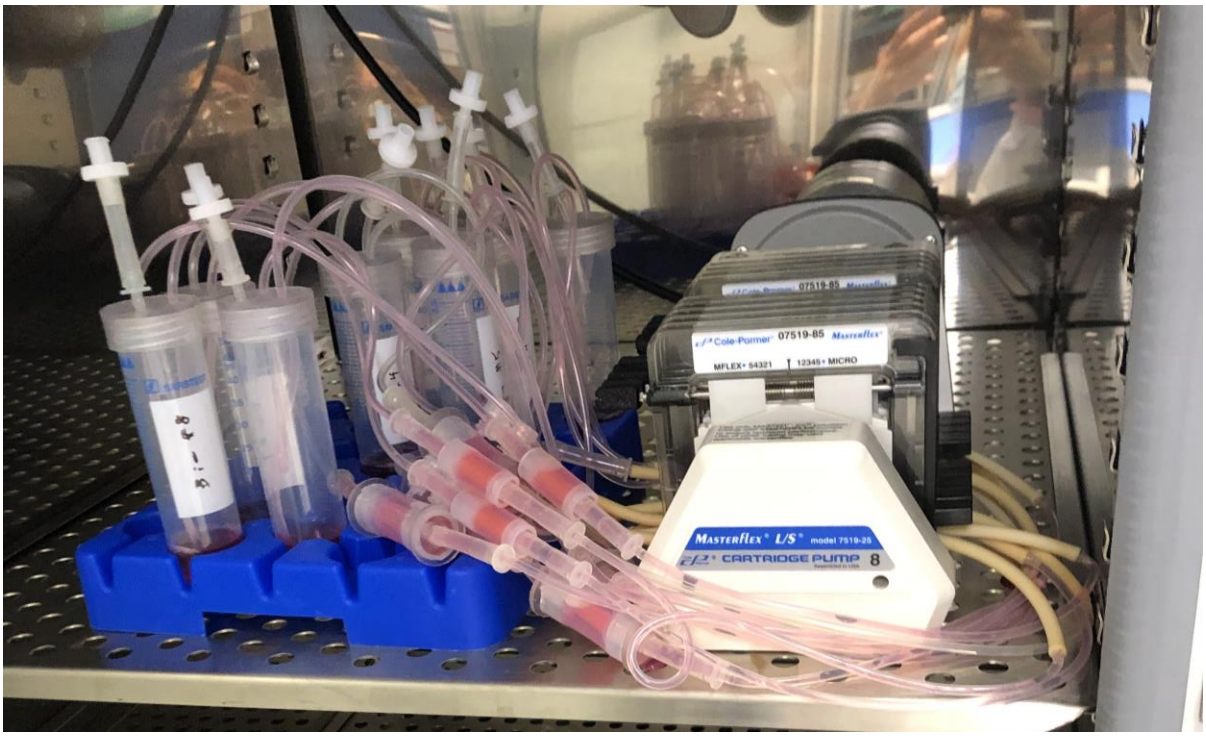

Figure 26: Representative image of the bioreactor system within the confined space of an incubator. This demonstrates the use of custom-made falcon caps to enable the use of falcon tubes for reservoirs.

4.2.3 Leak testing methods

Tissue chambers were cut to 33 mm using a custom-made tube cutting apparatus and threaded 1/16” to 1/8” ports were added to the end-caps and tightened using an 8 mm wrench before using a tubing with the same inner diameter as the PGA scaffold (1 mm ID) to mimic the scaffold while performing leak testing. Then, the end-caps were added to the cut tubing and holes were punched into the tubing with a 1.5 mm hole punch (Ted Pella) manually. The holes were punched with the intention of having their through-holes as close to the end caps as possible, as this reduces the dead space present and prevents bubbles from getting trapped. Then, two luer ports and caps were inserted into the through holes to complete the assembly of the tissue chamber system (Figure 27). In the first leak test of Design #1, additional conditions were added to try to eliminate the variables

on where leakage could occur. End-caps were either left in their original form, or epoxied with 5-minute epoxy (LePage), or wrapped in parafilm. The sampling ports were either left in their original form, not added to the system, or epoxied. For this test, there was only one sample of each condition and the test was ran once to help identify possible leakage points. For testing both Design #1 and Design #2, the bioreactor system was assembled in a non-sterile condition (assembly is the same as previously described in section 4.1.1.). For Design #1, the system was tested on a benchtop using water, and for Design #2, the bioreactor system was taken into the BSC and sterile technique was used to add media to the tissue chamber. In both cases, the system was hooked up to the peristaltic pump and left on circulation at ~0.7 mL/min for 7 days. When testing Design #2, the assembled system was rinsed with distilled water and dried with compressed air then the whole system was autoclaved to ensure the system was sterilized. These tissue chambers were left on a benchtop, submerged in a water bath or left in a cell culture incubator at 37ºC and 5% CO_2. Images of the Designs #1 and #2 were taken on day 0 and day 7 to identify if bubbles formed large enough to interfere with the scaffold (Appendix E).

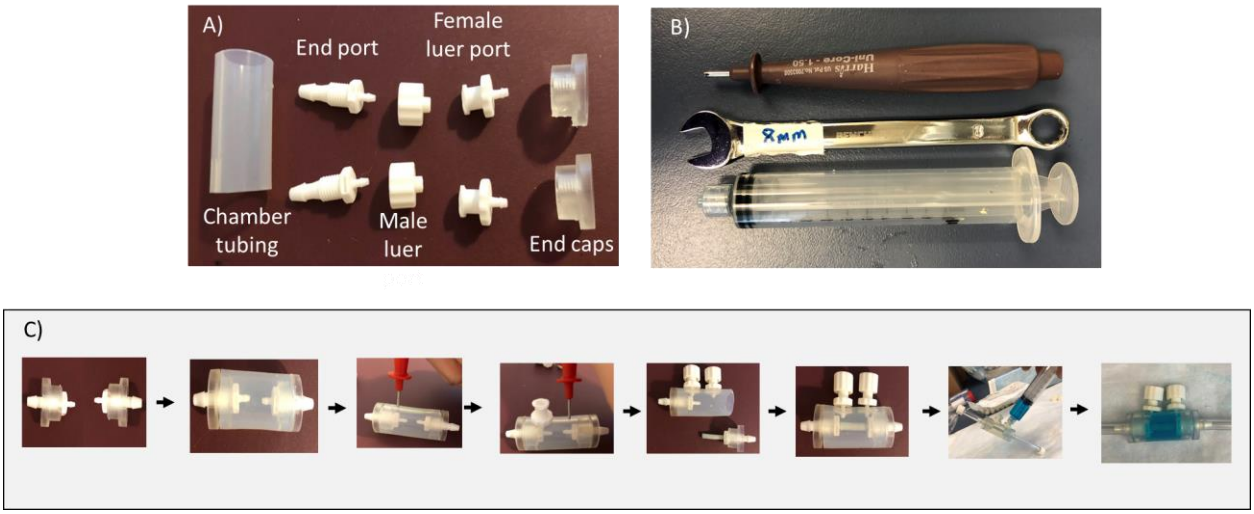

Figure 27: Tissue chamber assembly, A) tissue chamber parts include the tissue chamber, end ports, male luer ports, female luer caps, and end caps, B) the required parts for assembling the tissue chamber include an 8 mm wrench, a syringe and a 1.5 mm hole punch, C) the assembly process.

4.3 Results

4.3.1 Leak testing of designs #1 and #2

An overview of the results of testing Design #1 are shown in Table 6, where green indicates no bubbles formed, orange indicates bubbles formed, but they were not large enough to obstruct the scaffold, and red indicates bubbles formed that were large enough to obstruct the scaffold. Design #1 did not produce any outcomes that did not lead to bubble formation. Although, it was noticed that the original fabrication method, including no alterations to the sampling ports or end-caps resulted in small bubble formation that were not large enough to obstruct the interior scaffold. Additionally, it was observed that adding epoxy and parafilm to the end caps had a similar result. This also indicates that the extra steps did not show a substantial decrease in the bubble sizes that were produced. It was also noticed that adding epoxy to the sampling ports led to large bubble formation, and not adding sampling ports led to large bubble formation. Adding epoxy to the

sampling ports or end-caps was challenging as it required more manipulation of the system, and it required letting the system dry for longer time periods, which is not ideal when trying to produce high throughput experiments. Additionally, having no sampling ports would limit the system, since the purpose of sampling ports is to investigate secretion from brain cells.

Table 6: Performance of tissue chamber Design #1 under different conditions. Orange (triangle) represents small bubbles formed, although no obstruction of scaffold was present. Red (square) represents a bubble large enough to touch scaffold. These results represent 1 sample.

Sampling ports / End caps	Original	Epoxied	None
Original	▲	■	■
Epoxied	▲	■	**N/A**
Parafilm wrap	▲	■	■

An overview of the results of leak testing Design #2 are shown in Table 7. The results indicate that the only condition that did not produce bubbles were from the submerged condition. Every other condition produced bubbles large enough to obstruct the scaffold. These results are from a single experimental replicate, with three samples of each condition present (N=1 with n=3).

Table 7: Performance of tissue chamber Design #2 under different conditions. Green (circle) represents no bubbles formed, orange (triangle) represents small bubbles formed, although no obstruction of scaffold was present, red (square) represents a bubble formed and it was large enough to touch the scaffold. These results represent 3 samples.

	Submerged	Benchtop	Incubator
Design #2			
Original (unmodified) design			

4.4 Discussion

Modifications to the original tissue chamber design have been made and these changes allow for more stable scaffolds, and the ability to sample the brain side of the scaffold. The increase in diameter and the smoothness of the 3D printed biomedical clear resin allow for a tighter, more secure fit of the end-caps; therefore it is recommended to move forward with Design #2. Both modified Designs #1 and #2 produced bubbles in non-hydrated conditions. This leads to the recommendation to introduce a media exchange before day 7, as it is suspected that evaporation through the tubing is causing bubble to form throughout the experiment. Gas exchange is important for cell survival, so finding an optimal time-point for exchanging the media is essential for the optimization of this system.

Chapter 5: Conclusion

Throughout this work, multiple types of *in vitro* blood-brain barrier models have been developed. The conceptualization and development steps needed to produce capillary models using non-standard master mold fabrication processes, as well as the steps taken to begin the optimization of the cellular environment in either a 3D hydrogel, or on a planar ECM layer, have been described. Additionally, this thesis describes the advancement of a previously used bioreactors' tissue chamber to enable in-line sampling and improve the robustness by incorporating custom made pressure-fitting end-caps.

The collaborative nature of this project allowed for progress in both the microfluidic model development as well as an overall understanding of the key variables associated with cell culture optimization. The sections below highlight the main points of this thesis, and future recommendations.

5.1 Summary of microfluidic capillary chip development

The progress towards developing a functional microfluidic chip was based on optimizing a few key variables. Originally, at the beginning of this project, the physical chip's optimization was not the priority of the work, since much of the focus was put on optimizing the cellular compatibility with GelMA. Some of the key limitations associated with this 3D hydrogel-based chip are listed below.

- 6 w/v% GelMA, 0.6 v/v% LAP has not been previously used with HBMECs or primary astrocytes.

    - Although GelMA has been previously used in other tissue engineering applications, it was not previously optimized for the brain cells that we were using. To develop a hydrogel that is compatible with HBMECs and astrocytes requires a very specific microenvironment to survive.
- Throughout the chip experiments, there were many instances of leakage.
    - The leakage resulted in a lot of samples not being usable, as leakage can lead to non-consistent seeding densities, poor nutrient supply, and a higher risk of contamination. At this point in the project, the exact reason for leakage was unknown; therefore, it was not corrected.

Some of the key positive attributes of the 3D hydrogel development are listed below.

- The chip allows for in-line imaging as well as sampling of both the "blood" and "brain" sides.
- GelMA can be mechanically tuned and can hold a lumen shape.
    - Holding a lumen shape for long-term cell culture was the original goal, as developing an AD model would eventually require iPSC brain cells of the APOE 3/3 and 4/4 allele to be embedded into the hydrogel and allow them time to secrete amyloid plaque.

After realizing that the astrocytes and HBMECs were not compatible with GelMA in 3D (either in a well-plate or in-chip), and after seeing many instances of leakage with this chip design, this led to a simpler, more feasible microfluidic chip design, which was the planar 2D microfluidic chip, described in Chapter 3.

Originally, for the planar 2D chip, the complexity of including a hydrogel was removed; although, the aspect of including a static top reservoir to mimic the brain was added. This was a decision made with both collaborators, as it more closely represents the negligible flow present in the brain. This design consideration required the top channel to increase in height to ensure surface area to volume ratio was similar to that seen in standard cell culture. For instance, a 1 mm^2 cell area should have a height of approximately 5mm to ensure proper nutrient supply for multiple days. This is what is seen in Transwell® co-cultures, which have a 1:5 ratio. There were a few limitations that became evident after moving from the conceptualization phase to the fabrication phase of this planar 2D design (known as Design #1 in Chapter 3:). A few of the limitations associated with Design #1 are listed below.

- Including a PDMS layer with a height of >1mm was challenging to fabricate at a traditional photolithography facility, based on the limitations of the depth of penetration into the light-sensitive polymer.
    - This resulted in the need to use non-traditional methods (such as 3D printing) to produce these molds.
- The surface finish of the SLA molds was not sufficient to allow for PDMS-PDMS bonding.
- The cells were not confined to the bottom channel, based on a lack of compression on the membrane from the PDMS-PDMS sandwich that was holding it in place.

Design #1 was adjusted to include a top reservoir with a smaller width and an acrylic base into the printed part (now termed Design #2). This allowed cells to be confined to the channel; although now there were further limitations realized with Design #2. These are described blow.

- The imperfect fit of the acrylic base into the SLA mold resulted in a non-flat membrane which allowed leakage between the bottom and top channels.
- Adding the acrylic-base into the SLA mold resulted in needing more time to allow PDMS to cure (~2 days) since some of the PDMS would seep under the acrylic.

Upon realizing that the imperfect channel geometry was a factor in the amount of failed chips present, it was evident that a new method to create the master mold was needed, and this was the reasoning behind acquiring a DLP printer that was specifically made for PDMS master mold printing. At this stage, the PDMS-PDMS bonding issue was resolved, and more systematic errors were realized and further optimized. This includes:

- The insufficient sealing of the needles.
    - Using a higher gauge needle to make the mold of the inlets/outlets helped create a pressure-fitting inlet/outlet.
    - Using a PDMS moat surrounding the chip, needles and tubing led to a leak-free chip.

Throughout the transition from chip Design #2 to chip Design #3, I was consistently working to develop the cellular environment in parallel. Since the endothelial cells build up the wall of the blood vessel and provides the ability to regulate transport into the brain, it is very important to optimize parameters for this cell type first. Keeping in mind that the endothelial cell barrier will not be fully optimized until glial cells are added to the system, this led me to focus on defining the ECM coating, cell seeding density and duration of the experiment needed to form a confluent monolayer.

At this point, when using HBMECs, recommended starting parameters include:

- Using a coating of collagen IV (400 μg/mL), laminin (10 μg/mL) and fibronectin (100 μg/mL).
- Using a seeding density of at least 5 million cells/mL.
- Keeping the chips on pump for at least 5 days to allow the HBMECs to form a confluent monolayer.
    - Keeping in mind that further optimization will need to be performed.

Additionally, I would like to acknowledge the limitations of the HBMECs used in these experiments, as they were often used at passage 6, even though their supplier recommends to not expand these cells. Therefore, I would recommend using earlier passage number, if financially feasible.

At this point, many challenges associated with developing new microfluidic platforms have been overcome, and I believe that these findings will be beneficial to anyone who is working to develop a capillary model.

5.1.1 Future work associated with capillary model

Future work associated with the development of the 2D planar capillary chip involves further improvements to the physical microfluidic system, as well as the cellular environment. This is further described below.

5.1.1.1 Physical microfluidic system

Future work for the physical microfluidic system includes investigating a method to effectively incorporate higher flow rates into the system while reducing systematic errors. Recommendations for next steps are listed below.

- Switching to using a peristaltic pump to allow for higher flow rates while limiting the volume of reagents being used.
- Adjusting the method of connection between the chips' microbore tubing, and standard larger bore tubing that comes with peristaltic pumps.
    - Using autoclavable adapters would allow for the full tubing system to be assembled before taking it into the BSC to connect with the microfluidic chip.
- Implementing the ability to use a pipette when seeding cells.
    - Using a syringe does not provide accurate volumes to be dispensed into the chip, and it leads to needing a high safety factor (~5x volume in chip) when preparing to seed cells. The current system uses tubing with a small inner diameter that does not permit the use of standard P200 pipette tips to fit. There are luer-to-port adapters that can fit onto luer-lock dispensing tips, and this could serve to increase the diameter which could allow for a pipette to fit. Alternatively, changing the inlet/outlet needles to be slightly larger would allow for a larger bore tubing to be used, and this could potentially fit a pipette tip.
- Implement a method of reducing number of bubbles that encounter the cell culture area. Areas to explore include:
    - Implementing a degassing step when preparing media to perfuse through the system.

- Including either an in-line bubble trap or an on-chip bubble trap. Although, adding a bubble trap will increase the complexity of the chip, as more inlet and/or membrane interfaces would be required.

- Improve the in-line imaging capabilities of the chip. Areas to explore include:
  - Incorporating a thinner bottom layer (<2mm) of PDMS.
    - Thin PDMS can rupture during the PDMS-PDMS bonding stage of chip fabrication.
  - Implementing a coverslip glass at the channel interface.
    - Cover glass can shatter during the PDMS-glass bonding steps of chip fabrication.
- Improve the quality of the surface finish of the PDMS layers. Areas to explore include:
  - Adjusting the printing parameters used and quantifying the surface finish by the smoothness of the PDMS layers using scanning electron microscopy (SEM).
- Scaling production of the chips. This could be achieved by:
  - Changing the design of the chip to allow for instant connection with the pump of choice and adding an external or larger reservoir of media to the top channel to allow for less frequent media exchanges (>2 days). Once these adjustments are made and validated using low-cost PDMS as the polymer for making the multi-layered device, then looking into polymers that can be manufactured in higher throughput using techniques such as hot embossing would be suitable.

5.1.1.2 Cellular environment

As the physical system has been optimized to reduce leakage and systematic errors throughout the experiment, the cell layer would now be the primary focus of optimization.

The parameters selected in this work were based on literature review and preliminary experiments, typically using one experimental replicate. Developing a consistent endothelial monolayer will require more optimization of the microenvironment. Recommended next steps include:

- Optimizing the ECM coating experiment within the actual microfluidic chip and repeating the experiment 3x with at least 4 replicates to identify a finalized solution of ECM to use, and the respective individual protein concentrations.
    - Including the concentrations used in this thesis in the experiment: collagen IV (400 μg/mL), laminin (10 μg/mL) and fibronectin (100 μg/mL).
    - Quantifying the endothelial monolayer for confluency and tight junction maturity to conclude on what coating to use.
- Adding factors to the media to further enhance the endothelial monolayer.
    - For instance, Gray *et al.* demonstrated an increase in mature junction when treating HBMECs with cAMP (97).
- Optimizing the microenvironment for glial cells.
    - Use ratios of pericytes:astrocyte cells as seen in the human brain.
    - Use a mixed media that contains the same ratio of pericyte:astrocyte media in the top channel.

Once the BBB model is established, it can then be used for investigating AD pathology. To investigate AD, recommended next steps include:

- Following the methodology described by Robert *et al.* (22). This includes using recombinant Aß40 and Aß42 and adding it into the "brain" side of the microfluidic chip to represent Aß that is present in aging individuals.
- Using HDL from normolipidemic individuals and testing HDL's effect on clearing the Aß from the brain.
- Move away from primary cells to using iPSC lines from different APOE genotyped individuals and differentiating the iPSCs into glial cells that would produce endogenous Aß in the "brain" channel and see if the effects remain.

5.2 Summary of tissue chamber modifications

Advancements to the tissue chamber have been made to allow for in-line sampling and improve the robustness of the overall system by creating custom pressure-fitting end caps. To fit the sampling ports, the size and the material of the tissue chamber tubing had to be adjusted, and therefore, experiments have been performed to identify if these adjustments had any negative effects on bubble formation within the tissue chamber. After running the modified bioreactor with circulating flow and monitoring for bubbles, it was observed that the newly designed tissue chamber had similar bubble formation as seen with the old design. This led to the conclusion that future experiments should be conducted with the new design, and that more frequent media exchanges should occur (<7 days).

5.2.1 Future work associated with tissue chamber

Future work associated with the tissue chamber include getting feedback on the ease of assembling the tissue chamber from multiple individuals within UBC and at other institutions. Additionally, as this system has been previously used to study Aß clearance, recommended next steps include:

- Performing Aß adsorption tests on the tissue chamber tubing and the end-caps.
    - If there are issues with adsorption in the tubing, I would recommend seeking a new tubing that has the same inner dimeter, thickness, and autoclavability and doing a similar test.
    - Further, if there is Aß adsorption into the end-caps, I would outsource manufacturing of the end-caps to a hot embossing facility, and select polypropylene as the material, as this has been previously reported to have low adsorption properties (133).

Bibliography

1. Bennet TJ, Shen B, Siwik J, Pan S. Airway-on-a-Chip: Development and in Vitro Validation of a Microfluidic Cell Culture Model for Chronic Obstructive Pulmonary Disease. 2020 IEEE 33rd …. 2020;
2. Uhl EW, Warner NJ. Mouse models as predictors of human responses: evolutionary medicine. Curr Pathobiol Rep. 2015;3(3):219–223.
3. Hodge RD, Bakken TE, Miller JA, Smith KA, Barkan ER, Graybuck LT, et al. Conserved cell types with divergent features in human versus mouse cortex. Nature. 2019 Sep;573(7772):61–68.
4. Chiaradia I, Lancaster MA. Brain organoids for the study of human neurobiology at the interface of in vitro and in vivo. Nat Neurosci. 2020 Dec;23(12):1496–1508.
5. Sidhaye J, Knoblich JA. Brain organoids: an ensemble of bioassays to investigate human neurodevelopment and disease. Cell Death Differ. 2021 Jan;28(1):52–67.
6. Qian X, Song H, Ming G-L. Brain organoids: advances, applications and challenges. Development. 2019 Apr 16;146(8).
7. Whitesides GM, Ostuni E, Takayama S, Jiang X, Ingber DE. Soft lithography in biology and biochemistry. Annu Rev Biomed Eng. 2001;3:335–373.
8. Cucullo L, Hossain M, Puvenna V, Marchi N, Janigro D. The role of shear stress in Blood-Brain Barrier endothelial physiology. BMC Neurosci. 2011 May 11;12:40.
9. Garcia-Polite F, Martorell J, Del Rey-Puech P, Melgar-Lesmes P, O'Brien CC, Roquer J, et al. Pulsatility and high shear stress deteriorate barrier phenotype in brain microvascular endothelium. J Cereb Blood Flow Metab. 2017 Jul;37(7):2614–2625.

10. DeStefano JG, Xu ZS, Williams AJ, Yimam N, Searson PC. Effect of shear stress on iPSC-derived human brain microvascular endothelial cells (dhBMECs). Fluids Barriers CNS. 2017 Aug 4;14(1):20.

11. Reinitz A, DeStefano J, Ye M, Wong AD, Searson PC. Human brain microvascular endothelial cells resist elongation due to shear stress. Microvasc Res. 2015 May;99:8–18.

12. Wang YI, Abaci HE, Shuler ML. Microfluidic blood-brain barrier model provides in vivo-like barrier properties for drug permeability screening. Biotechnol Bioeng. 2017 Jan;114(1):184–194.

13. Gray KM, Stroka KM. Vascular endothelial cell mechanosensing: New insights gained from biomimetic microfluidic models. Semin Cell Dev Biol. 2017 Nov;71:106–117.

14. Onken MD, Mooren OL, Mukherjee S, Shahan ST, Li J, Cooper JA. Endothelial monolayers and transendothelial migration depend on mechanical properties of the substrate. Cytoskeleton (Hoboken). 2014 Dec;71(12):695–706.

15. Georges PC, Miller WJ, Meaney DF, Sawyer ES, Janmey PA. Matrices with compliance comparable to that of brain tissue select neuronal over glial growth in mixed cortical cultures. Biophys J. 2006 Apr 15;90(8):3012–3018.

16. Canfield SG, Stebbins MJ, Faubion MG, Gastfriend BD, Palecek SP, Shusta EV. An isogenic neurovascular unit model comprised of human induced pluripotent stem cell-derived brain microvascular endothelial cells, pericytes, astrocytes, and neurons. Fluids Barriers CNS. 2019 Aug 7;16(1):25.

17. Patterson C. World alzheimer report 2018. 2018;

18. Deane R, Sagare A, Hamm K, Parisi M, Lane S, Finn MB, et al. apoE isoform-specific disruption of amyloid beta peptide clearance from mouse brain. J Clin Invest. 2008 Dec;118(12):4002–4013.

19. Nielsen HM, Chen K, Lee W, Chen Y, Bauer RJ, Reiman E, et al. Peripheral apoE isoform levels in cognitively normal APOE ε3/ε4 individuals are associated with regional gray matter volume and cerebral glucose metabolism. Alzheimers Res Ther. 2017 Jan 30;9(1):5.

20. Sacre SM, Stannard AK, Owen JS. Apolipoprotein E (apoE) isoforms differentially induce nitric oxide production in endothelial cells. FEBS Lett. 2003 Apr 10;540(1-3):181–187.

21. Robert J, Stukas S, Button E, Cheng WH, Lee M, Fan J, et al. Reconstituted high-density lipoproteins acutely reduce soluble brain Aβ levels in symptomatic APP/PS1 mice. Biochim Biophys Acta. 2016 May;1862(5):1027–1036.

22. Robert J, Button EB, Yuen B, Gilmour M, Kang K, Bahrabadi A, et al. Clearance of beta-amyloid is facilitated by apolipoprotein E and circulating high-density lipoproteins in bioengineered human vessels. Elife. 2017 Oct 10;6.

23. Sweeney MD, Kisler K, Montagne A, Toga AW, Zlokovic BV. The role of brain vasculature in neurodegenerative disorders. Nat Neurosci. 2018 Oct;21(10):1318–1331.

24. Schaeffer S, Iadecola C. Revisiting the neurovascular unit. Nat Neurosci. 2021 Sep;24(9):1198–1209.

25. Cipolla MJ. The Cerebral Circulation. Colloquium Series on Integrated Systems Physiology: From Molecule to Function. 2009 Jan;1(1):1–59.

26. Bell RD, Winkler EA, Sagare AP, Singh I, LaRue B, Deane R, et al. Pericytes control key neurovascular functions and neuronal phenotype in the adult brain and during brain aging. Neuron. 2010 Nov 4;68(3):409–427.

27. Armulik A, Genové G, Mäe M, Nisancioglu MH, Wallgard E, Niaudet C, et al. Pericytes regulate the blood-brain barrier. Nature. 2010 Nov 25;468(7323):557–561.

28. Thanabalasundaram G, Schneidewind J, Pieper C, Galla H-J. The impact of pericytes on the blood-brain barrier integrity depends critically on the pericyte differentiation stage. Int J Biochem Cell Biol. 2011 Sep;43(9):1284–1293.

29. Yang AC, Stevens MY, Chen MB, Lee DP, Stähli D, Gate D, et al. Physiological blood-brain transport is impaired with age by a shift in transcytosis. Nature. 2020 Jul 1;583(7816):425–430.

30. Keaney J, Campbell M. The dynamic blood-brain barrier. FEBS J. 2015 Nov;282(21):4067–4079.

31. Ben-Zvi A, Lacoste B, Kur E, Andreone BJ, Mayshar Y, Yan H, et al. Mfsd2a is critical for the formation and function of the blood-brain barrier. Nature. 2014 May 22;509(7501):507–511.

32. Jamieson JJ, Linville RM, Ding YY, Gerecht S, Searson PC. Role of iPSC-derived pericytes on barrier function of iPSC-derived brain microvascular endothelial cells in 2D and 3D. Fluids Barriers CNS. 2019 Jun 6;16(1):15.

33. Ito R, Umehara K, Suzuki S, Kitamura K, Nunoya K-I, Yamaura Y, et al. A Human Immortalized Cell-Based Blood-Brain Barrier Triculture Model: Development and Characterization as a Promising Tool for Drug-Brain Permeability Studies. Mol Pharm. 2019 Nov 4;16(11):4461–4471.

34. Appelt-Menzel A, Cubukova A, Günther K, Edenhofer F, Piontek J, Krause G, et al. Establishment of a Human Blood-Brain Barrier Co-culture Model Mimicking the

Neurovascular Unit Using Induced Pluri- and Multipotent Stem Cells. Stem Cell Rep. 2017 Apr 11;8(4):894–906.

35. Lippmann ES, Al-Ahmad A, Azarin SM, Palecek SP, Shusta EV. A retinoic acid-enhanced, multicellular human blood-brain barrier model derived from stem cell sources. Sci Rep. 2014 Feb 24;4:4160.

36. Yamazaki Y, Shinohara M, Yamazaki A, Ren Y, Asmann YW, Kanekiyo T, et al. ApoE (Apolipoprotein E) in Brain Pericytes Regulates Endothelial Function in an Isoform-Dependent Manner by Modulating Basement Membrane Components. Arterioscler Thromb Vasc Biol. 2020 Jan;40(1):128–144.

37. Grubb S, Cai C, Hald BO, Khennouf L, Murmu RP, Jensen AGK, et al. Precapillary sphincters maintain perfusion in the cerebral cortex. Nat Commun. 2020 Jan 20;11(1):395.

38. Hamilton NB, Attwell D, Hall CN. Pericyte-mediated regulation of capillary diameter: a component of neurovascular coupling in health and disease. Front Neuroenergetics. 2010 May 21;2.

39. Kovacs-Oller T, Ivanova E, Bianchimano P, Sagdullaev BT. The pericyte connectome: spatial precision of neurovascular coupling is driven by selective connectivity maps of pericytes and endothelial cells and is disrupted in diabetes. Cell Discov. 2020 Jun 16;6:39.

40. Rustenhoven J, Jansson D, Smyth LC, Dragunow M. Brain pericytes as mediators of neuroinflammation. Trends Pharmacol Sci. 2017 Mar;38(3):291–304.

41. Herland A, van der Meer AD, FitzGerald EA, Park T-E, Sleeboom JJF, Ingber DE. Distinct Contributions of Astrocytes and Pericytes to Neuroinflammation Identified in a 3D Human Blood-Brain Barrier on a Chip. PLoS One. 2016 Mar 1;11(3):e0150360.

42. Brown LS, Foster CG, Courtney J-M, King NE, Howells DW, Sutherland BA. Pericytes and neurovascular function in the healthy and diseased brain. Front Cell Neurosci. 2019 Jun 28;13:282.

43. Sweeney MD, Zhao Z, Montagne A, Nelson AR, Zlokovic BV. Blood-Brain Barrier: From Physiology to Disease and Back. Physiol Rev. 2019 Jan 1;99(1):21–78.

44. Abbott NJ. Astrocyte-endothelial interactions and blood-brain barrier permeability. J Anat. 2002 Jun;200(6):629–638.

45. Heithoff BP, George KK, Phares AN, Zuidhoek IA, Munoz-Ballester C, Robel S. Astrocytes are necessary for blood-brain barrier maintenance in the adult mouse brain. Glia. 2021 Feb;69(2):436–472.

46. Petzold GC, Murthy VN. Role of astrocytes in neurovascular coupling. Neuron. 2011 Sep 8;71(5):782–797.

47. Liu C-Y, Yang Y, Ju W-N, Wang X, Zhang H-L. Emerging Roles of Astrocytes in Neuro-Vascular Unit and the Tripartite Synapse With Emphasis on Reactive Gliosis in the Context of Alzheimer's Disease. Front Cell Neurosci. 2018 Jul 10;12:193.

48. Hyvärinen T, Hagman S, Ristola M, Sukki L, Veijula K, Kreutzer J, et al. Co-stimulation with IL-1β and TNF-α induces an inflammatory reactive astrocyte phenotype with neurosupportive characteristics in a human pluripotent stem cell model system. Sci Rep. 2019 Nov 15;9(1):16944.

49. Giovannoni F, Quintana FJ. The role of astrocytes in CNS inflammation. Trends Immunol. 2020 Sep;41(9):805–819.

50. Macaulay N, Zeuthen T. Glial K^+ clearance and cell swelling: key roles for cotransporters and pumps. Neurochem Res. 2012 Nov;37(11):2299–2309.

51. Araque A, Carmignoto G, Haydon PG. Dynamic signaling between astrocytes and neurons. Annu Rev Physiol. 2001;63:795–813.

52. Fellin T. Communication between neurons and astrocytes: relevance to the modulation of synaptic and network activity. J Neurochem. 2009 Feb;108(3):533–544.

53. Mathiisen TM, Lehre KP, Danbolt NC, Ottersen OP. The perivascular astroglial sheath provides a complete covering of the brain microvessels: an electron microscopic 3D reconstruction. Glia. 2010 Jul;58(9):1094–1103.

54. Kubotera H, Ikeshima-Kataoka H, Hatashita Y, Allegra Mascaro AL, Pavone FS, Inoue T. Astrocytic endfeet re-cover blood vessels after removal by laser ablation. Sci Rep. 2019 Feb 4;9(1):1263.

55. Spampinato SF, Bortolotto V, Canonico PL, Sortino MA, Grilli M. Astrocyte-Derived Paracrine Signals: Relevance for Neurogenic Niche Regulation and Blood-Brain Barrier Integrity. Front Pharmacol. 2019 Nov 21;10:1346.

56. Menezes MJ, McClenahan FK, Leiton CV, Aranmolate A, Shan X, Colognato H. The extracellular matrix protein laminin α2 regulates the maturation and function of the blood-brain barrier. J Neurosci. 2014 Nov 12;34(46):15260–15280.

57. Wuest DM, Wing AM, Lee KH. Membrane configuration optimization for a murine in vitro blood-brain barrier model. J Neurosci Methods. 2013 Jan 30;212(2):211–221.

58. Tao-Cheng JH, Nagy Z, Brightman MW. Tight junctions of brain endothelium in vitro are enhanced by astroglia. J Neurosci. 1987 Oct;7(10):3293–3299.

59. Lee S-W, Kim WJ, Choi YK, Song HS, Son MJ, Gelman IH, et al. SSeCKS regulates angiogenesis and tight junction formation in blood-brain barrier. Nat Med. 2003 Jul;9(7):900–906.

60. Neal EH, Marinelli NA, Shi Y, McClatchey PM, Balotin KM, Gullett DR, et al. A Simplified, Fully Defined Differentiation Scheme for Producing Blood-Brain Barrier Endothelial Cells from Human iPSCs. Stem Cell Rep. 2019 Jun 11;12(6):1380–1388.

61. Katt ME, Xu ZS, Gerecht S, Searson PC. Human Brain Microvascular Endothelial Cells Derived from the BC1 iPS Cell Line Exhibit a Blood-Brain Barrier Phenotype. PLoS One. 2016 Apr 12;11(4):e0152105.

62. Canfield SG, Stebbins MJ, Morales BS, Asai SW, Vatine GD, Svendsen CN, et al. An isogenic blood-brain barrier model comprising brain endothelial cells, astrocytes, and neurons derived from human induced pluripotent stem cells. J Neurochem. 2017 Mar;140(6):874–888.

63. Oberheim NA, Takano T, Han X, He W, Lin JHC, Wang F, et al. Uniquely hominid features of adult human astrocytes. J Neurosci. 2009 Mar 11;29(10):3276–3287.

64. Middeldorp J, Boer K, Sluijs JA, De Filippis L, Encha-Razavi F, Vescovi AL, et al. GFAPdelta in radial glia and subventricular zone progenitors in the developing human cortex. Development. 2010 Jan;137(2):313–321.

65. Guttenplan KA, Liddelow SA. Astrocytes and microglia: Models and tools. J Exp Med. 2019 Jan 7;216(1):71–83.

66. Zhang Y, Sloan SA, Clarke LE, Caneda C, Plaza CA, Blumenthal PD, et al. Purification and Characterization of Progenitor and Mature Human Astrocytes Reveals Transcriptional and Functional Differences with Mouse. Neuron. 2016 Jan 6;89(1):37–53.

67. Thomsen MS, Routhe LJ, Moos T. The vascular basement membrane in the healthy and pathological brain. J Cereb Blood Flow Metab. 2017 Oct;37(10):3300–3317.

68. Reed MJ, Damodarasamy M, Banks WA. The extracellular matrix of the blood-brain barrier: structural and functional roles in health, aging, and Alzheimer's disease. Tissue Barriers. 2019 Sep 11;7(4):1651157.

69. Ljubimova JY, Fujita M, Khazenzon NM, Ljubimov AV, Black KL. Changes in laminin isoforms associated with brain tumor invasion and angiogenesis. Front Biosci. 2006 Jan 1;11:81–88.

70. Thomsen MS, Birkelund S, Burkhart A, Stensballe A, Moos T. Synthesis and deposition of basement membrane proteins by primary brain capillary endothelial cells in a murine model of the blood–brain barrier. J Neurochem. 2017 Mar;140(5).

71. Hallmann R, Hannocks M-J, Song J, Zhang X, Di Russo J, Luik A-L, et al. The role of basement membrane laminins in vascular function. Int J Biochem Cell Biol. 2020 Oct;127:105823.

72. Yurchenco PD. Integrating Activities of Laminins that Drive Basement Membrane Assembly and Function. Curr Top Membr. 2015 Jun 25;76:1–30.

73. McKee KK, Harrison D, Capizzi S, Yurchenco PD. Role of laminin terminal globular domains in basement membrane assembly. J Biol Chem. 2007 Jul 20;282(29):21437–21447.

74. Eigenmann DE, Xue G, Kim KS, Moses AV, Hamburger M, Oufir M. Comparative study of four immortalized human brain capillary endothelial cell lines, hCMEC/D3, hBMEC, TY10, and BB19, and optimization of culture conditions, for an in vitro blood-brain barrier model for drug permeability studies. Fluids Barriers CNS. 2013 Nov 22;10(1):33.

75. Gray KM, Katz DB, Brown EG, Stroka KM. Quantitative Phenotyping of Cell-Cell Junctions to Evaluate ZO-1 Presentation in Brain Endothelial Cells. Ann Biomed Eng. 2019 Jul;47(7):1675–1687.

76. Tilling T, Korte D, Hoheisel D, Galla HJ. Basement membrane proteins influence brain capillary endothelial barrier function in vitro. J Neurochem. 1998 Sep;71(3):1151–1157.

77. Relou IA, Damen CA, van der Schaft DW, Groenewegen G, Griffioen AW. Effect of culture conditions on endothelial cell growth and responsiveness. Tissue Cell. 1998 Oct;30(5):525–530.

78. Seo S, Kim H, Sung JH, Choi N, Lee K, Kim HN. Microphysiological systems for recapitulating physiology and function of blood-brain barrier. Biomaterials. 2020 Feb;232:119732.

79. Kaarj K, Yoon J-Y. Methods of Delivering Mechanical Stimuli to Organ-on-a-Chip. Micromachines (Basel). 2019 Oct 14;10(10).

80. Ando J, Yamamoto K. Effects of shear stress and stretch on endothelial function. Antioxid Redox Signal. 2011 Sep 1;15(5):1389–1403.

81. Holmgren M, Wåhlin A, Dunås T, Malm J, Eklund A. Assessment of cerebral blood flow pulsatility and cerebral arterial compliance with 4D flow MRI. J Magn Reson Imaging. 2020 May;51(5):1516–1525.

82. DeStefano JG, Jamieson JJ, Linville RM, Searson PC. Benchmarking in vitro tissue-engineered blood-brain barrier models. Fluids Barriers CNS. 2018 Dec 4;15(1):32.

83. Koutsiaris AG, Tachmitzi SV, Batis N, Kotoula MG, Karabatsas CH, Tsironi E, et al. Volume flow and wall shear stress quantification in the human conjunctival capillaries and post-capillary venules in vivo. Biorheology. 2007;44(5-6):375–386.

84. Poon C. Measuring the density and viscosity of culture media for optimized computational fluid dynamics analysis of *in vitro* devices. BioRxiv. 2020 Aug 25;

85. Maalouf A, Gadonna M, Bosc D. An improvement in standard photolithography resolution based on Kirchhoff diffraction studies. J Phys D, Appl Phys. 2009 Jan 7;42(1):015106.

86. Hwang Y, Paydar OH, Candler RN. 3D printed molds for non-planar PDMS microfluidic channels. Sensors and Actuators A: Physical. 2015 May;226:137–142.

87. Linville RM, DeStefano JG, Sklar MB, Chu C, Walczak P, Searson PC. Modeling hyperosmotic blood-brain barrier opening within human tissue-engineered in vitro brain microvessels. J Cereb Blood Flow Metab. 2020;40(7):1517–1532.

88. Griep LM, Wolbers F, de Wagenaar B, ter Braak PM, Weksler BB, Romero IA, et al. BBB on chip: microfluidic platform to mechanically and biochemically modulate blood-brain barrier function. Biomed Microdevices. 2013 Feb;15(1):145–150.

89. Park T-E, Mustafaoglu N, Herland A, Hasselkus R, Mannix R, FitzGerald EA, et al. Hypoxia-enhanced Blood-Brain Barrier Chip recapitulates human barrier function and shuttling of drugs and antibodies. Nat Commun. 2019 Jun 13;10(1):2621.

90. Maoz BM, Herland A, Henry OYF, Leineweber WD, Yadid M, Doyle J, et al. Organs-on-Chips with combined multi-electrode array and transepithelial electrical resistance measurement capabilities. Lab Chip. 2017 Jun 27;17(13):2294–2302.

91. Chueh B, Huh D, Kyrtsos CR, Houssin T, Futai N, Takayama S. Leakage-free bonding of porous membranes into layered microfluidic array systems. Anal Chem. 2007 May 1;79(9):3504–3508.

92. Sip CG, Folch A. Stable chemical bonding of porous membranes and poly(dimethylsiloxane) devices for long-term cell culture. Biomicrofluidics. 2014 May;8(3):036504.

93. Sellgren KL, Butala EJ, Gilmour BP, Randell SH, Grego S. A biomimetic multicellular model of the airways using primary human cells. Lab Chip. 2014 Sep 7;14(17):3349–3358.

94. Hemmilä S, Cauich-Rodríguez JV, Kreutzer J, Kallio P. Rapid, simple, and cost-effective treatments to achieve long-term hydrophilic PDMS surfaces. Appl Surf Sci. 2012 Oct;258(24):9864–9875.

95. Stone NL, England TJ, O'Sullivan SE. A novel transwell blood brain barrier model using primary human cells. Front Cell Neurosci. 2019 Jun 6;13:230.

96. Sances S, Ho R, Vatine G, West D, Laperle A, Meyer A, et al. Human iPSC-Derived Endothelial Cells and Microengineered Organ-Chip Enhance Neuronal Development. Stem Cell Rep. 2018 Apr 10;10(4):1222–1236.

97. Gray KM, Jung JW, Inglut CT, Huang H-C, Stroka KM. Quantitatively relating brain endothelial cell-cell junction phenotype to global and local barrier properties under varied culture conditions via the Junction Analyzer Program. Fluids Barriers CNS. 2020 Feb 11;17(1):16.

98. Katt ME, Linville RM, Mayo LN, Xu ZS, Searson PC. Functional brain-specific microvessels from iPSC-derived human brain microvascular endothelial cells: the role of matrix composition on monolayer formation. Fluids Barriers CNS. 2018 Feb 20;15(1):7.

99. Katt ME, Shusta EV. In vitro Models of the Blood-Brain Barrier: Building in physiological complexity. Curr Opin Chem Eng. 2020 Dec;30:42–52.

100. Adriani G, Ma D, Pavesi A, Kamm RD, Goh ELK. A 3D neurovascular microfluidic model consisting of neurons, astrocytes and cerebral endothelial cells as a blood-brain barrier. Lab Chip. 2017 Jan 31;17(3):448–459.

101. Wevers NR, Kasi DG, Gray T, Wilschut KJ, Smith B, van Vught R, et al. A perfused human blood-brain barrier on-a-chip for high-throughput assessment of barrier function and antibody transport. Fluids Barriers CNS. 2018 Aug 31;15(1):23.

102. Shin Y, Choi SH, Kim E, Bylykbashi E, Kim JA, Chung S, et al. Blood-Brain Barrier Dysfunction in a 3D In Vitro Model of Alzheimer's Disease. Adv Sci (Weinh). 2019 Oct 16;6(20):1900962.

103. Lee S, Chung M, Lee S-R, Jeon NL. 3D brain angiogenesis model to reconstitute functional human blood-brain barrier in vitro. Biotechnol Bioeng. 2020 Mar;117(3):748–762.

104. Winkelman MA, Kim DY, Kakarla S, Grath A, Silvia N, Dai G. Interstitial flow enhances the formation, connectivity, and function of 3D brain microvascular networks generated within a microfluidic device. Lab Chip. 2021 Dec 21;22(1):170–192.

105. Partyka PP, Godsey GA, Galie JR, Kosciuk MC, Acharya NK, Nagele RG, et al. Mechanical stress regulates transport in a compliant 3D model of the blood-brain barrier. Biomaterials. 2017;115:30–39.

106. Faley SL, Neal EH, Wang JX, Bosworth AM, Weber CM, Balotin KM, et al. iPSC-Derived Brain Endothelium Exhibits Stable, Long-Term Barrier Function in Perfused Hydrogel Scaffolds. Stem Cell Rep. 2019 Mar 5;12(3):474–487.

107. van Dijk CGM, Brandt MM, Poulis N, Anten J, van der Moolen M, Kramer L, et al. A new microfluidic model that allows monitoring of complex vascular structures and cell interactions in a 3D biological matrix. Lab Chip. 2020 May 19;20(10):1827–1844.

108. Bouhrira N, DeOre BJ, Sazer DW, Chiaradia Z, Miller JS, Galie PA. Disturbed flow disrupts the blood-brain barrier in a 3D bifurcation model. Biofabrication. 2020 Feb 27;12(2):025020.

109. Yu F, Kumar NDS, Foo LC, Ng SH, Hunziker W, Choudhury D. A pump-free tricellular blood-brain barrier on-a-chip model to understand barrier property and evaluate drug response. Biotechnol Bioeng. 2020 Apr;117(4):1127–1136.

110. Moya ML, Triplett M, Simon M, Alvarado J, Booth R, Osburn J, et al. A Reconfigurable In Vitro Model for Studying the Blood-Brain Barrier. Ann Biomed Eng. 2020 Feb;48(2):780–793.

111. Dessalles CA, Ramón-Lozano C, Babataheri A, Barakat AI. Luminal flow actuation generates coupled shear and strain in a microvessel-on-chip. Biofabrication. 2021 Oct 20;14(1).

112. Linville RM, DeStefano JG, Sklar MB, Xu Z, Farrell AM, Bogorad MI, et al. Human iPSC-derived blood-brain barrier microvessels: validation of barrier function and endothelial cell behavior. Biomaterials. 2019;190-191:24–37.

113. Grifno GN, Farrell AM, Linville RM, Arevalo D, Kim JH, Gu L, et al. Tissue-engineered blood-brain barrier models via directed differentiation of human induced pluripotent stem cells. Sci Rep. 2019 Sep 27;9(1):13957.

114. Seo S, Choi C-H, Yi KS, Kim SU, Lee K, Choi N, et al. An engineered neurovascular unit for modeling neuroinflammation. Biofabrication. 2021 May 5;13(3).

115. Park J, Wetzel I, Marriott I, Dréau D, D'Avanzo C, Kim DY, et al. A 3D human triculture system modeling neurodegeneration and neuroinflammation in Alzheimer's disease. Nat Neurosci. 2018 Jul;21(7):941–951.

116. Blanchard JW, Bula M, Davila-Velderrain J, Akay LA, Zhu L, Frank A, et al. Reconstruction of the human blood-brain barrier in vitro reveals a pathogenic mechanism of APOE4 in pericytes. Nat Med. 2020 Jun 8;26(6):952–963.

117. Arulmoli J, Wright HJ, Phan DTT, Sheth U, Que RA, Botten GA, et al. Combination scaffolds of salmon fibrin, hyaluronic acid, and laminin for human neural stem cell and vascular tissue engineering. Acta Biomater. 2016 Oct 1;43:122–138.

118. O'Grady BJ, Balotin KM, Bosworth AM, McClatchey PM, Weinstein RM, Gupta M, et al. Development of an N-Cadherin Biofunctionalized Hydrogel to Support the Formation of Synaptically Connected Neural Networks. ACS Biomater Sci Eng. 2020 Oct 12;6(10):5811–5822.

119. Potjewyd G, Kellett KAB, Hooper NM. 3D hydrogel models of the neurovascular unit to investigate blood-brain barrier dysfunction. Neuronal Signal. 2021 Dec;5(4):NS20210027.

120. Takamura T, Motosugi U, Sasaki Y, Kakegawa T, Sato K, Glaser KJ, et al. Influence of Age on Global and Regional Brain Stiffness in Young and Middle-Aged Adults. J Magn Reson Imaging. 2020 Mar;51(3):727–733.

121. Tcw J, Wang M, Pimenova AA, Bowles KR, Hartley BJ, Lacin E, et al. An Efficient Platform for Astrocyte Differentiation from Human Induced Pluripotent Stem Cells. Stem Cell Rep. 2017 Aug 8;9(2):600–614.

122. Preman P, Tcw J, Calafate S, Snellinx A, Alfonso-Triguero M, Corthout N, et al. Human iPSC-derived astrocytes transplanted into the mouse brain undergo morphological changes in response to amyloid-β plaques. Mol Neurodegener. 2021 Sep 25;16(1):68.

123. Lippmann ES, Azarin SM, Kay JE, Nessler RA, Wilson HK, Al-Ahmad A, et al. Derivation of blood-brain barrier endothelial cells from human pluripotent stem cells. Nat Biotechnol. 2012 Aug;30(8):783–791.

124. Soofi SS, Last JA, Liliensiek SJ, Nealey PF, Murphy CJ. The elastic modulus of Matrigel as determined by atomic force microscopy. J Struct Biol. 2009 Sep;167(3):216–219.

125. Okumura N, Ueno M, Koizumi N, Sakamoto Y, Hirata K, Hamuro J, et al. Enhancement on primate corneal endothelial cell survival in vitro by a ROCK inhibitor. Invest Ophthalmol Vis Sci. 2009 Aug;50(8):3680–3687.

126. Heo YS, Cabrera LM, Song JW, Futai N, Tung Y-C, Smith GD, et al. Characterization and resolution of evaporation-mediated osmolality shifts that constrain microfluidic cell culture in poly(dimethylsiloxane) devices. Anal Chem. 2007 Feb 1;79(3):1126–1134.

127. Duffy DC, McDonald JC, Schueller OJ, Whitesides GM. Rapid Prototyping of Microfluidic Systems in Poly(dimethylsiloxane). Anal Chem. 1998 Dec 1;70(23):4974–4984.

128. Razavi Bazaz S, Kashaninejad N, Azadi S, Patel K, Asadnia M, Jin D, et al. Rapid softlithography using 3d-printed molds. Adv Mater Technol. 2019 Oct;4(10):1900425.

129. Wong AD, Ye M, Levy AF, Rothstein JD, Bergles DE, Searson PC. The blood-brain barrier: an engineering perspective. Front Neuroengineering. 2013 Aug 30;6:7.

130. Pediaditakis I, Kodella KR, Manatakis DV, Le CY, Hinojosa CD, Tien-Street W, et al. Modeling alpha-synuclein pathology in a human brain-chip to assess blood-brain barrier disruption. Nat Commun. 2021 Oct 8;12(1):5907.

131. Brown JA, Pensabene V, Markov DA, Allwardt V, Neely MD, Shi M, et al. Recreating blood-brain barrier physiology and structure on chip: A novel neurovascular microfluidic bioreactor. Biomicrofluidics. 2015 Sep;9(5):054124.

132. Huh D, Kim HJ, Fraser JP, Shea DE, Khan M, Bahinski A, et al. Microfabrication of human organs-on-chips. Nat Protoc. 2013 Nov;8(11):2135–2157.

133. Kofanova OA, Mommaerts K, Betsou F. Tube polypropylene: A neglected critical parameter for protein adsorption during biospecimen storage. Biopreserv Biobank. 2015 Aug;13(4):296–298.

134. Bacabac RG, Smit TH, Cowin SC, Van Loon JJWA, Nieuwstadt FTM, Heethaar R, et al. Dynamic shear stress in parallel-plate flow chambers. J Biomech. 2005 Jan;38(1):159–167.

Appendices

Appendix A Representative images of endothelial cells seeded on 6 w/v% GelMA

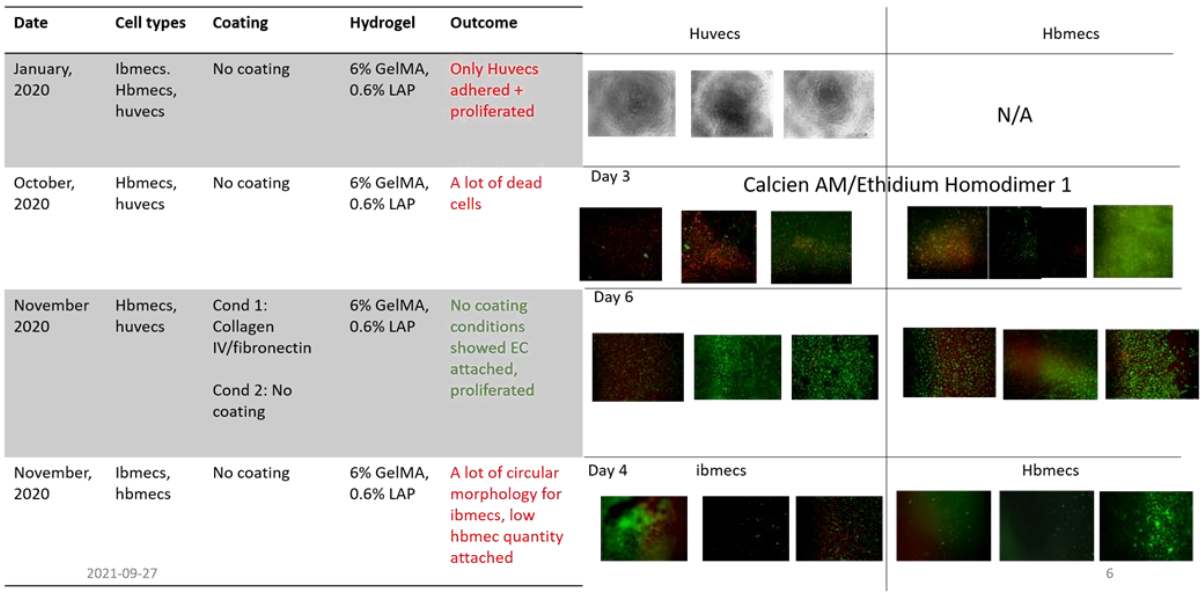

Figure A 1: Visual representation of endothelial cell outcomes from seeding on top of 6 w/v% GelMA.

Appendix B Shear stress calculations

Shear Stress in hydrogel-based capillary model:

Reynold's Number calculation for 3D hydrogel with lumen of 200um in diameter

$$Re = \frac{\rho U L}{\mu}$$

p=density of fluid (assume water) = 1000 kg/m^3
U=velocity = 60ul/hr
L= characteristic length = diameter of channel = 200um
u (mu) = dynamic viscosity of liquid (assume water) = 8.9 x 10^-4 Pa*s

$$Re = \frac{1000\frac{kg}{m^3} * \frac{0.53mm}{s} * \frac{m}{1000mm} * 200\,um * \frac{m}{1x10^6 um}}{8.9x10^{-4} Pa * s} = \frac{0.000106\frac{kg}{m*s}}{8.9\,x\frac{10^{-4}kgm}{s^2} * s} = 0.119$$

Poiseuille Law's Assumptions:

- Newtonian fluid→ Can generalize blood and water as Newtonian fluid
- Circular cross section
- Straight, inelastic walls
- Steady, laminar flow

Shear stress Calculation (3d hydrogel with 200um diameter lumen):

$$\tau = \frac{8\mu U}{d}$$

Given:
Q = 60 ul/hr
d= 200um
u (mu) = 0.94 cP for DMEM media

Solve:

$$U = Q * A$$

$$U = 60\left(\frac{ul}{h} * \frac{h}{60mins} * \frac{mins}{60s} * \frac{mm^3}{ul}\right) * \frac{\pi\left(200um * \left(\frac{mm}{1000um}\right)\right)^2}{4}$$

$$U = 0.53\frac{mm}{s}$$

0.94 cP = 0.0094 dyn/cm2

$$\tau = \frac{8 * 0.0094\frac{dyn*s}{cm^2} * \frac{0.53mm}{s}}{0.2mm} = \mathbf{0.199}\frac{\boldsymbol{dyn}}{\boldsymbol{cm^2}}$$

Shear stress Calculation (1mm^2 rectangular top channel using flow rate of 1100ul/min (peristaltic pump) vs. 60ul/hr (syringe pump)):

Assumptions:
Parallel-plate flow chamber – equation from (134)
Newtonian fluid
Steady flow
Infinitely wide parallel plates
For finite dimension – the fluid velocity profile remains parabolic between the plates

Given:
u = 0.94 cP for DMEM media
Q1 = 1100uL/min
Q2 = 60ul/hr
W=1mm
H=1mm

$$\tau = \frac{6\mu Q}{wh^2}$$

$$\tau = \frac{6 * 0.0094 \frac{dyn * s}{cm^2} * 1100 \frac{ul}{min} * \frac{mm^3}{ul} * \frac{min}{60s}}{(1mm)(1mm^2)} = \mathbf{1.034\ \frac{dyn}{cm^2}}$$

$$\tau = \frac{6 * 0.0094 \frac{dyn * s}{cm^2} * 60 \frac{ul}{hr} * \frac{mm^3}{ul} * \frac{hr}{3600s}}{(1mm)(1mm^2)} = \mathbf{0.00094\ \frac{dyn}{cm^2}}$$

Dial settings for peristaltic pump:

- 1: 6.3 ml/Hr = 0.105 ml/min
- 2: 25 ml/hr = 0.417 ml/min
- 3: 41 ml/hr = 0.68 ml/min
- **4: 58 ml/hr = 0.96 ml/min (select dial 4 on peristaltic pump)**
- 5: 79 ml/hr = 1.3 ml/min
- 6: 97 ml/hr = 1.6 ml/min
- 7: 116 ml/hr 1.9 ml/min
- 8: 136 ml/hr = 2.26 ml/min
- 9: 162 ml/hr = 2.7 ml/min
- 10: 175 ml/hr = 2.91 ml/min

Appendix C Protocol for fabricating PDMS chips at the Cheung Lab

1. MAKE 3D MOLD DESIGN

- Solidworks software:
    - Need to download Solidworks program on personal computer: https://ubc.onthehub.com/WebStore/Welcome.aspx
    - Tutorial on how to use Solidworks: https://blogs.solidworks.com/solidworksblog/2013/05/get-more-with-solidworks-tutorials.html
- Save Solidworks file as a SLDPRT and a .stl file (.stl file needed for use in Utility software)

2. PRINTING USING DLP PRINTER

- Open Utility.exe Software:
    - 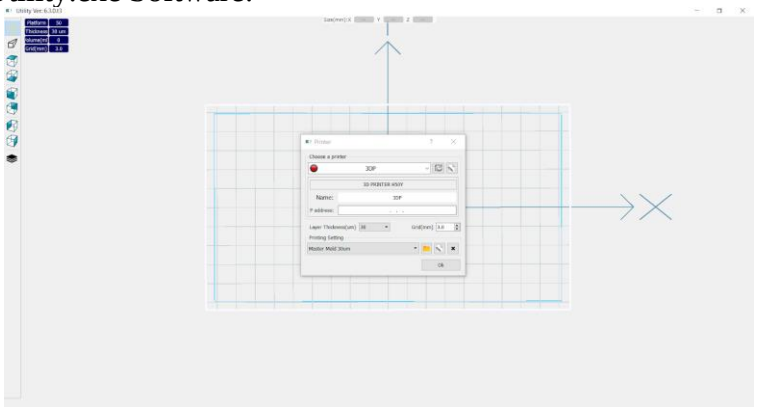

Figure A 2: Open Utility software and this page should open.

- Ensure 30um layer thickness, and master mold 30um print parameters are selected
- Click OK

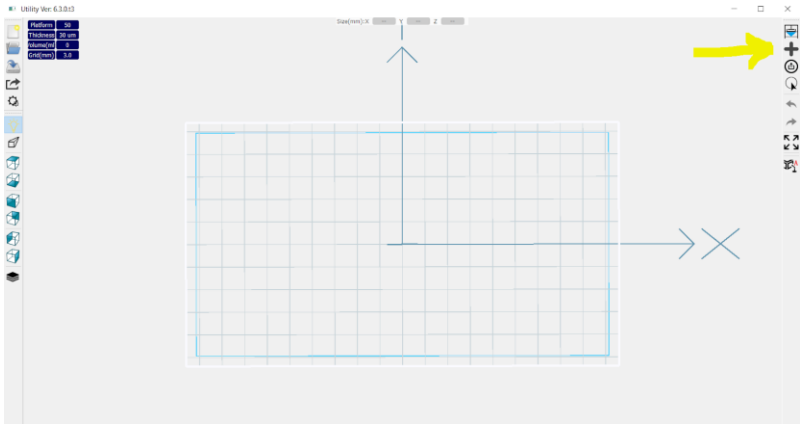

Figure A 3: Click + icon and upload the STL parts of choice.

- Click + icon and upload the STL parts of choice.
  - Click the item of preference

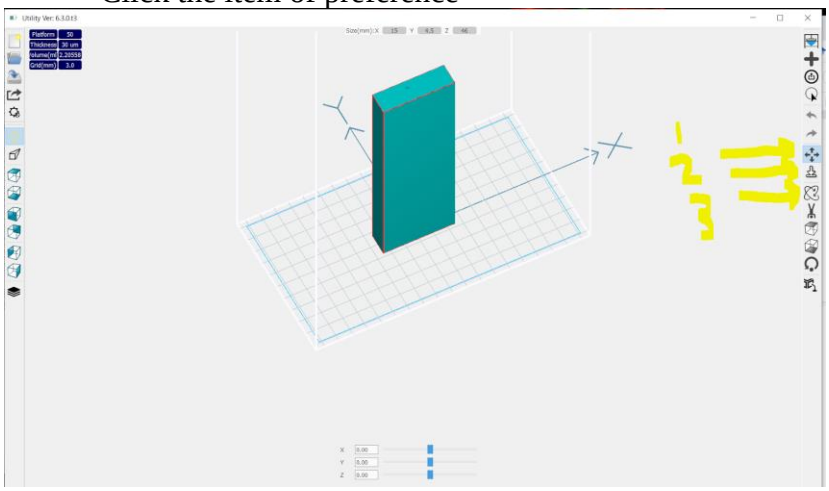

Figure A 4: Utility software functions.

  - Move the item using (1) button
  - Ground the item to be flat with the z position 0 with the (2) button
  - Rotate the item by clicking (3)
    - Adjust x/y/z by 90degree increments
- Get ready to print by uploading to print button

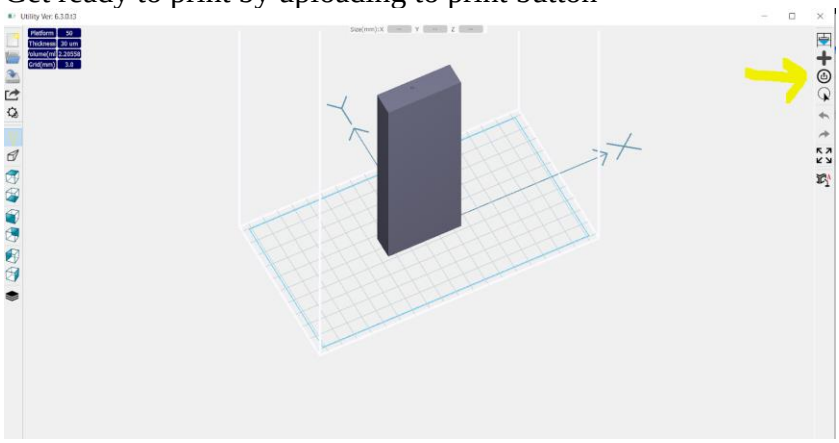

Figure A 5: Utility software upload print.

- Enter semi-auto mode pops up, Click NO

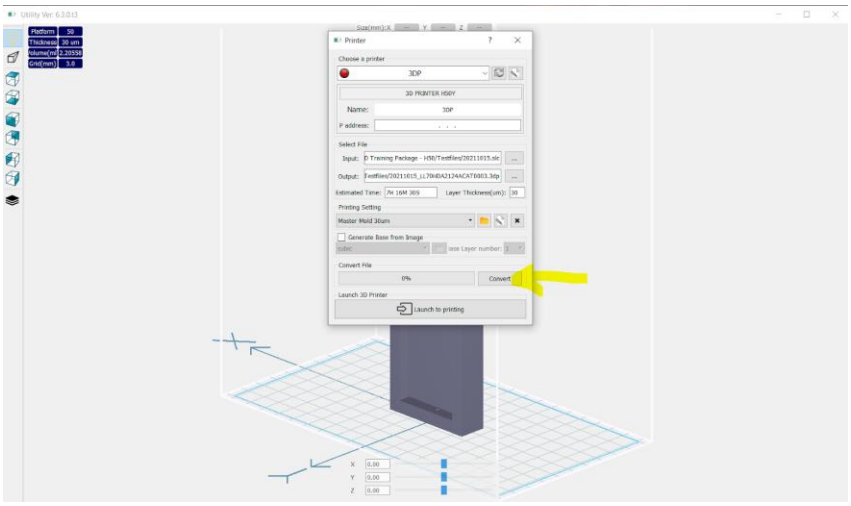

Figure A 6: Utility software convert print to .3DP file.

- Double check parameters are what you want
- Click “convert”
- Wait for conversion to reach 100% then click the 3 dots (...)
-

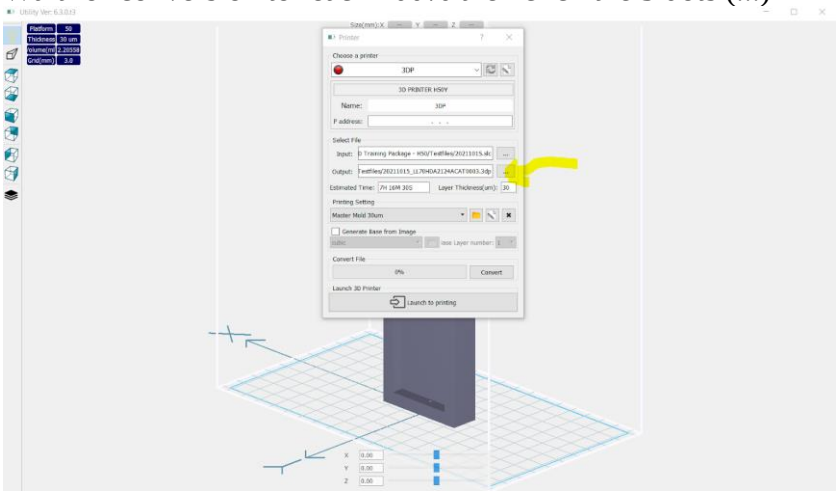

Figure A 7: Utility software how to save file.

- Then drag + drop into usb file and re-name to desired name
    - Ensure file is a (.3dp) file now

On the printer:

- Insert USB to front of printer
    - Click “print” on left icon
    - Choose USB
    - Find file and select
    - Click “Save as”
    - Write file name with date, name, description
    - Click Next

        - Save to: printer
        - It is saved. Can re-print multiple times now.

3. POST-PROCESSING

- Remove prints with the scraper + utility knife
    - Put parts into 1st >95% IPA bath for 10-20 minutes
    - Use compressed air to dry off parts
    - Put parts into second IPA bath for 10-20 minutes
    - Use compressed air to dry off parts
    - At this point, parts shouldnot have any resin on it. Resin shows up as a glossy area.
    - Put parts in UV chamber for 40 minutes on one side, and 20 minutes on other side. Use 40 minutes for the side in contact with PDMS.

4. CASTING CHIPS

Weigh out PDMS:

- Use THINKY cups to weigh out
    - Smaller cup: <55g of PDMS used
    - Larger cup: >55g of PDMS used
- Clean cups before use
    - If already solidified → use spatula to break and discard in garbage
    - If still liquid → place in oven for it to cure/solidify then use spatula
    - Can use airline (tube with yellow handle on right side of room) to blow out old residue from molds
- Use VWR scale to weigh out
    - Press ON
    - Add tissue and cup on top → weigh and record
    - Tare scale
    - Measure out 2 ingredients
        - SYLGARD 184 Silicone Elastomer Base (wide, short, cylindrical container with green stripe around the top, labeled “Cheung Lab”)
        - SYLGARD 184 Silicone Elastomer Curing Agent (tall, skinny bottle)
            - Crosslinking agent → required to enabled liquid solidify
        - Add base:curing agent at 10:1 ratio
            - Ratio gives desired stiffness of PDMS
    - Estimate total mass of PDMS needed to fill # of chips
        - Each chip needs ~4g PDMS
        - # of chips x 4 = X g of base to measure out
        - Measure out X/10 g of curing agent

Mix base and curing agent:

- Mix manually with popsicle stick (on shelf directly above scale)
- Securely place lid on cup

    - May need to clean out leftover PDMS from previous use using spatula
- Place cup into THINKY machine
    - If smaller cup → use adaptor
    - If larger cup → place cup directly in
    - Make sure cup's grooves are correctly lined up with the slot
- Set counter balance setting to approximately the mass of container + ingredients inside
- Turn on THINKY machine by closing lid and pressing START
    - Speed stays at 2000
    - Machine will automatically mix it one direction, then switch to opposite direction before stopping

Pour PDMS into mold:

- Insert 25G needles into the 3D printed molds
- Place post-processed 3D-printed molds into clean petri dish → can pour PDMS directly on top
- Take cup out of THINKY machine once spin is done
- Hand pour the PDMS over the molds
    - PDMS will overflow a little bit
- Place dish of molds with PDMS into desiccator to minimize air bubbles for ~20 minutes
    - Stack multiple dishes using weights inside desiccator if desired
    - Place large lid on top of desiccator
    - Turn yellow handle from perpendicular with tube → in line with tube
    - Twist red valve until no hissing sound from the air
    - Lift large lid to check vacuum has been created → entire desiccator should come up
    - After ~20min, turn yellow handle back to perpendicular with tube
    - Twist red valve perpendicular to edge of lid to stop vacuum
    - Lift lid → should lift easily without lifting the bottom of desiccator
    - Most bubbles should be gone from the PDMS
        - If some were underneath other plates, the bubbles may have remained
- If no strict requirement for height of chips → use folded filter paper or popsicle stick to flatten out the top of the PDMS
- If want strict height of chips → use tweezers to lay transparency film onto of the chips with PDMS. Be careful to move in one swift motion to avoid bubble formation.

Cure PDMS in oven:

- Place dishes into 65 deg oven to cure PDMS
    - Open oven by pressing white rectangle in the middle of the handle
    - Oven in PDMS room set to 65deg → heat allows PDMS to cure
- Leave in oven overnight
    - Fastest: 1.5 hours
    - Longest: a few days
- Clean any tools used with ethanol.

5. PDMS-PDMS BONDING (CHEUNG LAB)

- Take chips out from oven
- Cut PDMS layers out from the 3D-printed mold
    - Use scalpel to cut around edge of chip, a needle to lift up corners and edges of chip
    - Collect chips ready for next stage in a petri dish
- Bring petri dish to PDMS room, along with a glass slide fully covered in tape
    - Remove dust from PDMS layers by using Scotch tape and compressed air
    - Use tweezers to lift and align the membrane over the bottom PDMS layers' channel
    - Place glass slide with PDMS layers (bottom layer with membrane on it) inside plasma cleaner
- Turn ON plasma cleaner
    - Large red air tank on the right side of room: check 3 things from right to left
        - Turn large grey circular knob OPEN (counterclockwise)
        - Check red knob is OPEN by twisting a little both ways → should be loose and easy to twist rather than tight one way
            - Meter should be at ~18 000 kPa
        - Check small black knob is open by twisting a little both ways → should be loose and easy to twist rather than tight one way
            - Meter should be at ~100 kPa
    - Follow the clear tube towards the plasma cleaner
        - Turn grey handle from perpendicular to in line with tube
        - Don't move black round dial
        - Turn black handle from in line to perpendicular with the tube → allows door to fully close and vacuum to start
    - Physically push door in with hand while clicking the Pump switch ON, then keep pushing the door in until fully closed
    - Wait for digital display above the machine to turn on and for the number to reach below 600 mTorr
    - Click Power switch ON → wait ~10 seconds until a purple hued light can be seen through the window of the machine
    - RF level dial always remains at HI
- Set 1 min timer → PDMS is being treated for 1 min
- Once 1 min over, turn both Pump and Power switches OFF simultaneously
    - If needed, switch Power OFF first
- Slowly twist black handle to allow the vacuum to disappear → should hear hissing sound of air flowing → door opens on its own once vacuum is fully gone
- Remove glass slide with chips on it → chips are done being treated
    - Align chips manually and press down for ~30 seconds.
    - Put bonded chip into the oven for ~1-2 hours to complete bonding.
- Turn OFF plasma cleaner
    - Turn grey valve back to perpendicular with tube
    - Twist large grey circular knob on top of large air tank to CLOSED

- Leave machine door closed

6. CHIP LEAK TESTING

- Remove bonded chips from oven and let them cool to room temperature (~ 10 minutes)
- Cut 3" pieces of tygon tubing
  - Cut as many inlet/outlet ports you will have
- Take pliers and remove the luer connection off ½" straight 22G needles
- Manually attach the tygon tubing (RK-06419-01, Cole-Parmer Microbore Tubing, 0.02" x 0.06" OD) to the needles until about ½ of the needle is covered with tubing
  - Test the tubing + needles for blockages by using a syringe loaded with PBS with food dye and dispense liquid through the tubing + needle
- Add the 22G needle into the chip inlets/outlets
  - Again, test the chip leakage by using a syringe loaded with PBS and food dye to dispense liquid into through the chip
  - Be sure to push the syringe slowly as we don't want to rupture the PET membrane
    - Observe the path of PBS to make sure it flows through the bottom or top channel only and does not leak out the sides or PDMS orflow into the top channel

7. PDMS MOAT

- Place three (optional) assembled PDMS chips side-by-side and tape them together.
- Individually tape the tubing so that the top channel and bottom channel tubing do not overlap
  - Tape all pieces of tape together
- Put the connected chips into a container that has a flat bottom where the chips will lay
  - Any container will do – as long as the bottom is flat
  - The larger the container, the more PDMS you will use, but the smaller the container, the more difficult it is to place the connected PDMS chips and keep their needles straight, so this can be done by trying a couple containers first
  - Suggested containers include rectangular petri dishes, hard plastic covers from glass slide containers

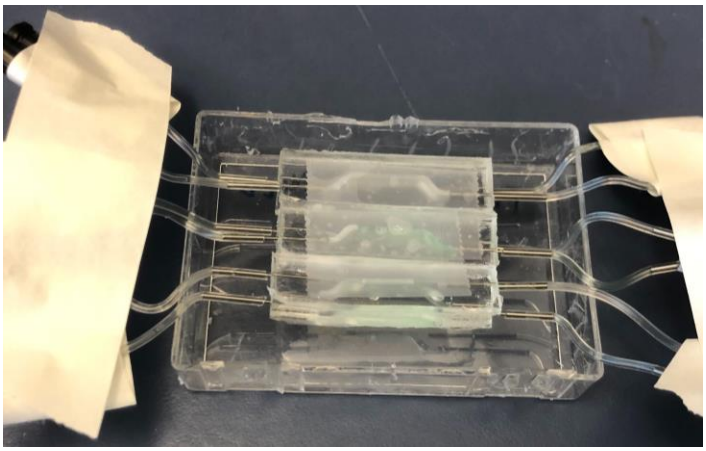

Figure A 8: Three assembled chips taped together and ready for PDMS moat.

- Put the container into a large 150mm petri dish

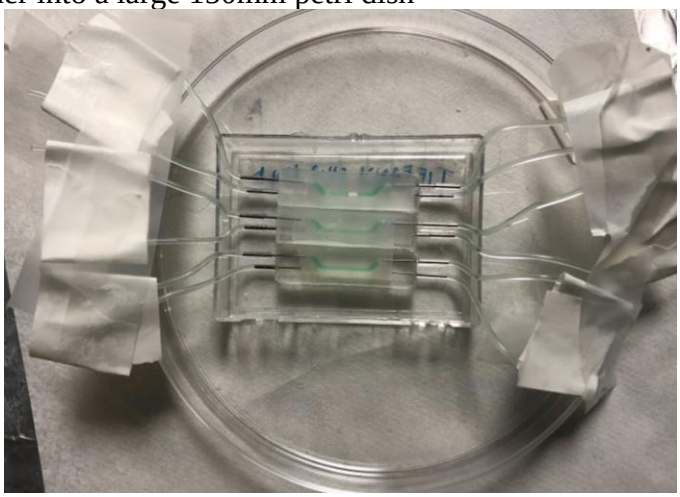

Figure A 9: When prepping for PDMS, include extra petri dish to catch extra resin.

- Pour 10:1 PDMS (make the same way as in section 4: CASTING CHIPS) around the chip until it reaches a height that covers all inlets and outlets
- Place the chips into the desiccator for ~40 minutes
- Remove the petri dish and add a piece of acrylic that will fit the size of the 3 chips and add a weight to weigh down the chips
- Place the chips with weight into the oven overnight
- Remove the acrylic weights and use a scalpel to remove the chips from the container

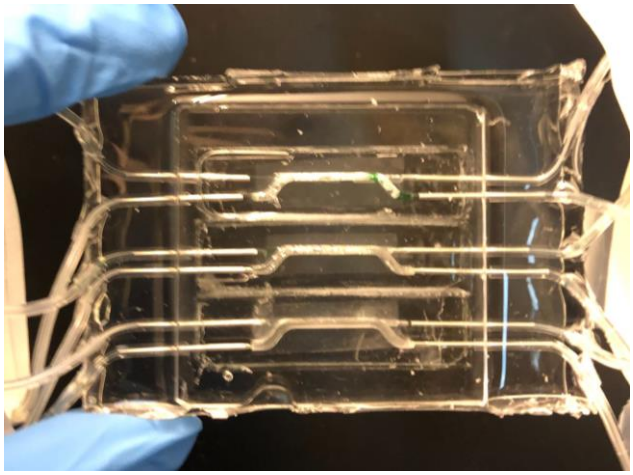

Figure A 10: Image of final PDMS moat embedded chips.

- Insert 22G needles into the ends of the tubing
- Add male luer caps to the luer lock needles

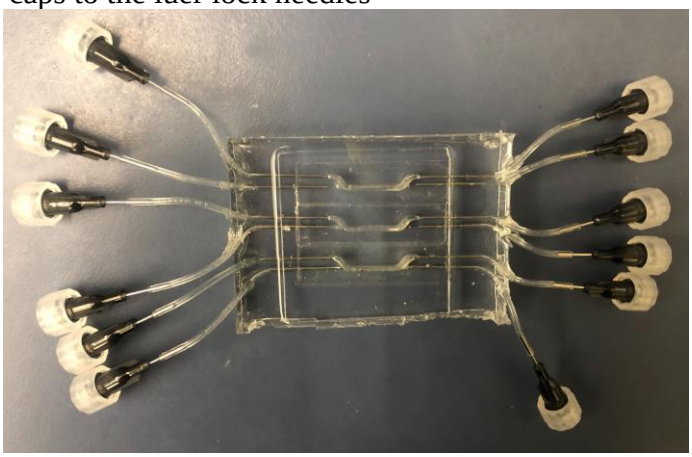

Figure A 11: Add needles to ends of tubign when prepping for a chip experiment containing cells.

- Now, cut 3’ and 1’ pieces of tygon tubing for each chip that you are using in the experiment
- Place 22g needles with luer locks into one end of the 3’ long piece and both ends of the 1’ long tubing
    - Flow pbs through to make sure the tubing and needles are cleared
- Put tubing with needles into small autoclave bag
- Place twice as many male to male luer lock adapters as you have chips into another autoclave bag
- For every set of 3 chips, place a custom made 50mL flacon cap that has 3 inlet holes and a standard 50mL falcon tube into a small autoclave bag

Figure A 12: Items to autoclave before a chip experiment that will include cells.

- Autoclave everything that's in an autoclave bag at 121C for 30 minutes (Grav 30 cycle)
    - Use secondary containers when autoclaving

Appendix D Bioreactor cost breakdown of old design and new design

Table A 1: Cost breakdown for the original bioreactor system.

Company	Description	Part number	Cost	Quantity	Link	Amount per each bioreactor run	Frequency of use	Cost / bioreactor ($)
Nordson Medical	Male Luer to 500 Series Barb, 1/16" (1.6 mm) ID Tubing (May be used with separate stationary lock ring; FSLLR), Animal-Free Natural Polypropylene	MLSL004-6005	$0.1803/ea - 100pcs minimum	100	https://www.nordsonmedical.com/Shop/Fluid-Management/Products/MLSL004-6005	per 4 ports	change every 3 uses	0.2404
Fisher Scientific	Dow Corning™ Silastic™ Laboratory Tubing (3.3 mm ID, 6.35 mm OD)	Catalog Num. 11-189-15L	$280.03 / Pack of 50 Each	1	https://www.fishersci.ca/shop/products/dow-corning-silastic-laboratory-tubing-24/1118915l	per 4 inches	change every 3 uses	0.01257911111
Fisher Scientific	Thermo Scientific™ Nalgene™ Pharma-Grade Platinum-Cured Silicone Tubing (3/8" ID and 1/16" thick) 11 psig at 73°F (23°C)	Catalog No.14-179-118	$511.66 / Case of 50 Each	1	https://www.fishersci.ca/shop/products/nalgene-pharma-grade-platinum-cured-silicone-tubing/14179118	per inch	change every 3 uses	0.005683888889
Fisher Scientific	Dow Corning™ Silastic™ Laboratory Tubing (3.13 mm OD, 1.6mm ID)	Catalog No.11-189-15G	$199.06 / Pack of 50 Each	1	https://www.fishersci.ca/shop/products/dow-corning-silastic-laboratory-tubing-24/1118915g?showTab=accessoriesTab	per 2 feet	change every 3 uses	0.05308266667
Confluent Medical Technologies	Non-woven PGA biofelt (1.0 mm x 70 mg/cc, 20 x 30 cm sheet)	Invoice #: 278164	2393.00 each	1	N/A - need invoice	16 scaffolds (2.4 x 12.4 cm) = 29.76 cm2 out of (20 x 30 = 600 cm2) so total # scaffolds = 600 cm2 / 29.76 cm2 = 20.16 16-scaffold-pieces so 20.16 x 16 scaffolds = 322.56 scaffolds (~1 / 320 sheets)	1	7.478125
Cole-Parmer	Masterflex L/S® Precision Pump Tubing, PharMed® BPT, L/S 14; 25 ft	Catalog RK-06508-14	$200.38CAD / PKG OF 1 (25 ft)	1	https://www.coleparmer.ca/i/masterflex-l-s-precision-pump-tubing-pharmed-bpt-l-s-14-25-ft/0650814?searchterm=RK-06508-14	per bioreactor use	change every 3 uses	2.0038
Nordson Medical	Straight Through Tube Fitting with 400 Series Barbs, 1/16" (1.6 mm)	N410-6005	$0.3478/ea - 100pcs minimum	1	https://www.nordsonmedical.com/Shop/Fluid-Management/Products/N410-6005	2 per bioreactor	change every 3 uses	0.6956

							Total ($/bioreactor)	**10.48927067**

Table A 2: Cost breakdown for the modified bioreactor system.

Company	Description	Part number	Cost	Quantity	Link	Amount per each bioreactor run	Frequency of use	Cost / bioreactor ($)
Fisher Scientific	Dow Corning™ Silastic™ Laboratory Tubing (3.3 mm ID, 6.35 mm OD)	Catalog Num. 11-189-15L	$280.03 / Pack of 50 Each	1	https://www.fishersci.ca/shop/products/dow-corning-silastic-laboratory-tubing-24/1118915l	per 4 inches	change every 3 uses	0.01257911111
Fisher Scientific	Dow Corning™ Silastic™ Laboratory Tubing (3.13 mm OD, 1.6mm ID)	Catalog No.11-189-15G	$199.06 / Pack of 50 Each	1	https://www.fishersci.ca/shop/products/dow-corning-silastic-laboratory-tubing-24/1118915g?showTab=accessoriesTab	per 2 feet	change every 3 uses	0.05308266667
Confluent Medical Technologies	Non-woven PGA biofelt (1.0 mm x 70 mg/cc, 20 x 30 cm sheet)	Invoice #: 278164	2393.00 each	1	N/A - need invoice	16 scaffolds (2.4 x 12.4 cm) = 29.76 cm2 out of (20 x 30 = 600 cm2) so total # scaffolds = 600 cm2 / 29.76 cm2 = 20.16 16-scaffold-pieces so 20.16 x 16 scaffolds = 322.56 scaffolds (~1 / 320 sheets)	1	7.478125
Cole-Parmer	Masterflex L/S® Precision Pump Tubing, PharMed® BPT, L/S 14; 25 ft	Catalog RK-06508-14	$200.38CAD / PKG OF 1 (25 ft)	1	https://www.coleparmer.ca/i/masterflex-l-s-precision-pump-tubing-pharmed-bpt-l-s-14-25-ft/0650814?searchterm=RK-06508-14	per bioreactor use	change every 3 uses	2.0038
Nordson Medical	Straight Through Tube Fitting with 400 Series Barbs, 1/16" (1.6 mm)	N410-6005	$0.3478/ea - 100pcs minimum	1	https://www.nordsonmedical.com/Shop/Fluid-Management/Products/N410-6005	2 per bioreactor	change every 3 uses	0.2318666667
Nordson Medical	Female Luer Lug Style to Classic Series Barb, 1/16" (1.6 mm) ID Tubing, Animal-Free Natural Polypropylene	FTL10-6005	0.2102	1	https://www.nordsonmedical.com/Shop/Fluid-Management/Products/FTL10-6005	2 per bioreactor	change every 3 uses	0.1401333333
Nordson Medical	Male Luer Integral Lock Ring Plug, Closed at Grip, Animal-Free Natural Polypropylene	LP4-6005	0.1206	1	https://www.nordsonmedical.com/Shop/Fluid-Management/Products/LP4-6005	2 per bioreactor	change every 3 uses	0.0804
Nordson Medical	Panel Mount Reduction Connector 1/4-28 UNF to 200 Series Barbs, 1/8" (3.2 mm) and 1/16" (1.6 mm) ID Tubing, Animal-Free Natural Polypropylene	PMS230-210-6005	0.3606	1	https://www.nordsonmedical.com/Shop/Fluid-Management/Products/PMS230-6005	2 per bioreactor	change every 3 uses	0.2404
Shop3D	Custom-made end caps made with autocalvable biomedical clear resin	N/A	$15.80	1	Quote #1124083 (Print to order)	2 per biorector	change every 6 uses	$5.27
Cole-Parmer	Masterflex Transfer Tubing, Platinum-Cured Silicone, 1/2" ID x 11/16" OD; 25 ft	RK-95802-22	$356	25'	https://www.coleparmer.ca/p/masterflex-transfer-tubing-platinum-cured-silicone/41153	per 2 inches	change every 3 uses	$1
							Total ($/bioreactor)	**16.29816456**

Appendix E Observations of tissue chamber bubble tests

Table A 3: Observations seen with Design #1 after performing a 7 day experiment.

		Day 0		Day 7	
#	Description	Observations	image	image	Observations
1	End caps – normal Sampling ports - normal	One very small bubble ~1/8 width of tubing	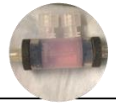	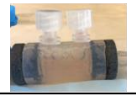	Discoloration Multiple small bubbles
2	End caps – normal Sampling ports – not present	Tiny bubbles	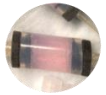		One bubble (~1/2 width of tubing) + small bubbles
3	End caps – parafilm Sampling ports – normal	Few tiny bubbles		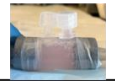	Small bubbles
4	End caps – normal Sampling ports – Epoxy	One bubble ~ 1/6 tubing width			One bubble ~1/2 width of tubing
5	End caps – parafilm Sampling ports – epoxy	One bubble ~ 1/3 tubing width			One bubble ~1/3 width of tubing
6	End caps – epoxy Sampling ports – epoxy	One bubble ~ 1/3 tubing width			One bubble ~1/3 width of tubing
7	End caps – parafilm Sampling ports – Not present	One bubble ~ 1/4 tubing width	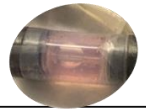		Slight discoloration One bubble ~1/2 width of tubing
8	End caps – epoxy Sampling ports – normal	No bubbles	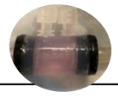	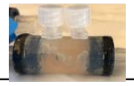	Discoloration Small bubbles

Table A 4: Obervations seen with tissue chamber Design #2 after a 7 day experiment.

Sample		Day 0		Day 7	
#	Description	Observations	Image	Image	Observations
1	End caps – Biomedical clear resin Sampling ports – polypropylene Tubing material: Masterflex® Transfer Tubing, Platinum-Cured Silicon	Filling of bioreactor chamber with media was successful. Minimal bubble formation.		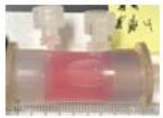	Bubbles approximately ¼ width of chamber formed. Bubbles are not big enough to interfere with scaffold.
2		Filling of bioreactor chamber with media was successful. Minimal bubble formation.	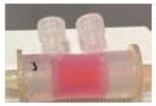		
3		Filling of bioreactor chamber with media was successful. Minimal bubble formation.			
4	Tubing: Thermo Scientific™ Nalgene™ Pharma-Grade Platinum-Cured Silicone Tubing Ports: Polypropylene	Filling of bioreactor chamber with media was successful. Minimal bubble formation.	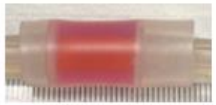	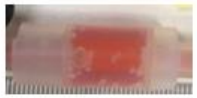	Small bubbles and large bubbles (1/2 width of chamber tubing) formed. In sample #6, bubble is big enough to interfere with scaffold.
5		Filling of bioreactor chamber with media was successful. Small bubble formation.	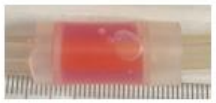		
6		Filling of bioreactor chamber with media was successful. Minimal bubble formation.			

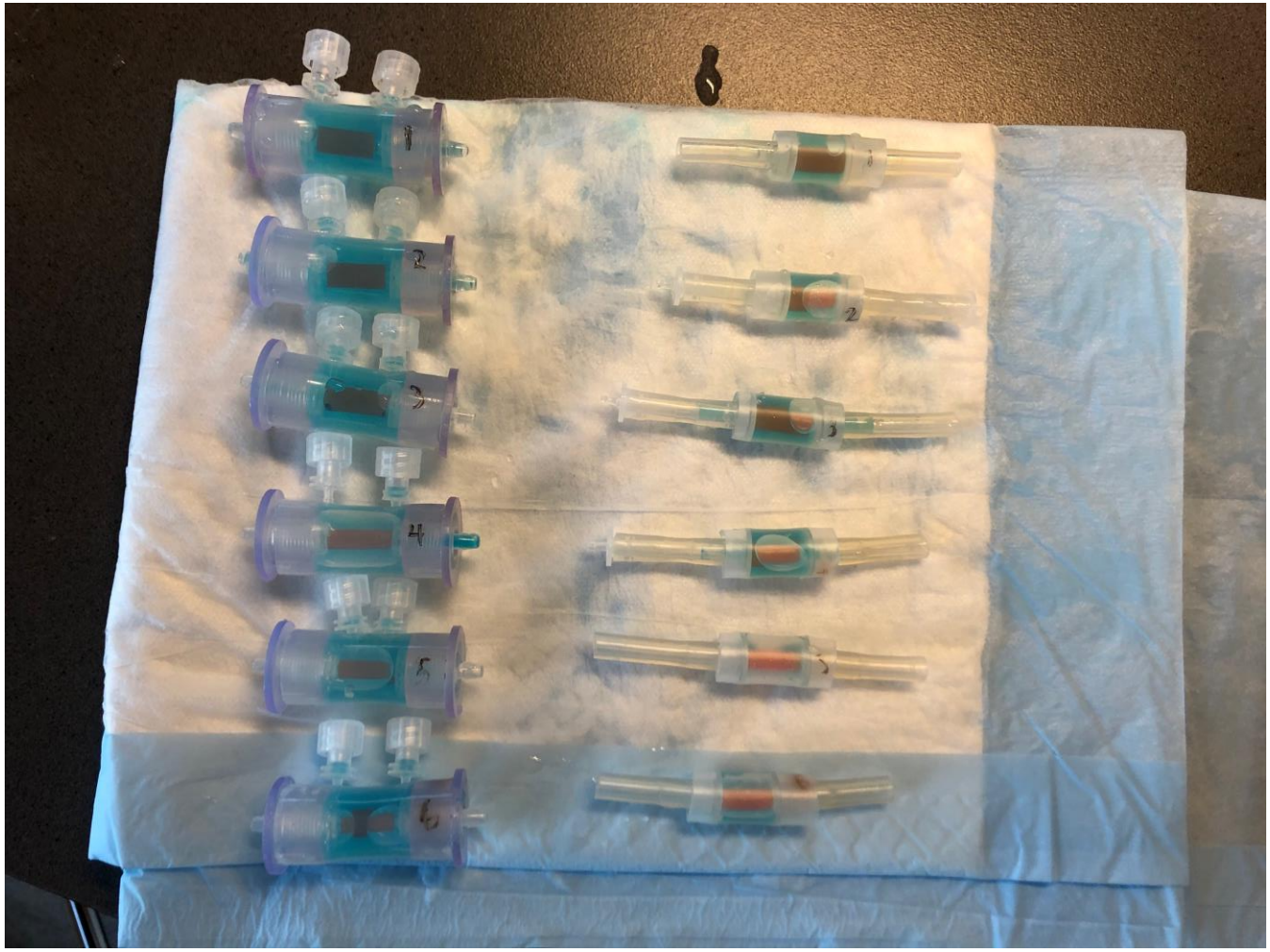

Figure A 13: Visual representation of tissue chamber Design #2 in hydrated (top 3 rows) and non-hydrated (bottom 3 rows) conditions for 7 days.